

INVESTIGATIONS OF THE ENZYMATIC MECHANISMS AND INHIBITION OF  
PROSTAGLANDIN E2 BIOSYNTHESIS

By

Michael C. Goodman

Dissertation

Submitted to the Faculty of the

Graduate School of Vanderbilt University

in partial fulfillment of the requirements for the degree of

DOCTOR OF PHILOSOPHY

in

Chemistry

May 11, 2018

Nashville, Tennessee

Approved:

Lawrence J. Marnett, Ph.D.

Charles R. Sanders, Ph.D.

Hassane S. Mchaourab, Ph.D.

John A. McLean, Ph.D.

*To my family*

*In loving memory of Dr. Richard Neil Armstrong,*

*who fostered a learning environment for many to further understand the world around us.*

## ACKNOWLEDGEMENTS

Graduate school has certainly been a challenge but has been made possible by so many wonderful people along the way. First and foremost, I would like to thank my parents for always supporting my academic and personal goals. Mom and Dad, you are both truly phenomenal role models and you always encouraged me to give my best effort in everything and to never quit anything, including little league football. I also thank my grandfather Lewis Cutliff, the epitome of a true gentleman. I have always looked up to you and appreciate the guidance and love you have given me for nearly thirty years of my life. I also attribute many of my greatest assets to my late great-grandmother, Lillian Cutliff, and my late grandmother, Maxine Cutliff. I value the love you shared with me and you are both dearly missed. I thank my grandparents, Stanley and Marjorie Goodman, for your love and encouragement as well. I am fortunate to have grown up with loving siblings, Amber, Adam, and Cole. Thank you all for always being there for me and taking care of your “baby brother.”

I want to thank the late Dr. Richard Armstrong for allowing me to join his lab shortly after beginning my graduate school studies. Your lab provided an ideal environment for training young scientists and connected us together on a personal level. Thank you for taking a chance on a boy from “Kan-tucky!” to pursue his dreams of making an impact in the scientific world. I also want to thank my colleagues from Dr. Armstrong’s lab who have become family. Dr. Matt Thompson, a fellow Kentuckian, thank you for guiding me from day one of my lab rotation to be a better scientist. Thanks for also killing me in the gym. Dr. Mary Keithly, thank you for being a wonderful resource in the beginning of my lab work and assisting me with many experiments. Kevin Jagessar, thanks for providing us with many laughs and “the wall.” Dr. Merced Malabanan, thanks for discussing life’s big questions with me and being a true friend. Finally, Dr. Kristin Droege, I especially thank you for being there for me in the last stretch of graduate school. I am thankful for you and Nathan and many stories we have shared together over 2 for 1 margaritas at Taco Mamacita.

I especially want to thank my current advisor, Dr. Lawrence Marnett, for allowing me to complete my doctoral studies in your lab, following the unfortunate passing of Dr. Armstrong. Larry, you are an incredible person and I am forever grateful that you have been there for me and accepted me into your lab for my final years of graduate school. You have provided adequate resources for my training and guidance for my future endeavors. I also want to specifically thank Dr. Charles “Chuck” Sanders, for stepping in a few years ago and giving me guidance for completing my graduate studies. I certainly couldn’t have finished without your willingness to help and I want to express how much I appreciate your mentorship for me, as well as other members of the Armstrong lab. I also want to thank Dr. Hassane Mchaourab for being a valued member of my committee and allowing me to gain experience through a rotation in your lab. Dr. John McLean, thank you for stepping in and agreeing to join my committee and being another resource of encouragement for completing my degree.

Next, I want to thank members of the Marnett lab for their camaraderie and assistance after I joined the lab. Brenda Crews, Jashim Uddin, Jim Galligan, Phil Kingsley, Orrette Wauchope, Michelle Mitchener, and James Wepy, it was truly a pleasure getting to know you all and work with you. I especially want to thank Kebreab Ghebreselasie for training me multiple days in cell culture. I also want to thank Dr. Shu Xu for being a wonderful mentor for me and assisting me with numerous tasks in the lab and for being a great friend. I am also very grateful for Dr. Carol Rouzer, another mentor who made my progress possible. I sincerely appreciate your willingness to spend a substantial amount of time investing in the improvements of my experiments and editing of manuscripts and other documents.

I want to thank many friends in my life who have made the graduate school journey much easier. To my best friend, Kevin, I appreciate your friendship and the encouragement you have provided for many years. I am grateful for the expeditions where we got to experience many sights in our great country during brief “breaks” in graduate school. Eric, thank you for keeping me grounded through frequent rock concerts and watching the Cats play basketball. Caroline, I am so glad that I had a “good ole Barren County” friend here in Nashville. Our constant rants about school enabled us to both survive. To all of my “family” at Mammoth Cave, I am very appreciative of the lifelong friendships that were formed many years ago. The

countless bonfires, card games, and laughter dispersed throughout the years have been filled with so many great memories I will forever cherish.

I want to thank many people at Vanderbilt University for making my graduate studies enjoyable. I am obliged to wonderful friends like Emily, Noah, and Drew, among so many others. You guys made my time outside of lab fun. I thank Sandra Ford, the “Vandy Mom,” for talking to me and engaging my interest one day in the summer of 2011 about the Chemistry graduate program when I was randomly in Nashville one day. I thank Dr. John York for assisting my transition to a new lab home and supporting me and other members of the Armstrong lab. I thank Jennifer Smith in the Department of Biochemistry for assisting me with scheduling various meetings. I thank the wonderful people in the administrative office including Anne Lara, Stephen Doster, and Becky Sanders.

I also want to thank some phenomenal people from other universities which have enabled my scientific career to flourish. I give many thanks to my undergraduate research advisor at the University of Kentucky, Dr. D. Allan Butterfield. I appreciate the opportunity to perform scientific research in your lab for two years and acquire many vital skills, including the ability to “think on my toes.” I want to thank Dr. Ralf Morgenstern at the Karolinska Institutet in Stockholm, Sweden for being a fantastic collaborator with my work from Dr. Armstrong’s lab. I especially thank you for allowing me to visit Sweden for the first time in 2015 to complete some work at Karolinska. It was a privilege to return two years later and I appreciate your hospitality and friendship. I also thank Dr. Hans Hebert for allowing me to work in his lab for a period in 2017, learning many new biochemical techniques. I sincerely appreciate the guidance of Dr. Caroline Jegerschöld for my time in the lab and all of the other wonderful colleagues I had the pleasure of meeting and working with.

Finally, I would like to thank the Lord for providing me with this opportunity, allowing me to experience this ever-evolving creation, and grow each day as a part of it.

These studies were supported by the National Institutes of Health R01 GM030910 (R.N.A.), R01 CA089450 (L.J.M.), the Vanderbilt Institute of Chemical Biology, and the Vanderbilt Center in Molecular Toxicology Training Grant (NIH T32 ES702839 (M.C.G.)).

# TABLE OF CONTENTS

	Page
DEDICATION .....	ii
ACKNOWLEDGEMENTS .....	iii
LIST OF TABLES .....	viii
LIST OF FIGURES .....	ix
LIST OF ABBREVIATIONS .....	xii
 Chapter	
I. Introduction.....	1
Inflammation .....	1
Eicosanoids.....	2
Cytochromes P450 Pathway.....	3
Lipoxygenase Pathway.....	4
Cyclooxygenase Pathway.....	5
Cyclooxygenase Mechanism.....	7
Cyclooxygenase Structure.....	10
Cyclooxygenase Isoform Differences.....	11
Cyclooxygenase Functions as a Heterodimer .....	13
Molecular Basis of COX Inhibition.....	14
Substrate-selective Inhibition of COX.....	20
Prostaglandin Isomerization .....	23
PGE Synthase.....	23
mPGES-1.....	24
MAPEG Proteins.....	24
mPGES-1 .....	25
mPGES-1 Function.....	26
mPGES-1 Structure .....	27
mPGES-1 Mechanism .....	28
mPGES-1 Inhibition .....	31
Purpose of these studies .....	35
II. Materials and Methods .....	37
Materials.....	37
Methods.....	37
III. Molecular Basis of Cyclooxygenase-2 Inhibition by Ibuprofen and Mefenamic Acid .....	50
Results.....	51
Discussion .....	59
Conclusions .....	62

IV. Dual Cyclooxygenase-Fatty Acid Amide Hydrolase Inhibitor Exploits Novel Binding Interactions in the Cyclooxygenase Active Site.....	63
Results.....	63
Discussion .....	76
Conclusions .....	79
V. Efforts Toward Investigating the Structural Dynamics of Cyclooxygenase-2 With Cryo Electron Microscopy.....	81
Results.....	82
Discussion .....	88
Conclusions .....	89
VI. Elucidation of the Chemical Mechanism of Human Inducible Microsomal Prostaglandin E2 Synthase 1.....	90
Results.....	90
Discussion .....	101
Conclusions .....	104
VII. Conclusions.....	106
Discussion .....	106
Future Studies.....	110
Concluding Remarks.....	113
Appendix	
A. Curriculum Vitae.....	114
REFERENCES.....	121

## LIST OF TABLES

Table	Page
1. Steady-state kinetic parameters for COX-2 .....	13
2. Steady-state kinetic parameters for mPGES-1 .....	26
3. IC <sub>50</sub> values for AA and 2-AG oxygenation in the presence of ibuprofen and mefenamic acid.....	53



## LIST OF FIGURES

Figures	Page
1. Chemical structure of arachidonic acid .....	2
2. Cytochromes P450 enzymatic pathway.....	3
3. Lipoxygenase enzymatic pathway .....	5
4. The Cyclooxygenase enzymatic pathway.....	6
5. Cyclooxygenase catalytic mechanism.....	9
6. Cyclooxygenase enzyme structure .....	11
7. COX-2 endocannabinoid substrates .....	12
8. Chemical structures of COX inhibitors .....	16
9. Crystal structure of diclofenac in the COX-2 active site.....	18
10. Crystal structure of ( <i>R</i> )-flurbiprofen in the COX-2 active site .....	21
11. Crystal structure of mefenamic acid in the COX-2 active site.....	22
12. PGH <sub>2</sub> isomerization to PGE <sub>2</sub> by the PGE synthases .....	23
13. mPGES-1 crystal structure.....	28
14. mPGES-1 catalytic mechanism.....	29
15. mPGES-1 active site with GSH and crystallographic water.....	30
16. Chemical structures of mPGES-1 inhibitors.....	32
17. IC <sub>50</sub> curves for mCOX-2 inhibition by ibuprofen.....	52
18. IC <sub>50</sub> curves for mCOX-2 inhibition by mefenamic acid .....	54
19. Time course assay for COX-2 substrate oxygenation in the presence of mefenamic acid .....	56
20. Heme oxidation in the presence of ibuprofen or mefenamic acid.....	58
21. Heme oxidation in the presence of ibuprofen or mefenamic acid.....	58
22. Chemical structures of ( <i>R</i> )- and ( <i>S</i> )-flurbiprofen and ( <i>S</i> )-ARN2508 .....	64
23. Crystal structure of ( <i>S</i> )-ARN2508 in the COX-2 channel .....	65
24. Inhibition of oCOX-1 with ARN2508.....	66

25. Inhibition of mCOX-2 with ARN2508, with or without pre-incubation .....	67
26. Kinetics of the time-dependent inhibition of mCOX-2 by ( <i>S</i> )-ARN2508 .....	69
27. Inhibition of mCOX-2 mutants with ARN2508.....	70
28. Peptide coverage of digested wild-type COX-2 following incubation with ( <i>S</i> )-ARN2508.....	71
29. Kinetics of the time-dependent inhibition of S530A and S530T mCOX-2 by ( <i>S</i> )-ARN2508.....	73
30. Dose response of ( <i>S</i> )-ARN2508 with 30 s preincubation.....	74
31. Kinetics of LNA inhibition by ( <i>S</i> )-ARN2508 and ( <i>S</i> )-flurbiprofen .....	75
32. SDS-PAGE gel of COX-2 reconstituted nanodiscs following size-exclusion.....	82
33. Negative stain EM of COX-2 reconstituted nanodiscs.....	83
34. SDS-PAGE gel of purified COX-2 reconstituted nanodiscs following IMAC and size-exclusion.....	84
35. Native PAGE gel of COX-2 nanodiscs .....	85
36. Negative stain EM of COX-2 reconstituted nanodiscs following IMAC and size-exclusion.....	86
37. 2D class averages of COX-2 nanodisc particles from Cryo-EM .....	87
38. 3D model of electron density from COX-2 nanodiscs .....	88
39. SDS-PAGE gel of wild-type human mPGES-1 .....	91
40. GST activity assay in the presence of wild-type mPGES-1.....	92
41. <sup>1</sup> H-NMR spectra of the oxygen analogue (GOH) and the desthio analogue (GH) of glutathione .....	93
42. PGH <sub>2</sub> isomerization with GSH, GOH, and GH.....	94
43. PGH <sub>2</sub> isomerization with GSH and competition with increasing concentrations of GOH .....	95
44. PGH <sub>2</sub> isomerization with GOH and competition with increasing concentrations of GSH .....	95
45. Stopped-flow kinetics of mPGES-1 .....	96
46. Confirmed peptide coverage of mPGES-1 using LC-MS/MS .....	98
47. PGH <sub>2</sub> isomerization in the presence of wild-type and S127A mPGES-1 .....	99
48. MDA fluorescence assay to assess the activity of wild-type, S127A, and S127C mPGES-1 .....	100
49. PGH <sub>2</sub> isomerization to assess the activity of S127A and S127C mPGES-1 enzymes.....	100

50. PGH<sub>2</sub> isomerization to assess the activity of S127C mPGES-1 purified with GSH or GSO<sub>3</sub><sup>-</sup> ..... 101

## LIST OF ABBREVIATIONS

2-AG	2-archidonoylglycerol
12-HHT	12 <i>L</i> -hydroxy-5,8,10-heptadecatrienoic acid
12-HOTrE	12-hydroxy-octadecatrienoic acid
15-PGDH	15-hydroxyprostaglandin dehydrogenase
15d-PGJ <sub>2</sub>	15-deoxy- $\Delta$ 12,14-prostaglandin J <sub>2</sub>
A <sub>280</sub>	Absorbance of protein at 280 nm
AA	Arachidonic acid
ABTS	2,2'-azino- <i>bis</i> (3-ethylbenzothiazoline-6-sulphonic acid)
AEA	Arachidonoylethanolamide
APHS	2-acetoxyphenylhept-2-ynyl sulfide
$\beta$ -DDM	n-Dodecyl- $\beta$ -D-maltoside
$\beta$ -OG	n-Octyl- $\beta$ -D-glucoside
C10M	n-Decyl- $\beta$ -D-maltoside
CDNB	1-chloro-2,4-dinitrobenzene
CHAPS	3-[(3-cholamidopropyl)dimethylammonio]-1-propanesulfonate
CID	Collision-induced dissociation
COX	Cyclooxygenase
CPGES	Cytosolic PGE <sub>2</sub> synthase
cPLA <sub>2</sub>	Cytosolic PLA <sub>2</sub>
DEDTC	Diethyldithiocarbamate
DHET	Dihydroxyeicosatrienoic acid
DMSO	Dimethyl sulfoxide
DSL	Differential static light scattering
DTT	Dithiothreitol

EET	Epoxyeicosatrienoic acid
EGF	Epidermal growth factor
EM	Electron microscopy
ER	Endoplasmic reticulum
EP	PGE <sub>2</sub> receptor
EX	Eoxin
FAAH	Fatty acid amide hydrolase
FAE	Fatty acyl ethanolamides
FLAP	5-LOX-activating protein
GH	$\gamma$ -L-Glu-L-AlaGly
GOH	$\gamma$ -L-Glu-L-SerGly
GPCR	G protein-coupled receptor
GSH	Glutathione
GSO <sub>3</sub> <sup>-</sup>	Glutathione sulfonate
GST	Glutathione <i>S</i> -transferase
HDX-MS	Hydrogen-Deuterium Exchange Mass Spectrometry
HETE	Hydroxyeicosatetraenoic acid
His <sub>6</sub> -tag	Hexahistidine affinity tag
HPETE	Hydroperoxyeicosatetraenoic acid
HSP90	Heat-shock protein 90
IL	Interleukin
IMAC	Immobilized metal affinity chromatography
IPTG	Isopropyl $\beta$ -D-1-thiogalactopyranoside
LA	Linoleic acid
LC-MS/MS	Liquid chromatography-tandem mass spectrometry

LNA	Linolenic acid
LOX	Lipoxygenase
LPS	Lipopolysaccharide
LT	Leukotriene
LTA4H	LTA <sub>4</sub> hydrolase
LTC4S	Leukotriene C <sub>4</sub> synthase
LX	Lipoxin
MAPEG	Membrane-associated proteins in eicosanoid and glutathione metabolism
MBD	Membrane binding domain
mCOX-2	Murine COX-2
MDA	Malondialdehyde
MGST	Microsomal glutathione <i>S</i> -transferase
mPGES-1	Microsomal PGE <sub>2</sub> synthase-1
mPGES-2	Microsomal PGE <sub>2</sub> synthase-2
MSP	Membrane-scaffold protein
MWCO	Molecular weight cut off
NAGly	N-arachidonylglycine
NSAID	Nonsteroidal anti-inflammatory drug
oCOX-1	Ovine COX-1
OD <sub>600</sub>	Optical density of cell culture at 600 nm
P450	Cytochrome P450
PA	Palmitic acid
PC	Phosphatidylcholine
PDB	Protein data bank
PE	Phosphatidylethanolamine
PG	Prostaglandin

PGG	Prostaglandin glyceryl ester
PGI <sub>2</sub>	Prostacyclin
PI	Phosphatidylinositol
PLA <sub>2</sub>	Phospholipase A <sub>2</sub>
POPC	1-palmitoyl-2-oleoyl- <i>sn</i> -glycero-3-phosphocholine
POX	Peroxidase
PPHP	5-phenyl-4E-pentenyl-1-hydroperoxide
PS	Phosphatidylserine
PUFA	Polyunsaturated fatty acid
SAR	Structure-activity relationship
sEH	Soluble epoxide hydrolase
TBA	Thiobarbituric acid
THC	$\Delta^9$ - tetrahydrocannabinol
TM	Transmembrane
TNF- $\alpha$	Tumor necrosis factor- $\alpha$
TX	Thromboxane

## CHAPTER I

### INTRODUCTION

#### Inflammation

Inflammation is an organism's protective response to an external chemical insult, physical injury, or harmful pathogen. When healthy tissue is damaged, there is an influx of immune cells that are transported from the blood to the site of injury. These cells include neutrophils, followed by monocytes, which can then differentiate into macrophages (1). With the increased presence of inflammatory leukocytes, various chemical species are released that are intended to eliminate the initial cause of injury from the affected site, clear any damaged tissue, and initiate the repair process. This acute phase of inflammation is characterized by five cardinal signs including pain, heat, redness, swelling, and loss of function (2). Typically, acute inflammation lasts for a few days, and the affected site of injury is successfully repaired by the controlled clearance of activated inflammatory cells and damaged tissue. However, if resolution is not achieved, inflammation can often last for extended periods of time, evolving to a chronic state. The loss of function of tissues in the affected area can often lead to organ failure and a plethora of diseases including neurodegeneration, cardiovascular diseases, inflammatory arthritis, cancer, and many others (3). Activated macrophages and neutrophils in an inflammatory site release a host of reactive oxygen and nitrogen species that serve to initiate a "chemical warfare" against the noxious pathogen. Many of these powerful chemical oxidants can also react with cellular macromolecules and modify their functions. Among the cellular components most prone to chemically react with these strong oxidant species are polyunsaturated fatty acids (PUFAs). These unsaturated carbon chains in the membrane bilayer of cells are susceptible to non-enzymatic oxidation due to the presence of *bis*-allylic hydrogen atoms (4). PUFAs can also be liberated from phospholipids in the membrane bilayer and enzymatically converted to various oxygenated bioactive lipid compounds that contribute to the pathology, or in some cases, the resolution of inflammation.



## Eicosanoids

One particular class of bioactive lipid molecules, the eicosanoids, is derived from arachidonic acid, an omega-6 fatty acid containing 20 carbons and 4 unsaturated carbon-carbon double bonds ( $\omega$ -6, 20:4) (AA) (Figure 1), or related 20-carbon PUFAs (5). AA is biosynthesized from the essential fatty acid linoleic acid ( $\omega$ 6, 18:2) (LA), which is supplied from the diet (6). AA is then incorporated into the phospholipid bilayer by fatty acyl-CoA synthetase and lysophospholipid acyltransferase (7). In the membrane bilayer, AA is esterified at the *sn*-2 position of the glycerol moiety of individual phospholipids, including phosphatidylcholine (PC), phosphatidylethanolamine (PE), and phosphatidylinositol (PI) (8). To release AA from the bilayer, the enzyme phospholipase A<sub>2</sub> (PLA<sub>2</sub>) hydrolyzes the acyl group at the *sn*-2 position. Among the three major classes of phospholipases, the calcium-dependent cytosolic PLA<sub>2</sub> (cPLA<sub>2</sub>) is abundantly expressed in many cells and plays a major role in liberation of AA from the membrane bilayer (9). Once hydrolyzed, free AA is metabolized enzymatically, forming various classes of eicosanoids. Perhaps the most well-studied class is known as the prostanoids, consisting of prostaglandins (PGs) and thromboxane (TX), formed via the cyclooxygenase (COX) pathway (10). Another family of enzymes, the cytochromes P450 (P450s), convert AA to various lipids including hydroxyeicosatetraenoic acids (HETEs) and epoxyeicosatrienoic acids (EETs) (11). Additional eicosanoids including leukotrienes (LTs), lipoxins (LXs), and eoxins (EXs) are produced from the lipoxygenase (LOX) enzyme family (12). The focus of this work involves PG synthesis in the COX pathway, but the P450 and LOX pathways will briefly be discussed.

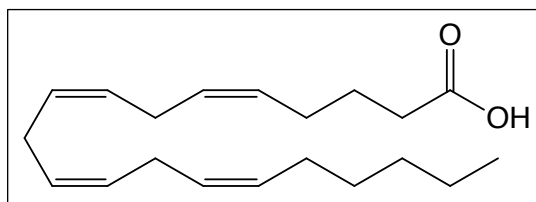


**Figure 1.** Chemical structure of arachidonic acid, the precursor for various bioactive eicosanoids.

## Cytochromes P450 Pathway

P450s are heme-containing enzymes that oxidize xenobiotic toxicants, clinically used drugs, and carcinogens (13). P450s are expressed in the liver as well as various tissues throughout the body and catalyze a wide range of reactions, including the epoxygenation of AA. Currently, there are 18 mammalian P450 families, encoding 57 genes in the human genome (14). Members of the 2C and 2J families of P450s add one molecule of oxygen to AA to form an epoxide at one of each of the four double bonds of the substrate, producing various EETs. Furthermore, the 4A and 4F families of CYP450s can hydroxylate the terminal carbon of AA, producing 20-HETE (15). EETs function as autocrine or paracrine signaling molecules in the cardiovascular system where they produce vasorelaxation, and down-regulate several pro-inflammatory signaling pathways (16). The terminally hydroxylated HETEs also exhibit anti-inflammatory effects by inhibiting the biosynthesis of LTs (17). EETs display rather short half lives in the cell, as they are hydrolyzed by epoxide hydrolases, producing dihydroxyeicosatrienoic acids (DHETs) (Figure 2). The enzyme primarily responsible for this reaction is soluble epoxide hydrolase (sEH). In contrast to the anti-inflammatory properties observed for EETs, their corresponding diols are thought to be pro-inflammatory or biologically inactive (5).

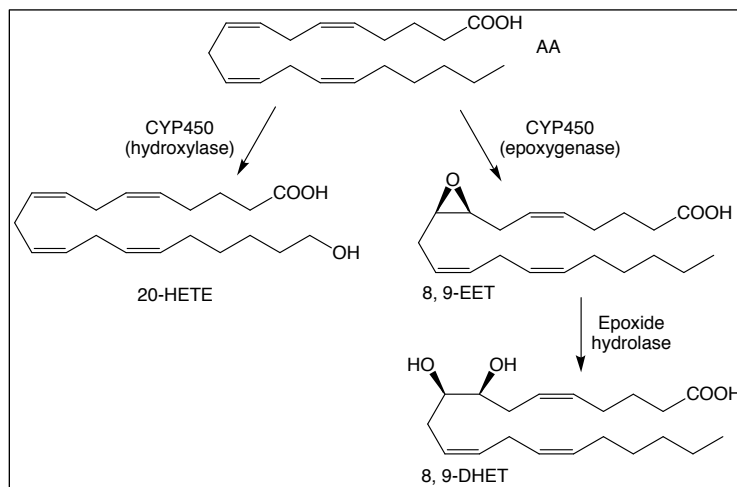


**Figure 2.** Cytochromes P450 enzymatic pathway. AA can be hydroxylated at its terminal carbon to form 20-HETE. Alternatively, it can be epoxygenated to form regio- and stereo-specific epoxyeicosatrienoic acids (EETs), which are then hydrolyzed by epoxide hydrolases to form dihydroxyeicosatrienoic acids (DHETs).

## Lipoxygenase Pathway

LOXs are non-heme, iron-containing dioxygenases that metabolize AA and other PUFAs to potent signaling molecules involved in acute and chronic inflammatory processes such as allergy and asthma (18). The LOX enzymes initiate catalysis by abstracting a hydrogen atom from a *bis*-allylic carbon of the substrate PUFA. Carbon-carbon double bond resonance and subsequent oxygen addition produces a peroxy radical, which is then enzymatically reduced to its corresponding hydroperoxide then to an alcohol, resulting in the regioselective and stereospecific addition of a hydroxyl group to a carbon on the PUFA (19). Various LOX isoforms have been studied, and each is named for the position of the carbon atom within AA to which molecular oxygen is added. In humans, six LOXs exist including 5-LOX, 12-LOX, 12*R*-LOX, 15-LOX, 15-LOX-2, and eLOX3 (20).

5-LOX, one of the most well-studied of the LOXs, has become a therapeutic target for anti-inflammatory drugs. 5-LOX catalyzes the first step in the biosynthesis of LTs, which are potent signaling compounds involved in allergic inflammation, atherosclerosis, and disorders of the respiratory system (21). The production of LTs results from a two-step conversion of AA by 5-LOX. Upon stimulation by pro-inflammatory signals, 5-LOX translocates to the nuclear membrane following the mobilization of intracellular calcium. Concurrently, AA is hydrolyzed from the membrane bilayer by cPLA<sub>2</sub>. Another membrane-bound protein, 5-LOX-activating protein (FLAP) is thought to act as a membrane scaffold for 5-LOX, enabling it to anchor to the membrane. FLAP also is thought to deliver AA to the 5-LOX active site, although the biochemical mechanism by which this occurs is still not fully understood (22). The first step of 5-LOX catalysis involves the oxidation of AA to 5-hydroperoxyeicosatetraenoic acid (5-HPETE), an unstable intermediate. 5-HPETE is then enzymatically reduced to its corresponding alcohol (5-HETE) or epoxidized to form the lipid epoxide LTA<sub>4</sub> (23). LTA<sub>4</sub> can be subsequently hydrolyzed by the enzyme LTA<sub>4</sub> hydrolase (LTA<sub>4</sub>H), forming LTB<sub>4</sub>, or conjugated with glutathione (GSH) to form the cysteinyl-leukotriene, LTC<sub>4</sub> by the enzyme LTC<sub>4</sub> synthase (LTC<sub>4</sub>S) (24) (Figure 3). Successive hydrolysis of LTC<sub>4</sub> yields LTD<sub>4</sub> and LTE<sub>4</sub>, potent mediators that reduce airflow to the alveoli and induce asthma (25). Various drugs have been developed to treat the allergic response and inflammatory disorders associated with the

increased presence of LTs, including zileuton (Zyflo), a 5-LOX inhibitor, and montelukast (Singulair), a cysteinyl LT receptor agonist (26,27). Furthermore, various inhibitors of FLAP have been developed to inhibit the biosynthesis of LTs. Currently, some inhibitors have been tested in clinical trials, but none has reached the market (28).

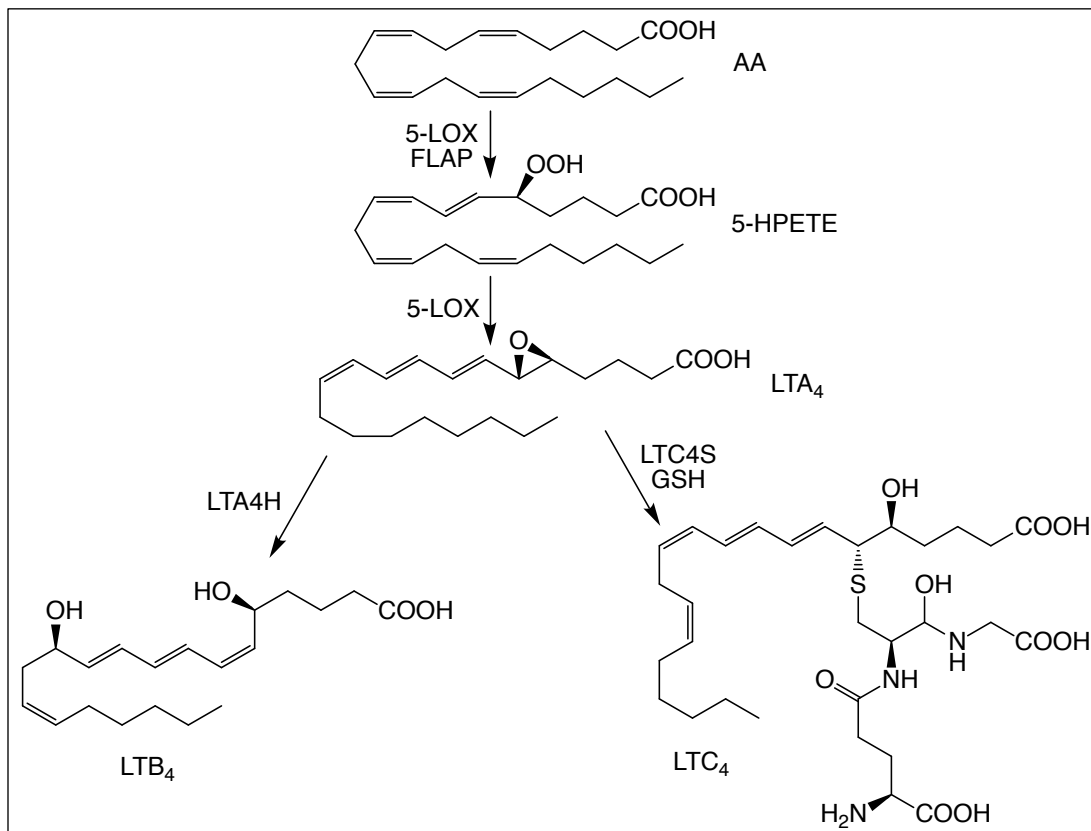


**Figure 3.** Lipoxigenase enzymatic pathway. AA is oxygenated by 5-LOX in the presence of FLAP. The intermediate is then converted to LTA<sub>4</sub>. Hydrolysis of LTA<sub>4</sub> by LTA<sub>4</sub>H yields LTB<sub>4</sub>. Alternatively, LTC<sub>4</sub>S can conjugate glutathione to LTA<sub>4</sub>, forming LTC<sub>4</sub>.

### Cyclooxygenase Pathway

In addition to the P450 and LOX biochemical pathways, AA and other PUFAs can be oxygenated by the COX enzymes. Initially, PG endoperoxides are produced, which can then be converted to PGs, including PGD<sub>2</sub>, PGE<sub>2</sub>, and PGF<sub>2α</sub>, PGI<sub>2</sub> (prostacyclin), or TXA<sub>2</sub> by downstream prostanoid synthases (Figure 4).

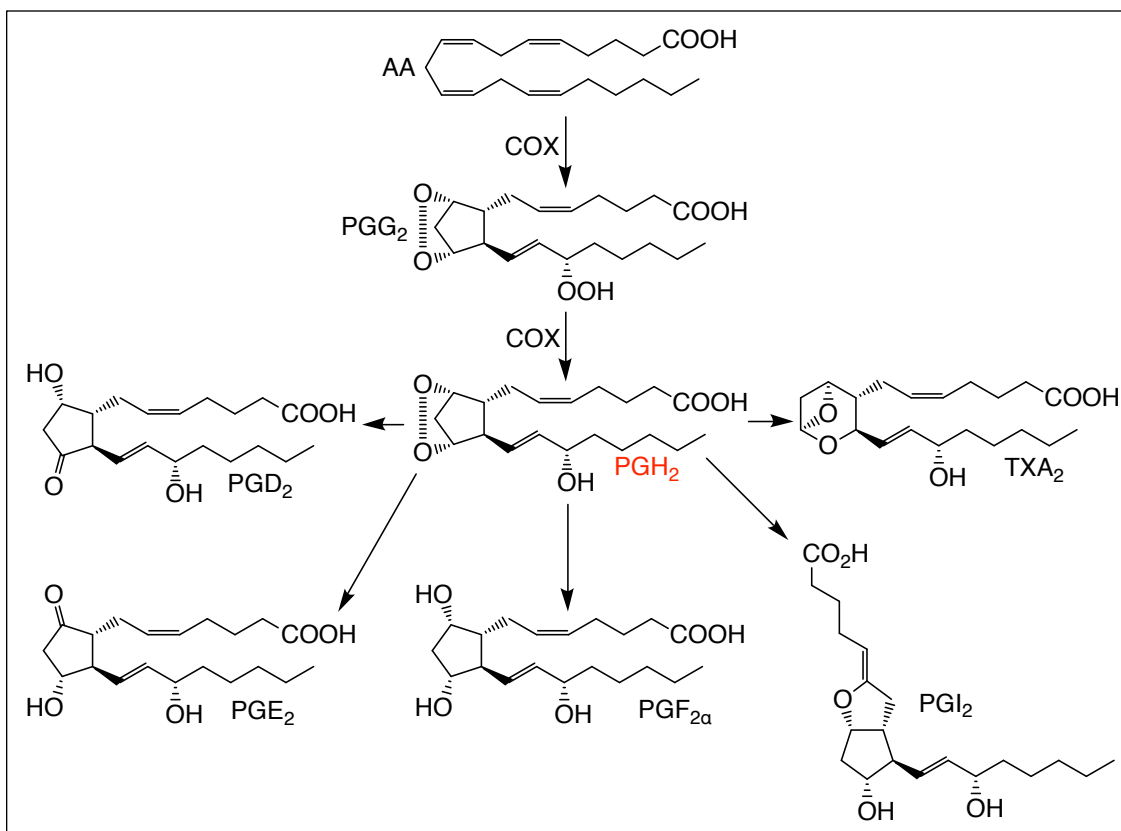


**Figure 4.** The Cyclooxygenase enzymatic pathway. AA is oxygenated to PGG<sub>2</sub>, which is then reduced to PGH<sub>2</sub> by the COX enzymes. PGH<sub>2</sub> is a substrate for various prostanoid synthases, producing PGs, prostacyclin (PGI<sub>2</sub>), and thromboxane.

There are two isoforms of COX, designated COX-1 and COX-2. COX-1 is constitutively expressed in most tissues and maintains homeostatic levels of PGs, which are crucial for normal cardiovascular and gastrointestinal functions. The expression of COX-2, however, is induced in the presence of various pro-inflammatory mediators such as cytokines, growth factors, and tumor promoters (29). Although their expression patterns differ, COX-1 and COX-2 enzymes share 60% sequence identity, and their three-dimensional structures are nearly superimposable (30). Since COX-1 and COX-2 both produce pro-inflammatory PGs, their inhibition has long been investigated through the development of nonsteroidal anti-inflammatory drugs (NSAIDs) including indomethacin, ibuprofen, and aspirin for the treatment of pain, fever, and inflammation (31). Since the expression of COX-2 is associated with the inflammatory response, various drugs were developed to selectively target its inhibition, while maintaining the normal physiological

function of COX-1. These COX-2-selective inhibitors (coxibs) were hypothesized to exploit the anti-inflammatory effects of traditional NSAIDs with fewer side effects. Coxibs such as celecoxib (Celebrex), rofecoxib (Vioxx), and valdecoxib (Bextra) displayed efficacious anti-inflammatory properties and decreased gastrointestinal toxicity. However, chronic use of coxibs in clinical trials of cancer prevention resulted in increased cardiovascular toxicity and the subsequent removal of all drugs of this class with the exception of celecoxib from the U.S. market (32).

### *Cyclooxygenase Mechanism*

The formation of PGs from AA was initially studied using cellular homogenates of ram seminal vesicles. The experiments showed that the radiolabeled AA was converted to radiolabeled PGE<sub>2</sub>, thus indicating fatty acids as biological precursors of PGs (33,34). Additional experiments using stereospecific, isotopically labeled fatty acid substrates indicated that the oxygenation is initiated by removal of the pro-*S* allylic hydrogen from carbon-13 of AA (35). From these studies, it was proposed that a free radical mechanism enables the oxygenation of AA to the hydroperoxy-endoperoxide intermediate PGG<sub>2</sub> followed by reduction of the hydroperoxyl group of PGG<sub>2</sub> by COX to yield PGH<sub>2</sub> (Figure 5). Thus, the enzyme catalyzes both a cyclooxygenase (COX) reaction, yielding PGG<sub>2</sub> and a peroxidase (POX) reaction to produce PGH<sub>2</sub>. The two reactions occur at distinct active sites, both of which are dependent on heme.

Following their expression in cells, the COX enzymes are structurally mature hemoproteins, but must first be activated by a hydroperoxide. To initiate catalysis, a two-electron reduction of the hydroperoxide substrate at the peroxidase active site oxidizes the ferric heme to an oxo-ferryl porphyrin cation radical. Since hydroperoxide activation is required to initiate COX catalysis, the enzyme exhibits a lag phase which complicates kinetic analysis *in vitro* (36). The COX enzyme also experiences self-inactivation before all substrate is consumed, with the process beginning instantaneously and in a concentration- and time-dependent manner (37). The mechanism of COX self-inactivation is not completely understood but could be due to covalent modification of the enzyme from substrate metabolism (38). The

identities of the initial hydroperoxide activator and reducing co-substrate *in vivo* are not known, but evidence suggests peroxynitrite could serve such a role (39).

The oxidized heme cation radical in the POX active site is subsequently reduced by a single electron from Tyr-385, reducing it back to a fully covalent oxy-ferryl protoporphyrin. The oxy-ferryl heme can further be reduced by an electron from a reducing co-substrate to its resting ferric state. The tyrosyl radical generated from Tyr-385 oxidation is close to the pro-*S* hydrogen of carbon-13 of AA bound in the cyclooxygenase active site. Abstraction of this hydrogen generates a radical on carbon-11, initiating the cyclooxygenase reaction. The carbon-centered radical reacts with molecular oxygen, forming an 11 (*R*)-hydroperoxyl radical. The radical then reacts with carbon-9, generating a cyclic endoperoxide with migration of the radical to carbon-8. This radical will then add to carbon-12, forming a new carbon-carbon bond. Eventually, the radical resonates to carbon-15 and reacts with a second molecule of oxygen, forming a hydroperoxyl radical which abstracts the hydrogen atom from Tyr-385 to yield the intermediate PGG<sub>2</sub>. The final step of the catalytic mechanism involves the reduction of the 15-hydroperoxide of PGG<sub>2</sub> to its corresponding alcohol, forming the final PGH<sub>2</sub> product (40). The regenerated tyrosyl radical can continue multiple substrate turnovers without additional peroxide activation.

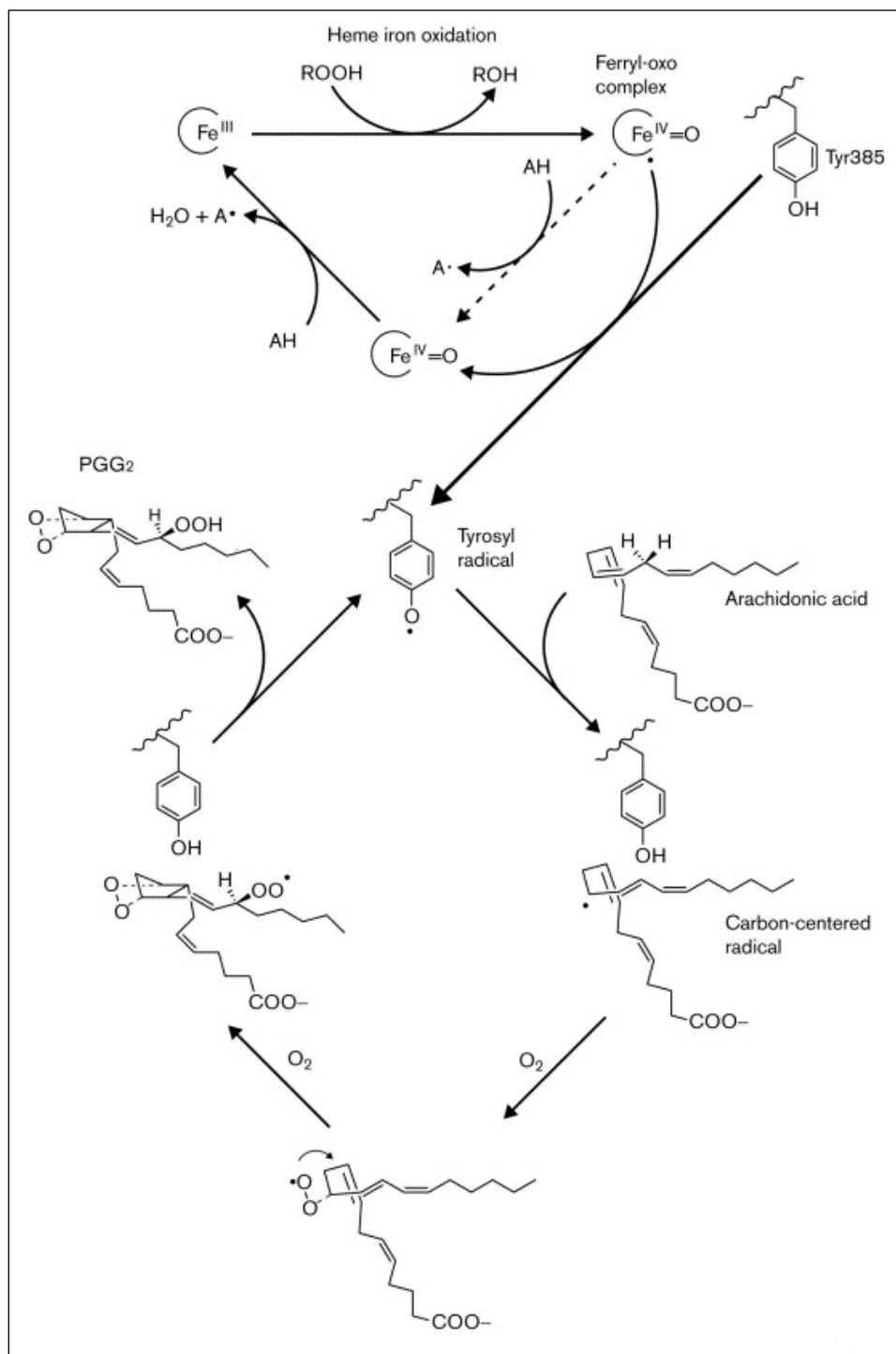


**Figure 5.** Cyclooxygenase catalytic mechanism. The activation of the enzyme by a hydroperoxide oxidizes the heme prosthetic group in the peroxidase site which can then oxidize Tyr-385, generating a tyrosyl radical. The abstraction of the 13-pro-(S)-hydrogen of AA by the tyrosyl radical initiates the branched chain radical mechanism in the cyclooxygenase active site. The reduction of the peroxy radical to form  $\text{PGG}_2$  regenerates the tyrosyl radical for multiple substrate turnovers. Reprinted from *Curr Opin Chem Biol.*, 4(5), Marnett, L.J., Cyclooxygenase mechanisms, 545-552, Copyright 2000, with permission from Elsevier (41).



### *Cyclooxygenase Structure*

Based on immunoelectron microscopy with antibodies specific to each isoform of the COXs, it was discovered that both COX-1 and COX-2 are found on the luminal surfaces of the endoplasmic reticulum (ER) as well as the inner and outer membranes of the nuclear envelope (42). The COX enzymes are homodimers, with COX-1 and COX-2 containing 576 and 581 amino acid residues, respectively, following the cleavage of their N-terminal signal peptides in the ER. Each monomer of approximately 70 kDa contains three distinct domains. Residues 34-72 make up the epidermal growth factor (EGF)-like domain, the function of which is still not fully understood, but most likely stabilizes the catalytic domain of the enzyme through disulfide bond formation. Residues 73-116 serve as a membrane binding domain (MBD), enabling the enzyme to anchor into the hydrophobic lipid bilayer. The remaining bulk of the enzyme consists of the catalytic domain, consisting of the two separate COX and POX active sites, which are separated by the heme prosthetic group (43) (Figure 6A). One heme per COX dimer is sufficient for full catalytic activity, suggesting half-of-sites reactivity (44). The POX site allows sufficient solvent accessibility to the heme to accommodate large alkyl peroxides such as PGG<sub>2</sub> and 15-HPETE. These peroxides have a higher affinity for the POX site and are reduced more efficiently than smaller peroxides such as hydrogen peroxide (45). The COX active site, which lies between the heme of the peroxidase site and the MBD, consists of a hydrophobic channel bent in an L-shaped conformation. The channel originates with a large “lobby” region in the MBD that is demarcated by a constriction formed by three residues, Arg-120, Tyr-355, and Glu-524. These residues form a constriction that must open to allow the entrance of substrates and inhibitors, into the upper portion of the active site (46). Above the constriction, the active site consists of a central channel that forms a near-right angle bend at Ser-530. This critical location of Ser-530 explains why its acetylation by aspirin inhibits PGG<sub>2</sub> formation. AA binds in this channel with the carboxyl group in close proximity to Arg-120 and Tyr-355 at the constriction site, carbon-13 aligned with the catalytic Tyr-385, and the ω-tail deep in the alcove above Ser-530. Tyr-385 is in favorable position to abstract the allylic hydrogen from carbon-13 when AA binds in the active site (Figure 6B). Beyond Tyr-385 and Ser-530, the ω-tail of AA

extends into a hydrophobic upper channel that lies between helices 2 and 17 consisting of residues Phe-205, Phe-209, Phe-210, Val-228, Ile-341, Val-344, Ile-377, Phe-381, and Leu-534 (10). The COX active site terminates at Gly-533. The mutation of Gly-533 to larger hydrophobic residues will not allow for the oxygenation of AA but will allow COX to oxygenate shorter chain fatty acids (46).

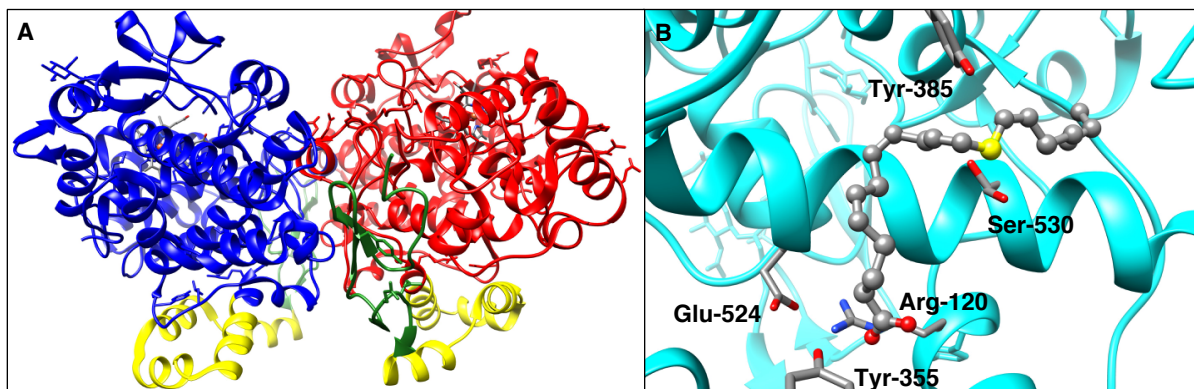


**Figure 6.** COX-2 enzyme structure. (A) The catalytic domains of each monomer, colored in red and blue, form noncovalent interactions at the dimer interface, playing a role in the allostery of the enzyme's activity. The membrane binding domains of both monomers, colored in yellow, anchor the enzyme to the lipid bilayer of the ER lumen. The EGF domain is colored in green. (B) AA in the active site of COX-2 along with residues at the constriction site, Ser-530 at the channel bend, and the catalytic Tyr-385 in close proximity to carbon-13 of AA (yellow). Figures generated from PDB entries 4Z0L and 3KRK (47,48).

### *Cyclooxygenase Isoform Differences*

The formation of PGs from COX-1 is proposed to maintain homeostatic biological functions, whereas the expression of COX-2 and concomitant increase in PG production is associated with an inflammatory or tumorigenic state. Other differences distinguish the isoforms of COX from one another in regard to various biochemical properties. Although both COX-1 and COX-2 oxygenate AA with similar catalytic parameters, COX-2 has been shown to be more sensitive to peroxide activation than COX-1. An approximately 10-fold lower concentration of hydroperoxide is necessary to initiate COX-2 than COX-1 activity, thus explaining the difference in their relative activities in cells with varying peroxide concentrations (49). One of the major biochemical differences between COX-1 and COX-2 is the size of their cyclooxygenase active sites. COX-2 contains a side pocket, consisting of residues Val-434, Arg-513, and Val-523. The corresponding residues in COX-1 are Ile-434, His-513, and Ile-523, thus making its active

site approximately 24% smaller than that of COX-2 (50). The larger volume of the COX-2 active site was exploited for the development of selective COX-2 inhibitors (51). Additional structural differences between the COX isoforms differentiates their ability to oxygenate particular substrates. Arg-120 in COX-1 is critical for binding of AA, but not necessarily for COX-2. If this residue is mutated to Gln in COX-1, the  $K_m$  for AA increases 1000-fold, but the same mutation in COX-2 does not alter the  $K_m$  or  $V_{max}$  for AA (52). Therefore, COX-2 can oxygenate neutral amide and ester derivatives of AA with much higher catalytic efficiency than COX-1. Some of these substrates include the endocannabinoids 2-archidonoylglycerol (2-AG) and arachidonylethanolamide (AEA) (53) (Figure 7). In fact, human and mouse COX-2 oxygenate 2-AG with a comparable catalytic efficiency (54) (Table 1). Both 2-AG and AEA are endogenous agonists for the CB<sub>1</sub> and CB<sub>2</sub> receptors which are also modulated by  $\Delta^9$ - tetrahydrocannabinol (THC), the psychoactive compound of the cannabis plant (55,56). COX-2 has also been shown to oxygenate additional amide substrates that COX-1 cannot. One such substrate is the lipoamino acid N-arachidonylglycine (NAGly), which possesses analgesic effects and suppresses inflammatory pain (57). COX-1 and COX-2 also differ in their ability to oxygenate other fatty acids with varying degrees of chain length and saturation including linoleic acid,  $\gamma$ -linolenic acid ( $\gamma$ -LNA), and  $\alpha$ -linoleic acid (58). One last difference between the COX isoforms is product formation following covalent acetylation by aspirin. The acetylation of Ser-530 of COX-1 completely inhibits substrate oxygenation. However, aspirin-mediated acetylation of COX-2 still allows the oxygenation of AA to form 15-HETE and 11-HETE, essentially transforming the enzyme to a lipoxygenase (59).

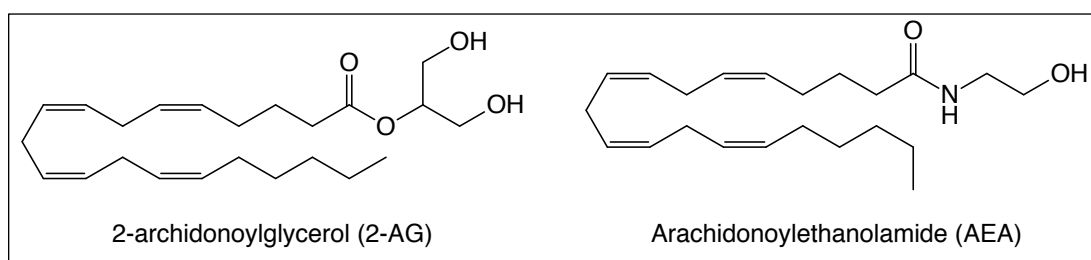


**Figure 7.** Additional COX-2 substrates, the endocannabinoids 2-AG and AEA. COX-2 oxygenates these substrates to prostaglandin glyceryl esters (PGGs) and prostaglandin ethanolamides (prostamides).

**Table 1.** Steady-state kinetic parameters for COX-2 isoforms in the presence of various substrates. Table was generated from from *Biochem Biophys Res Commun.*, 338(1), Rouzer, C.A. and Marnett, L.J., Structural and functional differences between cyclooxygenases: fatty acid oxygenases with a critical role in cell signaling, 34-44, Copyright (2005), with permission from Elsevier (60).

	$k_{cat}$ (s <sup>-1</sup> )	$K_M$ (μM)	$k_{cat}/K_M$ (s <sup>-1</sup> μM <sup>-1</sup> )
<b>Human COX-2</b>			
AA	15 ± 1	6.1 ± 0.6	2.4
2-AG	17 ± 1	4.4 ± 0.9	4.0
<b>Murine COX-2</b>			
AA	21 ± 2	8.2 ± 1.6	2.5
2-AG	11 ± 1	4.7 ± 0.8	2.3
AEA	0.1	24	0.0042
NAGly	6.3 ± 1.1	12 ± 1	0.54

#### *Cyclooxygenase Functions as a Heterodimer*

Each subunit of the COX enzyme dimer is structurally identical to the other with which it forms a series of non-covalent interactions at the dimer interface. Despite this structural identity, the monomers exhibit varying affinities for binding heme (44). The COX dimer binds one heme cofactor with high affinity in one monomer, which acts as the catalytic subunit. The opposite monomer binds heme with much lower affinity, and substantial data suggest that it allosterically regulates the activity of the catalytic monomer. Therefore, current kinetic and mutagenic data suggest that the enzyme functions as a heterodimeric enzyme (61). For example, COX-2 heterodimers that were expressed and purified with one native subunit and one subunit with a Y385F mutation displayed similar kinetic parameters as the COX-2 heterodimer with two native subunits. In fact, the heme cofactor was shown to bind with even higher affinity to the native subunit in the presence of the Y385F mutant subunit (62). Substrate oxygenation in the catalytic subunit of the COX heterodimer is modulated by occupancy of various compounds in the allosteric subunit. Many nonsubstrate fatty acids preferentially bind to the allosteric subunit and can stimulate the oxygenation of AA. Specifically, palmitic acid (PA) is an efficacious activator of the enzyme, increasing the catalytic conversion of AA to PGH<sub>2</sub> by approximately 80% (61). In other instances, nonsubstrate fatty acids can

significantly affect the oxygenation of a particular substrate. An example is the potentiation of 2-AG oxygenation by the nonsubstrate AA derivative, AM-8138 (13(*S*)-methylarachidonic acid). Upon binding in the COX-2 allosteric site, 2-AG oxygenation is increased approximately 3.5-fold, whereas AA oxygenation is unchanged (63). In addition to nonsubstrate molecules, COX substrates exert allosteric regulation of one another. Mitchener, et al. demonstrated that AA inhibits 2-AG oxygenation in a concentration-dependent manner, whereas 2-AG mildly stimulates AA oxygenation. This complex interplay between the COX substrates using a kinetic modeling system demonstrated that competition of AA and 2-AG substrates in both allosteric and catalytic subunits ultimately results in a preferential oxygenation of AA (64).

Despite the presence of over 70 X-ray crystal structures of COX-1 or COX-2 in complex with various substrates or inhibitors in the Protein Data Bank (PDB), the basis for the interaction between the catalytic and allosteric subunits of COX is still not fully understood. In nearly all crystal structures, both monomers of the enzyme are fully occupied with substrate or inhibitor, even when crystallized with substoichiometric amounts of ligand. Therefore, the enzyme preferentially crystallizes in a fully occupied form. Furthermore, few structural differences are noted either in the active site or at the dimer interface between liganded and apo-enzyme (65). In one experiment, COX-1 was crystallized with various NSAIDs and changes were observed in the occupancy of particular amino acid residues in a partially occupied subunit. In cases where one monomer of the enzyme was bound to an inhibitor and the other monomer was incompletely occupied, a loop region at the dimer interface consisting of residues 123-129 was observed in an alternate conformation. Based on this structural variation as well as previous cross-linking experiments demonstrate that this loop region could be involved in monomer cross-talk and could potentially affect interactions between each subunit (65).

### *Molecular Basis of COX Inhibition*

Numerous NSAIDs that nonselectively inhibit the activity of both COX-1 and COX-2 and coxibs that selectively inhibit COX-2 have been developed (66) (Figure 8). Inhibitors of the COX enzymes bind

in the COX active site in a noncovalent manner, with the exception of aspirin and 2-acetoxyphenylhept-2-ynyl sulfide (APHS), which transfer an acetyl group to Ser-530, or selectively to COX-2, respectively (31,67,68). The time-dependence of COX inhibition by aspirin, first described in 1971, was discovered to be due to acetylation of the active site Ser-530 residue (69). Mutating Tyr-385 to Phe is detrimental to aspirin acetylation of COX (70), suggesting that this residue plays a role in the reaction. Data suggest that Tyr-385 acts as a hydrogen bond donor to aspirin's acetyl group, thus stabilizing the tetrahedral intermediate formed during the reaction. Although aspirin acetylates both isoforms, it is between 10- and 100-fold more potent for acetylating COX-1 than COX-2 (71).

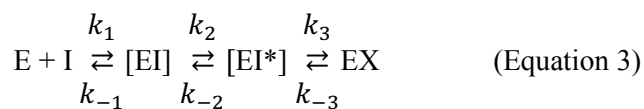
Most noncovalent NSAIDs and coxibs are generally classified as either rapidly reversible, competitive inhibitors or slow, tight-binding inhibitors. Rome and Lands described a kinetic model for time-dependent noncovalent COX inhibition using various inhibitors. Their data indicated that the kinetics of COX inhibition by the NSAIDs ibuprofen and mefenamic acid were consistent with the classical model of rapidly reversible competitive inhibition. In contrast, flurbiprofen and meclofenamic acid displayed time-dependent inhibition that became functionally irreversible, indicative of a two-step binding mechanism consisting of an initial rapid, reversible binding step of the inhibitor to the enzyme, followed by an essentially irreversible, time-dependent formation of the inhibitor-enzyme complex (72). For this two-step binding, a kinetic model was developed, where the initial inhibitor enzyme complex binding is represented by a dissociation constant ( $K_1$ ), followed by the functionally irreversible tight-binding step represented by the rate constant  $k_{inact}$  as seen in Equation 1:

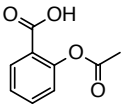
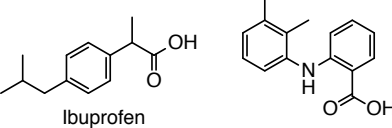
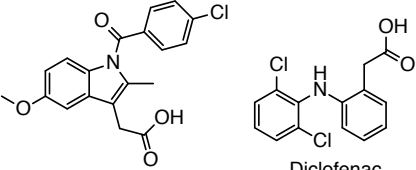
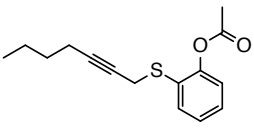
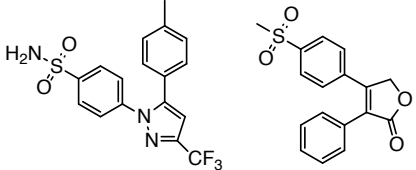


Following the initial kinetic description of COX inhibitor binding mechanisms, additional inhibitors were investigated, with most NSAIDs, like diclofenac and indomethacin, exhibiting a two-step binding mechanism (Equation 2):



Or a three-step binding mechanism as observed for COX-2 selective diarylheterocycles such as celecoxib (Equation 3):



	Covalent Inhibitors	Non-Covalent Inhibitors
Non-Selective Inhibitors	 Aspirin	<p><u>Rapid, reversible inhibitors (one step)</u></p>  Ibuprofen      Mefenamic Acid
		<p><u>Slow, tight-binding inhibitors (two step)</u></p>  Indomethacin      Diclofenac
COX-2 Selective Inhibitors	 APHS	<p><u>Slow, tight-binding inhibitors (three step)</u></p>  Celecoxib      Rofecoxib

**Figure 8.** Chemical structures of COX inhibitors.

Like the AA substrate, many NSAIDs contain a carboxylic acid moiety that forms noncovalent polar interactions with the COX enzymes. Multiple crystal structures of enzyme-inhibitor complexes in addition to site-directed mutagenesis studies have given further insight into the molecular basis of COX inhibition.

Residues at the constriction site form noncovalent interactions with many NSAIDs, most commonly with the carboxylate ion pairing with Arg-120 and/or forming a hydrogen bond with Tyr-355. Some time-dependent NSAIDs containing carboxylates like flurbiprofen and indomethacin form ion pairs with Arg-120 in COX-1. This interaction is crucial for their inhibition as mutation of Arg-120 to Glu eliminates their inhibitor effects (73). In COX-2 however, the mutation of Arg-120 does not abolish inhibition by indomethacin. Additional studies utilizing a methyl ester analogue of indomethacin revealed that binding to COX-1 became time-independent and that the carboxylate was required for its tight binding to the enzyme (72). For COX-2 inhibition, the methyl ester of indomethacin does not eliminate its time-dependence, but the inhibitor does bind to the enzyme with lower affinity (74,75). A crystal structure of COX-2 in complex with indomethacin shows that in addition to ion pairing to Arg-120, additional contacts are made with Tyr-355 at the constriction site, the chlorine atom interacts with Leu-384 at the top of the active site, and the 2'-methyl group projects into a hydrophobic pocket formed by the residues Val-349, Ala-527, Ser-530, and Leu-531 (51). A 2'-*des*-methyl analogue is a rapid, reversible inhibitor of COX-2 and, to some extent, of COX-1 (76). However, substituting the 2'-methyl group to a larger trifluoromethyl group produces a tight-binding inhibitor that is selective for COX-2 inhibition (77). Therefore, binding of the 2'-methyl group of indomethacin in the hydrophobic pocket is a crucial property for its time-dependent inhibition of COX. Mutating Arg-120 to Gln also decreases the potency of indomethacin and the trifluoromethyl analogue, indicating that both ion-pairing and hydrogen bonding interactions are important for these inhibitors (77).

In addition to Arg-120, the hydroxyl group of Tyr-355 is in favorable binding distance to the carboxylate of some NSAIDs (78). Tyr-355 has been found to have a determinant role in the enantiospecific inhibition of AA oxygenation by COX in the presence of 2-propionic acid inhibitors like flurbiprofen and ibuprofen. The (*S*)-enantiomer of flurbiprofen exhibits potent inhibition of AA oxygenation in the presence of wild-type enzyme, but the (*R*)-enantiomer is a poor inhibitor. However, the (*R*)-enantiomer of flurbiprofen has similar IC<sub>50</sub> values in the presence of wild-type enzyme and a Y355F mutant (79). The Y355F mutation also decreases the transition state energy of the slow-binding inhibition step for



flurbiprofen and indomethacin, thus indicating Tyr-355 is involved in the molecular mechanism of time-dependent inhibition for these inhibitors (80).

Other carboxylate-containing NSAIDs display either one- or two-step binding mechanisms but bind in the COX active site in a different orientation. Like indomethacin, diclofenac is a slow, tight-binding inhibitor of COX. However, the mutation of either Arg-120 to Ala or Tyr-355 to Phe does not affect the inhibitory potency of diclofenac. The crystal structure shows that diclofenac binds in the COX active site in an “inverted” orientation (Figure 9). Its carboxylate makes no contacts with Arg-120 or Tyr-355, but it does form hydrogen bonds with Tyr-385 and Ser-530 (81). Mutating Ser-530 to Ala is detrimental to diclofenac inhibition ( $IC_{50} > 50 \mu\text{M}$ ) and a Ser-530-Met mutation resulted in a 240-fold increase in the  $IC_{50}$  value for diclofenac relative to that of the wild-type enzyme (82). The selective COX-2 inhibitor lumiracoxib is a rapid, reversible inhibitor of AA oxygenation that also binds in an inverted orientation with its carboxylate forming hydrogen bonds with Tyr-385 and Ser-530. Mutating Ser-530 to Ala abolishes sensitivity to lumiracoxib inhibition (83). Lumiracoxib also contains a 5'-methyl group that clashes with the side chain of Leu-384 of COX-1, suggesting a mechanism for its selectivity of COX-2 inhibition over COX-1 (84).

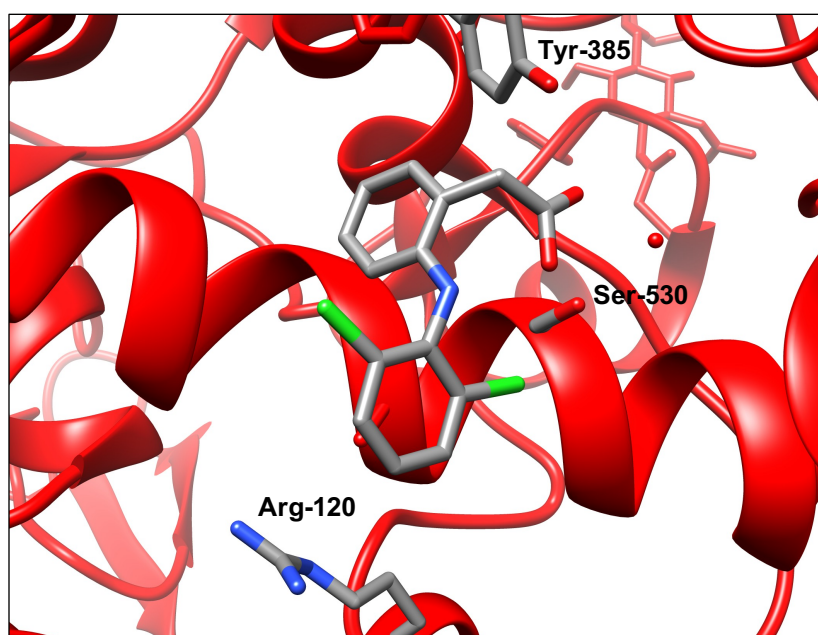


**Figure 9.** Crystal structure of diclofenac bound to active site of mCOX-2 (PDB: 1PXX).

Many of the coxibs designed to selectively inhibit COX-2 are of the diarylheterocycle class, consisting of inhibitors such as celecoxib, rofecoxib, valdecoxib, and etoricoxib. Celecoxib was evaluated for its ability to inhibit COX-1 and was found to exhibit competitive, reversible kinetics (85). For COX-2 inhibition, an initial competitive interaction is observed, followed by a time-dependent mechanism, forming a tight enzyme-inhibitor complex. Upon further investigation, it was determined that celecoxib actually binds to COX-2 in a three-step mechanism, with the final two steps being kinetically distinct based on the magnitudes of their rate constants (86). In comparing the sequences of COX-1 and COX-2, the only difference within in the central channel of the COX-2 active site not conserved in COX-1 is a Val-523 residue. If this residue is mutated to Ile in human COX-2, the coxibs lose their time-dependence of inhibition and the selectivity of the inhibitors for COX-2 is abolished, whereas NSAIDs like indomethacin show no difference in regard to their selectivity. The crystal structure of COX-2 in complex with a celecoxib analogue shows that its sulfonamide group binds in the side pocket of the active site next to Val-523. Thus, the insertion of the sulfonamide or methylsulfonyl groups of coxibs past Val-523 in the COX-2 active site dictates their time-dependent step for inhibition (51).

Time-dependence of COX-2 inhibition is also dependent on peripheral residues which are not part of the active site where NSAIDs bind. In COX-2, a Val-89 residue lies in a space in the lobby just outside of the active site, between helices B and D. Mutating this residue to a bulkier Trp residue reduced the size of the entrance into the active site from the lobby region. The mutation of adjacent His-90 residue to Trp further reduced the size of the entrance to a proposed alternative route for substrates and inhibitors to enter the active site. The increased steric bulk from these mutations transformed the kinetic behavior of rapid, reversible inhibitors of COX-2 such as ibuprofen and mefenamic acid into slow, tight-binding inhibitors. Single mutant studies and crystal structures indicated that Val-89 is the residue primarily responsible for the shift in inhibitor time-dependence and its mutation to a bulkier residue remodels the structure of the lobby route channel (87).

### *Substrate-selective Inhibition of COX*

Both the potency and the time-dependence of some COX inhibitors vary substantially depending on the substrate being utilized. The initial experiments describing COX inhibition by ibuprofen and mefenamic acid were based on the conversion of AA to PGs. Later experiments, however, revealed that these inhibitors display “substrate-selective” properties. Although both ibuprofen and mefenamic acid are weak, competitive inhibitors of AA oxygenation, they are potent, noncompetitive inhibitors of endocannabinoid oxygenation by COX-2. Based on these observations, it was proposed that binding of one molecule of each inhibitor in the allosteric subunit is sufficient to prevent the oxygenation of the endocannabinoid substrate in the catalytic subunit, thus preventing its oxygenation. However, a single inhibitor molecule in the allosteric subunit still allows AA oxygenation, and much higher concentrations of inhibitor are necessary to compete AA out of the catalytic site to prevent its oxygenation (88). This result thus reemphasizes the importance of the cross-talk between the monomers of the COX enzyme and the demonstrates how the presence of a compound in the allosteric subunit can affect the oxygenation of substrates in the catalytic subunit, especially for the endocannabinoids in the presence of COX-2.

Additional experiments investigated the substrate-selectivity of weak, reversible inhibitors as well as slow, tight-binding inhibitors. A particular class of NSAIDs, the propionic acids, display enantiospecificity for inhibiting the oxygenation of AA by the COX enzymes. As noted above, the (*S*)-enantiomers of these inhibitors including ibuprofen, flurbiprofen, and naproxen prevent the oxygenation of AA, but the (*R*)-enantiomers are poor inhibitors. With regard to 2-AG oxygenation, the weak, reversible inhibitors, including the (*R*)-propionic acids, are also potent inhibitors. Initial studies with site-directed mutagenesis and structure-activity relationships suggested that unfavorable binding of the (*R*)-propionic acids in the active site was due to steric clash between the inhibitor  $\alpha$ -methyl group and Tyr-355 (79). However, the crystal structure of COX-2 and (*R*)-naproxen revealed that the constriction site residues that form interactions with the inhibitor, Arg-120 and Tyr-355, can reposition themselves to sterically accommodate the  $\alpha$ -methyl group for favorable binding in the active site. Furthermore, Arg-120 is crucial

for binding of (*R*)-flurbiprofen to the enzyme, as mutation of Arg-120 to Gln eliminates inhibition (Figure 10). Thus, the binding of the (*R*)-propionic acids in the allosteric subunit of COX-2 likely induces a conformational change in the catalytic site, preventing the oxygenation of endocannabinoids (89).

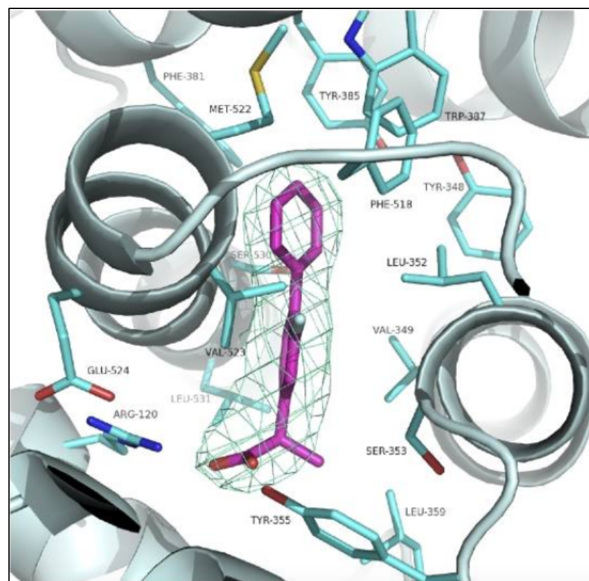


**Figure 10.** Crystal structure of (*R*)-flurbiprofen in the COX-2 active site. Ion-pairing of the inhibitor with Arg-120 is critical for its binding. Reprinted from *Nat Chem Biol.*, 7(11), Duggan, K., (*R*) Profens Are Substrate-Selective Inhibitors of Endocannabinoid Oxygenation by COX-2, 803-809, Copyright 2011, with permission from Nature America Inc. (89).

In addition to mefenamic acid, other fenamic acid inhibitors have been tested for their ability to inhibit COX activity in a substrate-selective manner. These inhibitors, including flufenamic acid, meclofenamic acid, and tolfenamic acid, are structurally similar to phenyl acetic acid NSAIDs such as diclofenac and lumiracoxib. Unlike many NSAIDs, the fenamates are observed to bind in the COX active site in an inverted orientation with their carboxylic acid moieties forming interactions with Tyr-385 and Ser-530 (Figure 11). Based on this observation and spectroscopic studies, it was found that the fenamates can quench the radical formed at the catalytic tyrosine and reduce the heme cofactor back to its resting state, essentially resetting the enzyme and requiring additional turnover of peroxide to continue substrate oxygenation. Endocannabinoid oxygenation requires higher concentrations of peroxide in comparison to

AA oxygenation (90). Therefore, the substrate-selectivity of these inhibitors may be, at least in part, dependent on the peroxide tone associated with their interactions with the enzyme active site (91).

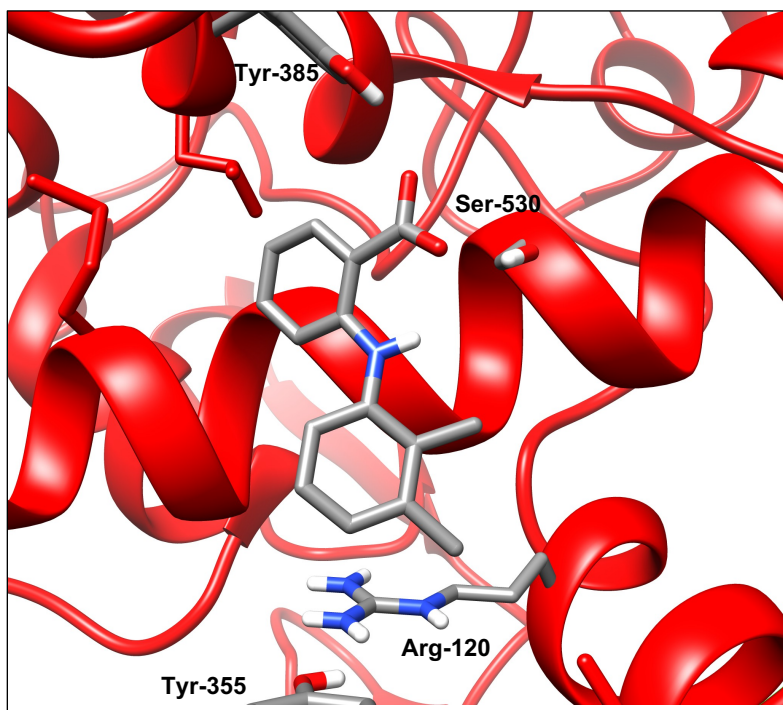


**Figure 11.** Crystal structure of mefenamic acid in the COX-2 active site. The inhibitor binds in an inverted orientation relative to many other NSAIDs, with its carboxylate group forming interactions with Tyr-385 and Ser-530. Figure generated from PDB 5IKR (91).

## Prostaglandin Isomerization

As described above, COX oxygenation of AA produces the product  $\text{PGH}_2$ . *In vivo*,  $\text{PGH}_2$  spontaneously decomposes into the prostanoids  $\text{PGD}_2$  and  $\text{PGE}_2$  with a half-life of approximately 90 – 100 seconds (92).  $\text{PGH}_2$  can also be enzymatically isomerized to various PGs,  $\text{PGI}_2$ , and  $\text{TXA}_2$  by various synthases. These prostanoids exhibit various biochemical processes by binding to their respective G protein-coupled receptors (GPCRs). Here, we focus on one of the isomerases that produced  $\text{PGE}_2$ .

### *PGE Synthase*

$\text{PGE}_2$  is a PG consisting of a cyclopentane nucleus bearing a keto group at carbon-9 and a hydroxyl group at carbon-11. It is isomerized from  $\text{PGH}_2$  by three separate PGE synthases (Figure 12), including cytosolic  $\text{PGE}_2$  synthase (CPGES), microsomal  $\text{PGE}_2$  synthase-1 (mPGES-1), and microsomal  $\text{PGE}_2$  synthase-2 (mPGES-2) (93).

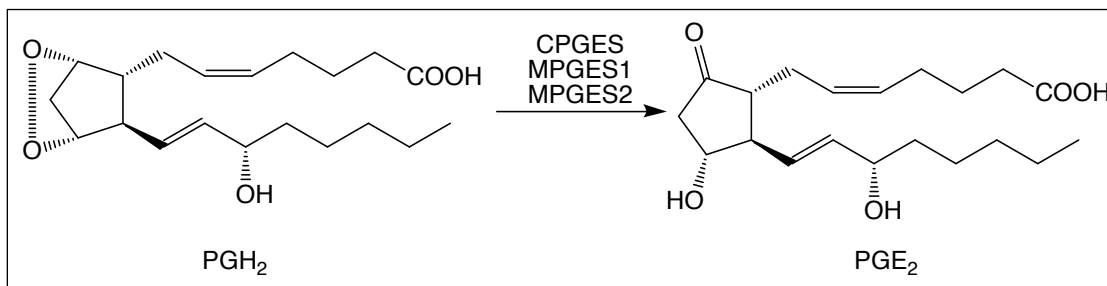


**Figure 12.**  $\text{PGH}_2$  isomerization to  $\text{PGE}_2$  by the PGE synthases.

As a member of the cytosolic glutathione *S*-transferase (GST) superfamily of enzymes, CPGES is a glutathione-dependent enzyme that is also identical to p23, a heat-shock protein 90 (HSP90)-binding protein (94). The enzyme is expressed in a wide variety of cells and tissues and preferentially isomerizes  $\text{PGH}_2$  that is derived from COX-1. Therefore, CPGES is believed to be functionally coupled to COX-1 to maintain homeostatic production of  $\text{PGE}_2$  in cells (95).

mPGES-2 was initially determined to be a membrane-bound enzyme containing both heme and GSH in its active site, and it was believed to catalyze  $\text{PGH}_2$  degradation to 12*L*-hydroxy-5,8,10-

heptadecatrienoic acid (12-HHT) (96). A subsequent study demonstrated that mPGES-2 isomerizes PGH<sub>2</sub> to PGE<sub>2</sub>. Furthermore, it was proposed that the enzyme was activated by a variety of compounds containing sulfhydryl groups in addition to GSH, including dihydrolipoic acid and dithiothreitol (DTT), and that heme was not involved in the enzymatic reaction (97). In order to clarify the role of heme, absorption and fluorescence experiments were utilized to investigate the heme association/dissociation with the enzyme. From these studies, it was determined that heme only binds to the enzyme in the presence of GSH. A low dissociation constant indicated that the heme binds tightly to the enzyme, but it can be dissociated by exposure to DTT, which produces heme-free enzyme that has the ability to isomerize PGH<sub>2</sub> to PGE<sub>2</sub> (98). mPGES-2 is constitutively expressed and isomerizes PGH<sub>2</sub> derived from both COX-1 and COX-2, thus making its physiological relevance less well understood (99).

#### mPGES-1

##### *MAPEG Proteins*

mPGES-1 is a member of the membrane-associated proteins in eicosanoid and glutathione metabolism (MAPEG). This family of enzymes includes several nonmammalian members and six mammalian members that can be divided into four subgroups based on their sequence alignments. Group I contains microsomal GSH transferase (MGST) 2, FLAP, and LTC<sub>4</sub>S. Group II contains only MGST3. Group III contains bacterial MAPEG members, and finally, group IV consists of MGST1 and mPGES-1 (100). Based on sequence alignments and hydropathy plots, it was predicted that the MAPEG proteins are composed of membrane-spanning helices (101). Initially, the structures of MGST1 and mPGES-1 were solved utilizing electron microscopy of two-dimensional crystals (102,103). Concurrently, X-ray crystal structures were obtained for LTC<sub>4</sub>S and FLAP (104,105). These structures revealed that the MAPEG proteins share similar characteristics; all are homotrimers of subunits that each comprise four transmembrane (TM) helices. Additionally, a molecule of GSH binds at the interface of adjacent subunits in each of the proteins with the exception of FLAP, which has not been shown to bind GSH (106).

The MAPEG proteins carry out various biological processes, including the catalytic production of PGE<sub>2</sub> and LTs, as well as the conjugation of GSH to various electrophiles for the purpose of excreting potentially toxic compounds. MGST1 can catalyze the nucleophilic substitution of GSH to the substrate 1-chloro-2,4-dinitrobenzene (CDNB) with the formation of a thiolate anion being a rate-determining step in enzyme turnover (107). MGST1 can also catalyze the conjugation of GSH to LTA<sub>4</sub> to form LTC<sub>4</sub>, the same enzymatic function as LTC4S (108). MGST2 has similar biochemical functions to those of MGST1, including the conjugation of GSH to electrophilic xenobiotics as well as to LTA<sub>4</sub>, although with reduced efficiency (109). MGST3 is unable to catalyze the conjugation of GSH to CDNB but can conjugate GSH to LTA<sub>4</sub> to form LTC<sub>4</sub>. Furthermore, both MGST2 and MGST3 exhibit GSH-dependent peroxidase activity by reducing 5-HPETE to 5-HETE (110). FLAP is the only mammalian member of the MAPEG family that does not bind GSH and utilize it as cofactor. In fact, FLAP technically does not have any known enzymatic activity. It was discovered by observing that an inhibitor, MK-886, inhibited the synthesis of LTA<sub>4</sub> in whole human leukocytes but not by purified 5-LOX (111). Eventually, the molecular target of a radio-labeled analogue of MK-886 was identified as FLAP, which is necessary for LT biosynthesis by 5-LOX in intact cells (112).

#### *mPGES-1*

As noted above, mPGES-1 is MAPEG protein that is most closely related to MGST1, with 38% sequence identity (113). mPGES-1 is a GSH-dependent membrane-bound enzyme, and its expression is induced by pro-inflammatory cytokines and growth factors such as bacterial lipopolysaccharide (LPS), interleukin-1 $\beta$  (IL-1 $\beta$ ), and tumor necrosis factor- $\alpha$  (TNF- $\alpha$ ) (114). It is also co-localized with COX-2 in the perinuclear membrane and the ER. This coupled localization is associated with the induced production of PGE<sub>2</sub> (115).



### *mPGES-1 Function*

mPGES-1 catalyzes the isomerization of PGH<sub>2</sub> to PGE<sub>2</sub>; the former is derived primarily from COX-2. mPGES-1 can also utilize PGG<sub>2</sub>, the intermediate from the COX reaction, as an alternative substrate with similar kinetic parameters (Table 2). From the initial characterization of the enzyme, its catalytic efficiency of PGH<sub>2</sub> turnover was found to be 310 mM<sup>-1</sup> s<sup>-1</sup>. Like MGST1, mPGES-1 can also catalyze the nucleophilic addition of GSH to CDNB, albeit at the relatively low specific activity of 0.8 μmol min<sup>-1</sup> mg<sup>-1</sup> (116). mPGES-1 can also reduce 5-HPETE with a specific activity of 0.043 μmol min<sup>-1</sup> mg<sup>-1</sup>. The latter alternative enzymatic activities of mPGES-1 are less efficient than those of other GSTs. Thus, these are most likely not relevant biological functions for mPGES-1 *in vivo*, but they do highlight the evolutionary similarity between the enzymes within the MAPEG family (116).

**Table 2.** Steady-state kinetic parameters for human mPGES-1 in the presence of various substrates. Table was generated from in *J Biol Chem.*, 278(25), Thorén, S. Human microsomal prostaglandin E synthase-1: purification, functional characterization, and projection structure determination. 22199-209, Copyright 2003 (116).

Substrate	$k_{\text{cat}}$ (s <sup>-1</sup> )	$K_M$ (mM)	$k_{\text{cat}}/K_M$ (s <sup>-1</sup> M <sup>-1</sup> )
PGG <sub>2</sub>	75 ± 4	0.160 ± 0.03	470 x 10 <sup>3</sup>
PGH <sub>2</sub>	50 ± 6	0.160 ± 0.04	310 x 10 <sup>3</sup>
GSH	21 ± 1	0.71 ± 0.2	30 x 10 <sup>3</sup>

mPGES-1, in conjunction with COX-2, causes a substantial increase in the formation of PGE<sub>2</sub> under pro-inflammatory conditions. PGE<sub>2</sub> is a key mediator of the inflammatory response in the cardiovascular system. All clinical hallmarks of inflammation including rubor (redness), tumor (swelling), dolor (pain), and fever are promoted by its cellular effects (117). PGE<sub>2</sub> is an unstable compound in the circulatory system. After only 1.5 min following intravenous injection, less than 5% of PGE<sub>2</sub> remains in the circulation due to its rapid metabolism to other compounds (118). It is converted *in vivo* primarily to its inactive metabolite 13,14-dihydro-15-keto PGE<sub>2</sub> by the enzyme 15-hydroxyprostaglandin dehydrogenase (15-PGDH) (119). Prior to its metabolism, PGE<sub>2</sub> is a potent lipid mediator. Its biochemical effects are initiated by binding to

one of four GPCRs, or type E prostanoid receptors (EP 1-4). Although an increase of PGE<sub>2</sub> is associated with pain and fever in an inflammatory state, it also exhibits anti-inflammatory and pro-resolving properties under some conditions *in vivo*. In the late phase of inflammation, PGE<sub>2</sub> suppresses the biosynthesis of pro-inflammatory mediators like TNF- $\alpha$  and IL-1 $\beta$ , while inducing the formation of anti-inflammatory resolvins and protectins (120). Furthermore, PGE<sub>2</sub> regulates renal blood flow, protects the gastrointestinal tract, and promotes wound healing (121). The contrasting biological effects from PGE<sub>2</sub> are the result of tissue-specific downstream signaling effects from each EP receptor as well as the dual function of individual receptors. Specifically, the EP4 receptor mediates pro-inflammatory processes in diseases like arthritis and also promotes tumor progression in cancers. Yet, the same receptor is involved in kidney development and wound healing, and it contributes to protective processes in the cardiovascular system (122).

#### *mPGES-1 Structure*

The first crystal structure of mPGES-1 with GSH bound was determined by electron diffraction of two-dimensional crystals to 3.5 Å (103). Later, in 2013, a 1.2 Å X-ray crystallographic three-dimensional structure was solved, providing greater molecular detail about the enzyme (123) (Figure 13A). Like the other MAPEG proteins, mPGES-1 is a homotrimer, consisting of monomers that contain four TMs each. Each monomer is stabilized by a group of polar residues, including Lys-26, Asn-74, Asp-75, Arg-110, and Thr-114 that are bridged by two water molecules, connecting TMs I, II, and III. An ~15 Å deep cavity formed from N-terminal portions of TMs II and IV and the C-terminus of TM I from one monomer and the cytoplasmic domain of the adjacent monomer is found at each monomer interface. A GSH molecule is bound in a U-shaped conformation in this pocket, forming hydrogen bonds to the side chains of residues Arg-73, Asn-74, Glu-77, His-113, Tyr-117, Arg-126, and Ser-127 from TMs II and IV and the Arg-38 side chain from TM I (Figure 13B). GSH is an essential cofactor for the stability and catalysis of mPGES-1. However, molecular simulations and hybridization experiments determined that only one GSH cofactor can bind to one of the pockets and form an active complex at any given time. Therefore, mPGES-1 exhibits one-third-of-sites reactivity (124). In each monomer, there is an insert consisting of 20 amino acids between

TMs I and II that forms a small positively charged domain (the C-domain), forming part of the active site. This is one prominent feature that illustrates the structural diversity observed within the MAPEG family, as this extra domain is not observed in other members. The space between the active site and the central cavity is blocked by an Arg-73 residue, which is observed to possess two discrete conformations. In one conformation, the residue coordinates to a carboxylate group of GSH and results in a separation of the cavities. In the alternate conformation, the residue interacts with the carbonyl group of the Leu-69 residue of an adjacent molecule and the solvent within the central cavity.

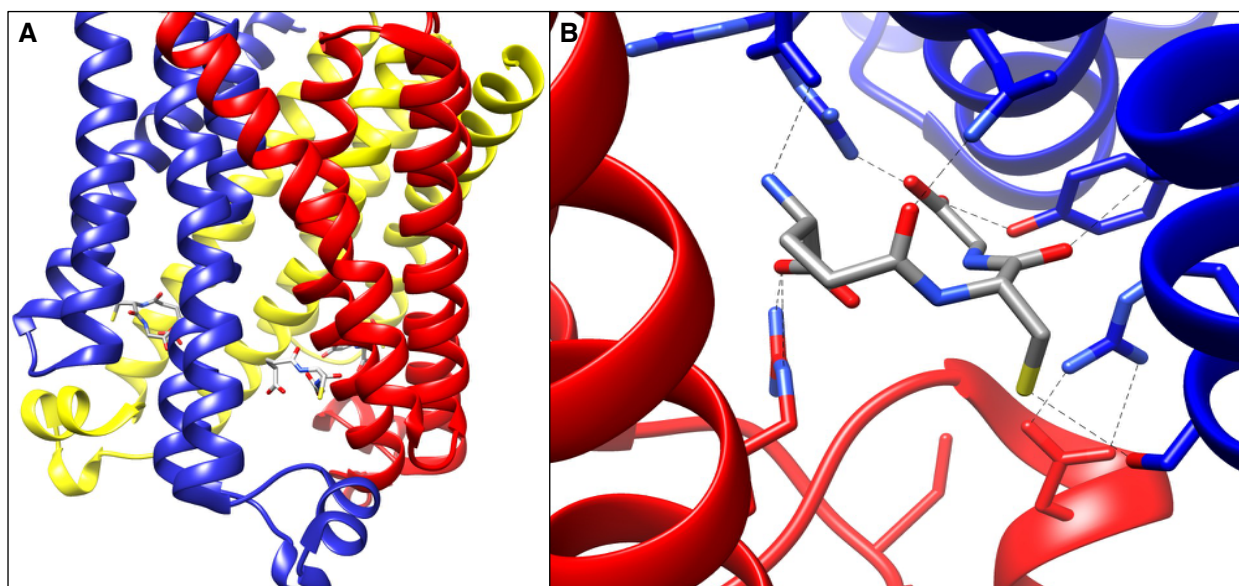


**Figure 13.** mPGES-1 crystal structure. (A) Each subunit of mPGES-1 containing four transmembrane helices is shown in blue, red, or yellow. At the interface of each subunit, the glutathione (GSH) cofactor forms noncovalent interactions and stabilizes the enzyme structure. (B) The active site of mPGES-1 with GSH. The thiolate (yellow) is in close proximity to Ser-127. Figure generated from PDB 4AL0 (123).

#### *mPGES-1 Mechanism*

Based on the high resolution, three-dimensional structure of the mPGES-1 enzyme from 2013, a mechanism of PGH<sub>2</sub> isomerization to PGE<sub>2</sub> was proposed. The structural data indicated that the hydroxyl group of Ser-127 is responsible for the formation and stabilization of the glutathione thiolate which exerts a nucleophilic attack on the oxygen atom at carbon-9 of the PGH<sub>2</sub> endoperoxide (123). Initially, it was thought that a highly conserved arginine residue was responsible for stabilizing the glutathione thiolate in

all members of the MAPEG family. The corresponding arginine residue, Arg-104 is necessary for forming the thiolate within the active site of LTC4S, initiating its conjugation to LTA<sub>4</sub> (125). Further investigation of the mPGES-1 chemical mechanism utilized structural dynamic analysis combined with site-directed mutagenesis and activity assays to determine that the isomerization of PGH<sub>2</sub> proceeded differently than hypothesized, and a new mechanism was proposed (Figure 14). From the structural refinement of the mPGES-1 crystal structure, it was determined that a crystallographic water is present in the active site (Figure 15).

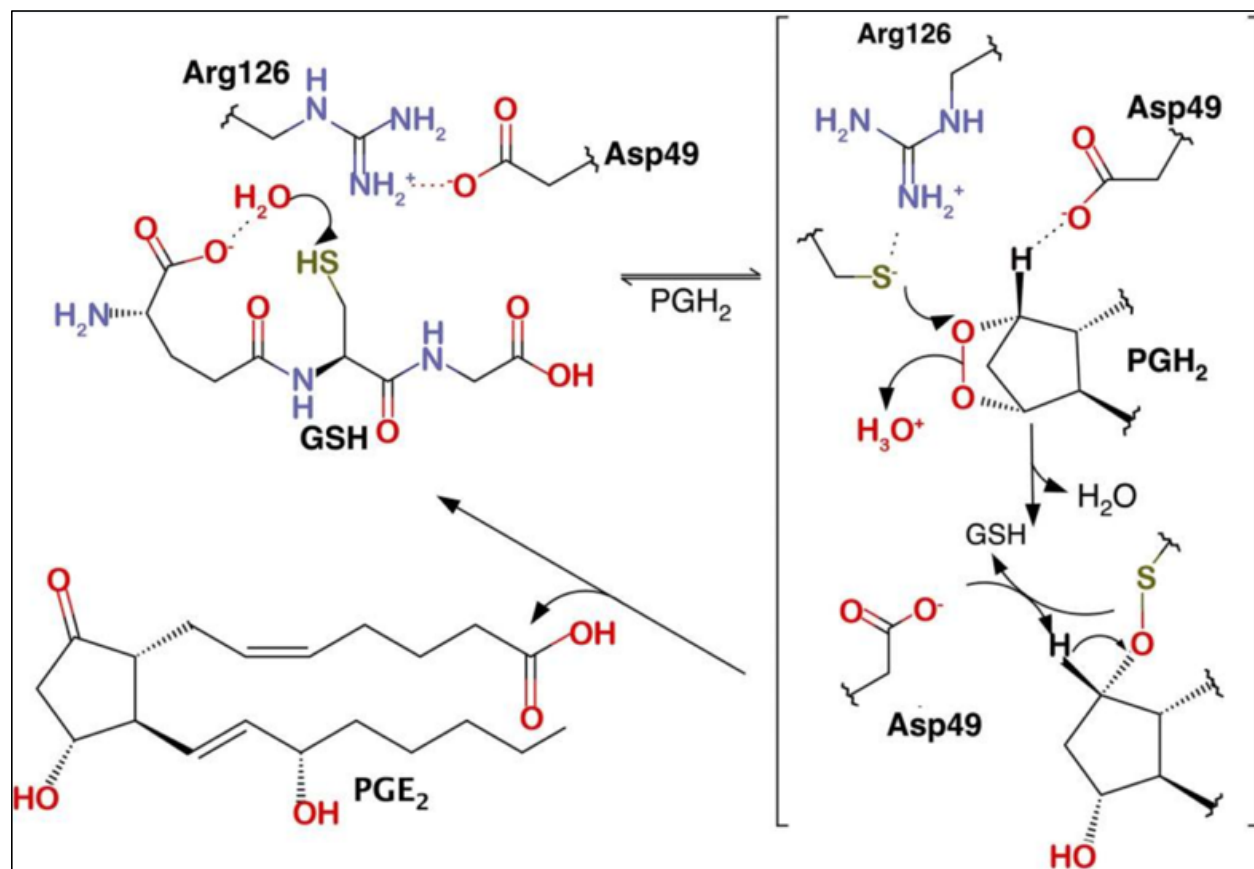


**Figure 14.** mPGES-1 catalytic mechanism. Asp-49 forms an interaction with Arg-126, enabling it to activate the thiolate of GSH for nucleophilic attack on the oxygen of carbon-9. A water molecule acts as a proton shuttle to transfer the GSH proton to the oxygen of carbon-11. Reprinted from *Proc Natl Acad Sci U.S.A.*, 113(4), Brock, JS., A dynamic Asp-Arg interaction is essential for catalysis in microsomal prostaglandin E2 synthase, 972-977, Copyright 2016, with permission from National Academy of Sciences (126).

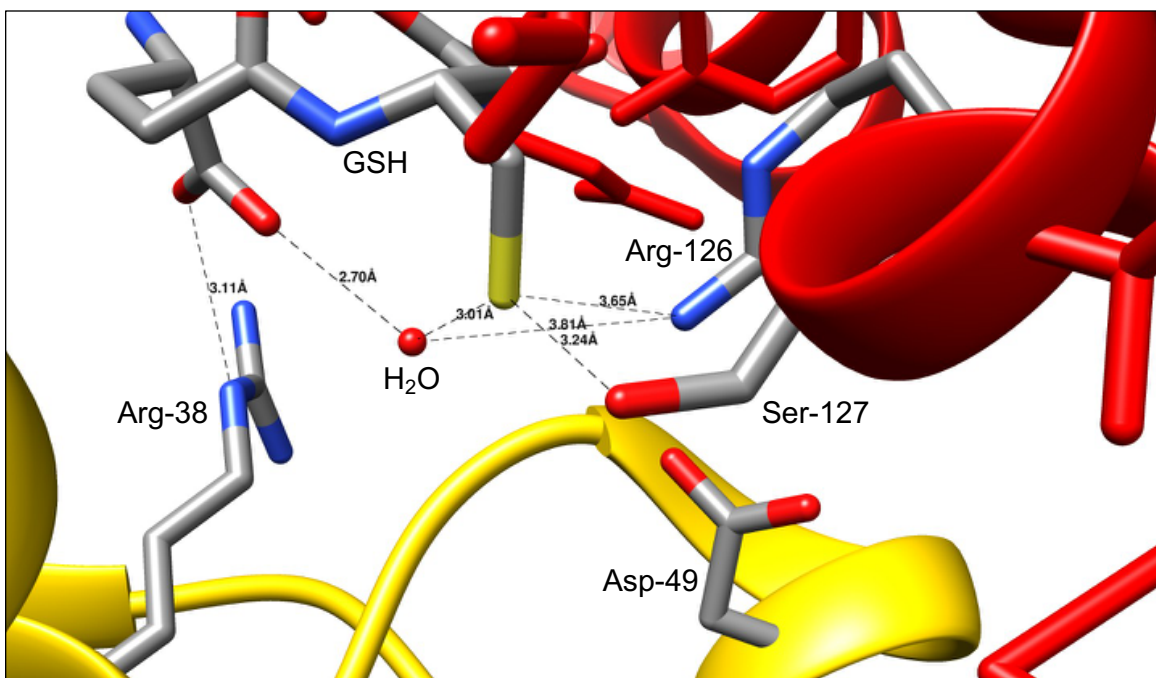


**Figure 15.** mPGES-1 active site with GSH and crystallographic water. Structural refinement and site-directed mutagenesis indicated that Ser-127 is not essential for catalysis, but Asp-49 and Arg-126, as well as the water molecule are crucial for isomerization. Figure generated from PDB 4AL0 (123,126).

With site-directed mutagenesis, it was also discovered that the Ser-127 proposed to stabilize the GSH thiolate was not necessary for enzyme catalysis; however, Asp-49 and Arg-126 are essential for activity. Based on this refinement, it was proposed that the Asp-49 modulates Arg-126 to activate the thiolate of GSH for its nucleophilic attack on the oxygen of carbon-9. The proton from GSH is then shuttled by the crystallographic water to protonate the oxygen of carbon-11. Following its liberation from Arg-126, Asp-49 can then function as a base to abstract the proton from carbon-9, generating the PGE<sub>2</sub> product and regenerating GSH (126). Further studies confirmed that Ser-127 is not essential for catalysis, but Asp-49 and Arg-126 are necessary for substrate isomerization (127). When Arg-126 of mPGES-1 is mutated to either alanine or glutamine, the enzyme becomes a reductase, producing PGF<sub>2α</sub> (128). The mutation to a charge-conserved lysine also produces PGF<sub>2α</sub>, but retains a low level of isomerization activity, indicating a positive charge at residue 126 is crucial for catalysis (126).

### *mPGES-1 Inhibition*

Since the inhibition of the COX enzymes is associated with adverse cardiovascular and gastrointestinal side effects, new ways to block the production of pro-inflammatory PGs have been sought. The induction of mPGES-1 along with COX-2 and the associated increase in PGE<sub>2</sub> production in response to inflammatory stimuli has led to considerable interest in mPGES-1 as a therapeutic target for the treatment of chronic inflammation (129). Shortly after its identification in the late 1990s, various inhibitors of mPGES-1 were developed in both the academic and pharmaceutical sectors (Figure 16). However, the development of potent mPGES-1 inhibitors for the treatment of chronic inflammatory diseases has been a challenge. Although some compounds have been developed which potently inhibit human mPGES-1, they substantially lose potency for the rat orthologue. Previous studies determined that this interspecies difference is due to the residues Thr-131, Leu-135, and Ala-138 in human mPGES-1, which function as gate keepers for the active site of the enzyme. These residues are located on TM IV and line the entrance to the active site between two subunits in the protein trimer. The corresponding residues in the rat isoform are bulkier and thus restrict access of the inhibitors into the active site (130). The human mPGES-1 crystal structure revealed that Arg-52 and His-53 in the C-domain may also contribute to the differences in inhibitor potency between human and rat isoforms but this was not confirmed by point mutations (123).

The first reported inhibitor of mPGES-1 was in 2001, MK-886, and two inhibitors have recently entered clinical trials. However, no mPGES-1 inhibitors have reached the market for treating chronic inflammation (131). An oxicam inhibitor developed by Pfizer Inc., PF-9184, was quite potent for mPGES-1 inhibition, exhibiting an IC<sub>50</sub> value of 16.5 nM in the presence of the recombinant human enzyme and having no effect on either COX-1 or COX-2 (132). Another inhibitor developed by Angelini Research Center was the carbazole benzamide, AF3442. The compound inhibited mPGES-1 in a specific manner with an IC<sub>50</sub> value of 60 nM for the recombinant human enzyme and 410 nM in LPS-stimulated monocytes. The inhibitor did not appear to affect the redirection of PGH<sub>2</sub> into other prostanoid synthase pathways (133).

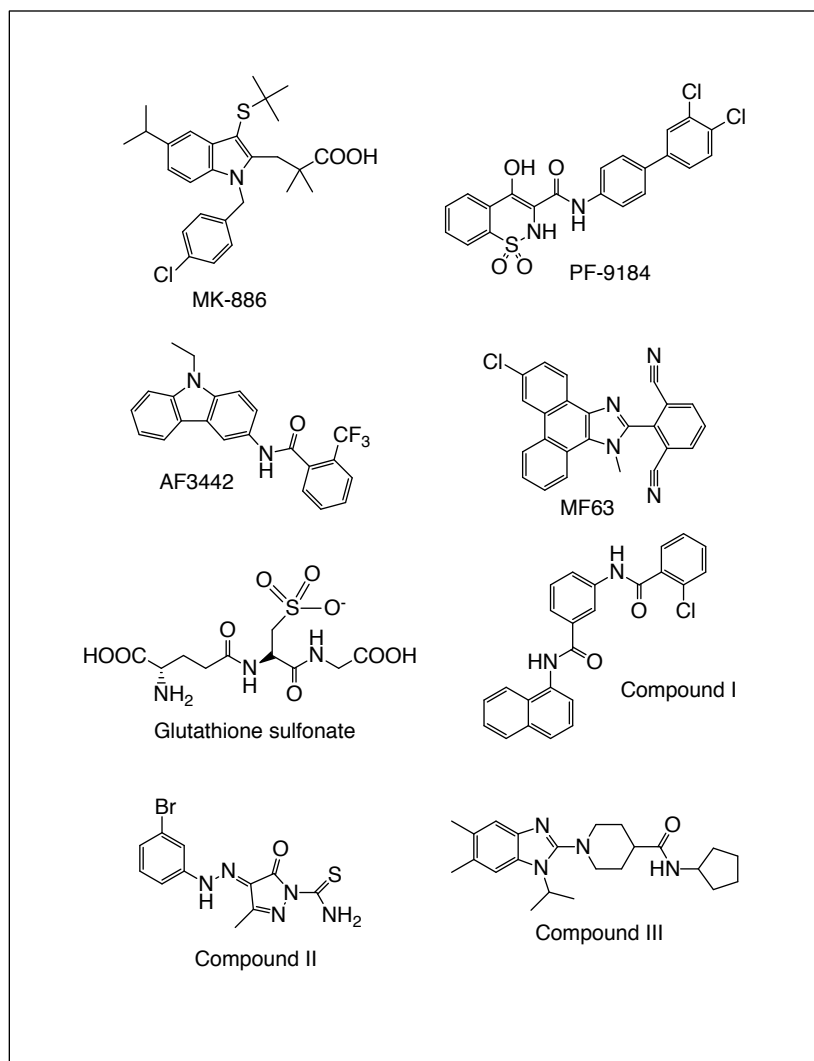


**Figure 16.** Chemical structures of mPGES-1 inhibitors.

Another potent phenanthrine imidazole inhibitor, MF63, developed by Merck Frosst displayed an  $IC_{50}$  of 1.3 nM for the human enzyme with a high selectivity over other prostanoid synthases. Moreover, gastrointestinal toxic side effects typically observed with NSAIDs were not caused by the administration of MF63 (134). Some of the most recent mPGES-1 inhibitors have exhibited sufficient potency in inhibiting both the human and rat enzymes in cell-free assays, *in vitro* cellular assays, and also *in vivo* models of inflammation. The pyrazolone known as compound II from NovaSAID AB inhibited PGE<sub>2</sub> production in synovial fibroblasts from patients having rheumatoid arthritis (135). Another inhibitor, a benzoimidazole

known as compound III from NovaSAID AB, exhibits a submicromolar  $IC_{50}$  in the presence of both human and rat recombinant enzymes. mPGES-1 inhibition was also investigated in mouse macrophages and A549 cells. In these systems, levels of other prostanoids were decreased, with most  $PGH_2$  being shunted to the prostacyclin pathway. In contrast, mPGES-1 knock-out mice displayed an increased production of  $TXA_2$  (136). More recently, additional analogues of the first mPGES-1 inhibitors have been optimized, and more inhibitors have been developed. From using X-ray crystallography and a high-throughput screening method with differential static light scattering (DSLS), four distinct inhibitors were further investigated to elucidate their structure-activity relationships with the enzyme and ultimately improve the efficacy of future inhibitors. From the crystal structures, it was observed that the inhibitors share a common binding mode, where each forms interactions with TM IV of one monomer and their head groups insert into the active site pocket above GSH (137).

Hydrogen-deuterium exchange mass spectrometry (HDX-MS) has been utilized to map the binding sites of different types of inhibitors to mPGES-1 (138). One inhibitor, glutathione sulfonate ( $GSO_3^-$ ), was shown to bind in the GSH binding site with an  $IC_{50}$  of 1.8 mM. With the introduction of the three additional oxygen atoms of the sulfonate group, the GSH binding site is disrupted, as indicated by the HDX-MS results. Other inhibitors that were examined included MF63, MK-886 from Merck (139), and an inhibitor known as compound I from NovaSAID AB (130). Based on dynamic HDX-MS studies, the majority of the enzyme peptides that are involved in inhibitor binding are found within a hydrophobic cleft consisting of TM I from one subunit and TMs II and IV from a neighboring subunit. It was shown that the three critical residues on TM IV that differ between the human and rat enzymes exhibited enhanced HDX kinetics in the presence of the aforementioned inhibitors (excluding  $GSO_3^-$ , which competes for the GSH binding site), indicating that this particular region is crucial for inhibitor binding (138).

In addition to synthetic inhibitors of mPGES-1, the degradation product of prostaglandin  $D_2$ , 15-deoxy- $\Delta^{12,14}$ -prostaglandin  $J_2$  (15d-PG $J_2$ ), has been shown by HDX-MS kinetics to inhibit mPGES-1 by covalent modification of Cys-59 and by noncovalent interaction at the  $PGH_2$  substrate binding site (140). The initial spontaneous dehydration of PGD $_2$  gives rise to the intermediate compound PGJ $_2$ , which will



then isomerize to form  $\Delta$ 12-PGJ<sub>2</sub>. This product spontaneously loses an additional molecule of water to yield 15d-PGJ<sub>2</sub> (141). Using a Cys-59-Ala mutant mPGES-1 enzyme, it was observed that inhibition with the 15d-PGJ<sub>2</sub> substrate was reversible with increasing concentrations of PGH<sub>2</sub> with an IC<sub>50</sub> value of 12  $\mu$ M. Based on these studies, 15d-PGJ<sub>2</sub> most likely inhibits mPGES-1 through its covalent adduction to the Cys-59 residue of the enzyme. However, since the concentration of 15d-PGJ<sub>2</sub> in the cell is unknown, no conclusion can be made regarding whether the covalent modification of MPEGS1 *in vivo* is of any significance (140).

## PURPOSES OF THESE STUDIES

COX-2 and mPGES-1 are both upregulated in the presence of pro-inflammatory stimuli and growth factors. Consistent with its role in inflammation, COX-2 is a therapeutic target through inhibition by NSAIDs and coxibs. In recent years, mPGES-1 has become another therapeutic target to selectively inhibit production of the pro-inflammatory PGE<sub>2</sub>. However, only recently two mPGES-1 inhibitors entered clinical trials, and none has yet reached the market.

The studies described herein further investigate the molecular mechanisms of both COX-2 and mPGES-1. Although NSAIDs have been thoroughly studied, it is still unknown how the occupancy of an inhibitor in one subunit can affect substrate oxygenation in the opposite subunit. The phenomenon of substrate-selectivity has been exhibited by various NSAIDs and many crystal structures of these inhibitors with COX-2 have been solved. However, this structural data is insufficient for defining the mechanistic properties of substrate-selectivity.

In Chapter III of this dissertation, two COX-2 inhibitors, ibuprofen and mefenamic acid, were used to assess the substrate-selective inhibition of COX-2 with AA and 2-AG substrates. The inhibitors bind to the enzyme active site in different orientations with regard to the position of their carboxylates. The NSAID flurbiprofen is structurally similar to ibuprofen and binds to the enzyme in the same orientation yet is not substrate-selective. Likewise, meclofenamic acid is similar in structure to mefenamic acid yet is also not substrate-selective. Therefore, the substrate-selectivity of ibuprofen and mefenamic acid for AA and 2-AG oxygenation were investigated with various experimental parameters, including a preincubation period of each inhibitor with the enzyme. Furthermore, the hydroperoxide PPHP was added to some reaction mixtures to examine the effect of enzyme activation in the presence of each inhibitor.

In Chapter IV, a COX-2•FAAH dual inhibitor, ARN2508, was utilized for structural and kinetic studies. Previously, it was shown that ARN2508 inhibits FAAH as well as both COX isoforms. These studies utilized a racemic mixture of the inhibitor. Herein, the (*S*)-enantiomer of ARN2508 was crystallized in complex with COX-2 in order to observe how the inhibitor bind to the enzyme active site. The inhibitory

kinetics of each ARN2508 enantiomer were also investigated. Various experimental conditions were tested including the absence or presence of a preincubation of the inhibitor with the enzyme. Mutations of active site residues were also completed to investigate how they affected binding of ARN2508 to the enzyme and its subsequent inhibitory kinetics.

In Chapter V, efforts to investigate the structural properties of the COX-2 homodimer were began in collaboration with the Karolinska Institutet. A membrane mimetic, nanodiscs, was used for the reconstitution of recombinant COX-2 and subsequent analysis by negative stain EM and Cryo-EM. The nanodisc platform provided a suitable environment for keeping the COX-2 enzyme stable in solution as well as exhibiting a sufficient molecular size for EM analysis. The structural analysis of COX-2 in nanodiscs could reveal more about its heterodimeric function. Although many X-ray crystal structures of the enzyme in complex with substrates and inhibitors have been solved, there is still limited information regarding the cross-talk of residues at the dimer interface of the enzyme. With recent improvements in Cryo-EM, it could be possible to investigate the structural dynamics of COX-2 in the presence of various substrates and/or inhibitors.

In Chapter VI, the molecular mechanisms of mPGES-1 were investigated. The development of potent mPGES-1 inhibitors for the treatment of chronic inflammatory diseases has been a challenge. Only recently, a high-resolution crystal structure of the enzyme was solved and proposed to involve the activation of a glutathione (GSH) thiolate by a Ser-127 residue in the active site. Here, site-directed mutagenesis studies conducted in collaboration with the Karolinska Institutet revealed that alternate residues in the enzyme active site, Asp-49 and Arg-126, are crucial for activity. Moreover, Ser-127 is not necessary for substrate isomerization. Based on these studies and further molecular refinement of the crystal structure, the molecular dynamics of the enzyme are better understood, setting the stage for the design of more potent mPGES-1 inhibitors.

## CHAPTER II

### MATERIALS AND METHODS

#### Materials

Buffer salts and common chemical reagents were purchased in the highest available quality from commercial vendors. Detergents were from Affymetrix Anatrace, Santa Clara, CA. AA was purchased from Nu-Chek Prep, Inc., Elysian, MN. Heme was purchased from Frontier Scientific, Inc., Logan, UT. 2-AG, PGE<sub>2</sub>-d<sub>4</sub>, 11β-PGE<sub>2</sub>, PGH<sub>2</sub>, PPHP, malondialdehyde, (*S*)-flurbiprofen, and α-linolenic acid were purchased from Cayman Chemical, Ann Arbor, MI. PGE<sub>2</sub>-G-d<sub>5</sub> was synthesized from chemicals purchased from Sigma-Aldrich, St. Louis, MO as previously described (54). Phosphatidylcholine was purchased from Avanti Polar Lipids, Alabaster, AL. Linearized baculovirus DNA and related reagents were purchased from Expressions Systems, LLC., Davis, CA. Sf9 cell culture reagents were from Life Technologies, Carlsbad, CA.

#### Methods

##### *Recombinant murine COX-2 expression and purification*

The cDNA of recombinant murine COX-2 (mCOX-2) was cloned into a pVL-1393 transfer vector and co-transfected with linearized baculovirus DNA (*Autographa californica* nuclear polyhedrosis virus). The virus containing the mCOX-2 gene was amplified in *Spodoptera frugiperda* Sf9 cells and the amplified virus stocks were subsequently used to infect larger Sf9 cell cultures. Cell cultures at a density of 1.2 x 10<sup>6</sup> cells/mL were infected with amplified virus and grown in an incubator shaker at 27°C, 140 rpm for 72 h. Cells were harvested by centrifugation and resuspended in homogenization buffer (25 mM Tris, pH 8.0, 250 mM sucrose, 1 mM EDTA, 1 mM diethyldithiocarbamate (DEDTC)). Cells were stirred until homogenous, and a 15% n-Decyl-β-D-maltoside (C10M) aqueous solution was added to the mixture

dropwise, giving a final C10M concentration of 1.5%. Cells were stirred for one additional hour at 4°C. Cells were sonicated (60% amplitude, 50% duty cycle, 2 minutes on, 4 minutes off) for 3-4 cycles using a Qsonica Q500 sonicator. Cellular debris was cleared by centrifugation in a Beckman-Coulter JA-20 rotor at 16,000 rpm, 4 °C, 30 min. Cellular lysate was loaded onto a Q Sepharose Anion Exchange column (28 mL column volume) equilibrated with Buffer A (20 mM Tris, pH 8.0, 0.1 mM EDTA, 0.1 mM DEDTC, 0.15% C10M). Following the lysate load, the column was washed with Buffer A at a flow rate of 2 mL/min until the absorbance ( $A_{280}$ ) returned to baseline. To elute mCOX-2, a linear gradient of Buffer A and an increasing concentration of Buffer B (20 mM Tris, pH 8.0, 1 M NaCl, 0.1 mM EDTA, 0.1 mM DEDTC, 0.15% C10M), 40% B over 12 column volumes, was applied, and peak fractions (6 mL) were collected. Fractions containing mCOX-2 were concentrated to approximately 2 mL and further purified with gel filtration on a HiLoad 16/600 Superdex 200 pg column (120 mL column volume) in size-exclusion buffer (25 mM Tris, pH 8.0, 0.1 mM EDTA, 50 mM NaCl, 0.3% n-Octyl- $\beta$ -D-glucoside ( $\beta$ -OG)), at a flow rate of 0.5 mL/min. Fractions (5 mL) containing the eluted protein were collected, pooled, and concentrated to approximately 1 mL, and frozen in aliquots at -80°C.

The above procedure was for the purification of mCOX-2 without an affinity tag. To optimize the purification, a C-terminal hexahistidine-tag (His<sub>6</sub>-tag) was cloned in frame with the mCOX-2 gene sequence. To purify the tagged enzyme, cell transfection and harvest were performed as described above. Harvested cells containing his-tagged mCOX-2 were resuspended in homogenization buffer (25 mM Tris-HCl, pH 8.0, 150 mM NaCl, 10 mM imidazole, 250 mM sucrose, 10% glycerol, 1.5% C10M (added dropwise)) and stirred until homogeneous. Cells were lysed as described above. Cell lysate was added to a gravity column containing Ni-NTA affinity resin, equilibrated with equilibration buffer (25 mM Tris, pH 8.0, 150 mM NaCl, 10 mM imidazole). Nonspecific proteins were washed with 10 column volumes of wash buffer (25 mM Tris, pH 8.0, 150 mM NaCl, 50 mM imidazole, 5% glycerol, 0.3%  $\beta$ -OG). mCOX-2 was eluted from the Ni-NTA column with five column volumes of elution buffer (wash buffer containing 150 mM imidazole). Eluted enzyme was concentrated to approximately 1 mL and purified with

gel filtration in size-exclusion buffer. Fractions were collected, concentrated to approximately 1 mL, and frozen in aliquots at -80°C.

#### *mCOX-2 Peroxidase Activity Assay*

To assess the POX activity of purified mCOX-2, a colorimetric assay observing the oxidation of 2,2'-azino-*bis*(3-ethylbenzothiazoline-6-sulphonic acid) (ABTS) in the presence of hydrogen peroxide was used. The assay was performed at room temperature (22 °C) on a Beckman-Coulter DU800 spectrophotometer. Each sample (total reaction volume of 1 mL) contained: 100 mM Tris, pH, 8, 15 nM mCOX-2, 30 nM heme, and 1 mM ABTS. The absorbance at 417 nm was measured as a blank. Next, H<sub>2</sub>O<sub>2</sub> was added to a final concentration of 50 μM, the solution was quickly mixed, and the absorbance at 417 nm was monitored for two minutes. The slope of the linear portion of the absorbance spectrum was used to calculate the POX activity of purified mCOX-2.

#### *mCOX-2 Heme Oxidation Assay*

The oxidation state of heme reconstituted with mCOX-2 was investigated spectroscopically based on a previously published method (91). In a quartz cuvette, 1 μM wild-type mCOX-2 was mixed with 1 μM heme in 100 mM Tris, pH 8.0. The formation of the oxidized heme radical cation was initiated by the addition of H<sub>2</sub>O<sub>2</sub> to a final concentration of 15 μM. The total reaction volume of each sample was brought to 600 μL with buffer. Wavelength scans from 390 to 620 nm were recorded. To monitor the ability to act as reducing co-substrates, various concentrations of inhibitors were pre-incubated with 1 μM wild-type mCOX-2 and 1 μM heme for at least 3 mins at room temperature in 100 mM Tris, pH 8.0. The absorbance at 409 nm was recorded for each sample as a blank before adding H<sub>2</sub>O<sub>2</sub> to initiate heme oxidation. Wavelength scans were recorded every 20 s to monitor the change in absorbance at 409 nm, corresponding to the reduction of compound II back to the resting ferric state.

### *mCOX-2 Activity and Inhibition Assay by Mass Spectrometry*

For assessing the catalytic activity of mCOX-2, 195  $\mu\text{L}$  of 15 nM enzyme was reconstituted with 30 nM heme in buffer containing 100 mM Tris, pH 8 and 500  $\mu\text{M}$  phenol. Samples were kept on ice until ready for use. Each sample was equilibrated at 37°C for at least three minutes before the addition of substrate. The desired substrate (5  $\mu\text{L}$ , AA or 2-AG) in dimethyl sulfoxide (DMSO) was added to the reaction buffer. If the hydroperoxide activator 5-phenyl-4E-pentenyl-1-hydroperoxide (PPHP) was used in the assay, the enzyme volume buffer was reduced to 190  $\mu\text{L}$  and 10  $\mu\text{L}$  of a mixture containing substrate and PPHP was added to the buffer. The final concentration of PPHP in each sample was 1  $\mu\text{M}$ . After adding substrate, the reaction mixture was quickly vortexed, and the reaction proceeded for 10 secs (or other specified reaction time). Each reaction was quenched with the addition of 200  $\mu\text{L}$  of ice-cold ethyl acetate containing 0.5% glacial acetic acid and 300 nM internal standards, either PGE<sub>2</sub>-d<sub>4</sub> or PGE<sub>2</sub>-G-d<sub>5</sub>. Each tube was thoroughly mixed and frozen at -80°C for at least 30 mins. The top organic layer was collected and evaporated to dryness under N<sub>2</sub> gas. The samples were then reconstituted in 150  $\mu\text{L}$  of 50% methanol/water and analyzed using liquid chromatography-tandem mass spectrometry (LC-MS/MS). Each sample was injected onto a Phenomenex Luna C18 (2) column (50 x 2 mm, 5  $\mu\text{M}$ ) with a gradient elution of 30-100% solvent B over 3 mins at a flow rate of 400  $\mu\text{L}/\text{min}$ . Solvent A contained 5 mM ammonium acetate, pH 3.6 and Solvent B contained 94% acetonitrile and 6% Solvent A. Selected reaction monitoring for the following transitions were analyzed:  $m/z$  370  $\rightarrow$  317 (PGE<sub>2</sub>/D<sub>2</sub>),  $m/z$  374  $\rightarrow$  321 (PGE<sub>2</sub>-d<sub>4</sub>),  $m/z$  444  $\rightarrow$  391 (PGE<sub>2</sub>/D<sub>2</sub>-G), and  $m/z$  449  $\rightarrow$  396 (PGE<sub>2</sub>-G-d<sub>5</sub>). For the COX-2 inhibition assays, the same analysis of PGs and PGGs was utilized. Inhibitors (mefenamic acid, ibuprofen, flurbiprofen, ARN2508) were dissolved in DMSO, and 5  $\mu\text{L}$  of each was added to the reaction buffer and preincubated with COX-2 for a designated time. Alternatively, inhibitors were added simultaneously with substrate in a total volume of 10  $\mu\text{L}$  DMSO to each reaction sample.

### *Inhibition of COX-2 Gly-533 mutants by (S)-ARN2508*

Inhibition kinetics with Gly-533 mutants were analyzed using UV-Visible Spectroscopy on a Beckman-Coulter DU800 Spectrophotometer. Enzyme (200 nM monomer) was resuspended in 590  $\mu$ L of assay buffer (100 mM Tris, pH 8.0) with one equivalent of heme. LNA (50  $\mu$ M) was then added, mixed and the absorbance at 235 nm was recorded for 2 min after approximately 5 s of dead time. Inhibitors in a DMSO stock were added for various preincubation times prior to adding substrate.

### *Reconstitution and Purification of mCOX-2 in Nanodiscs*

The incorporation of purified mCOX-2 into nanodisc membrane mimetics was investigated in collaboration with the laboratory of Dr. Hans Hebert at the Karolinska Institutet in Huddinge, Sweden. To prepare the nanodiscs, a molar ratio of 1300:10:1 of 1-palmitoyl-2-oleoyl-*sn*-glycero-3-phosphocholine (POPC):membrane-scaffold protein (MSP1E3D1):mCOX-2 (dimer) was used. POPC lipids (10 mg) in chloroform were dried under a stream of N<sub>2</sub> and then overnight in a vacuum desiccator. The following day, 263  $\mu$ L of 500 mM sodium cholate in nanodisc buffer (20 mM Tris, pH 7.5, 150 mM NaCl, 0.5 mM EDTA) was added to the dried lipids. Lipids were vortexed and sonicated until homogeneously resuspended into the buffer. Non-tagged MSP1E3D1 protein was added to the mixture along with purified mCOX-2 and  $\beta$ -OG detergent. The final concentrations of each component in the mixture were: 16 mM POPC, 32 mM cholate, 123  $\mu$ M MSP1E3D1, 12  $\mu$ M mCOX-2 (dimer), and 0.53%  $\beta$ -OG in a total volume of 822  $\mu$ L. The components were mixed at 4 °C for at least one hour. The mixture was split into two separate Eppendorf tubes and to each tube, 330 mg of SM-2 Bio-Beads (BioRad) was added. Following mixing overnight at 4 °C, Bio-Beads were removed by centrifugation. The supernatant containing mCOX-2-constituted nanodiscs was exchanged with nanodisc buffer without the addition of EDTA (20 mM Tris, pH 7.5, 150 mM NaCl) using centrifugal protein concentrator conical tubes. Following buffer exchange, the mixture was purified by immobilized metal affinity chromatography (IMAC) by incubating with Ni-NTA resin at 4 °C for at least one hour. The mixture was added to a gravity column, and the beads were washed with buffer



containing 20 mM Tris, pH 7.5, 150 mM NaCl, and 50 mM imidazole. mCOX-2 nanodiscs were eluted from the resin with buffer containing 20 mM Tris, pH 7.5, 150 mM NaCl, and 200 mM imidazole. Eluted nanodiscs were concentrated to 500  $\mu$ L and purified with size-exclusion chromatography in nanodisc buffer. The purity of fractions from the size-exclusion purification was assessed with SDS-PAGE. Moreover, the incorporation of mCOX-2 into nanodiscs was assessed using native PAGE in a 4-16% Bis-Tris gel (Novex). Samples were mixed with 4 X native PAGE sample buffer (Invitrogen). Blue native PAGE was performed by using light cathode buffer (native PAGE running buffer (Invitrogen) with 0.001% Coomassie G-250) in the cathode tank and native PAGE running buffer in the anode tank. Gels were run at a constant voltage of 150 V.

#### *COX-2:POPC Nanodisc Cryo-Electron Microscopy*

Vitrified samples were prepared using an FEI Vitrobot at 22 °C and 92% humidity. 3  $\mu$ L of COX-2:POPC nanodisc solution (final concentration  $\sim$ 35  $\mu$ g/mL) was applied onto 400 mesh glow-discharged Quantifoil R2/4 grids (Quantifoil Micro Tools GmbH, Germany). The sample was incubated on the grid for 10 s, blotted for 2-3 s and plunge-frozen into liquid ethane. Frozen grids were stored in liquid nitrogen. For cryo-electron microscopy, the grids were loaded into a Gatan 626 cryo-holder and transferred to a JEOL JEM2100F transmission electron microscope operated at 200 kV. Images were recorded at 2, 5-4  $\mu$ m defocus on a DE-20 direct electron detector (Direct Electron, LP, USA) at a magnification of  $\times$  50,000, resulting in a sampling distance of 1.24  $\text{\AA}$ /pixel. Each image was exposed for 2 s using a frame rate of 20 frames/s. The total accumulated dose/image was approximately 40-50  $e^-/\text{\AA}^2$ .

#### *COX-2:POPC Nanodisc Cryo-Electron Microscopy Image Processing*

The effect of sample drift for each frame was compensated using the DE\_process\_frames-2.7.1.py script. Image processing was performed using EMAN2 software. The templates for auto-picking were selected manually from the images and the auto-picked images were checked manually to remove bad particles. The total dataset consisted of 244 images and 65,164 particles. 2D class averages were calculated

from a smaller set of particles to see the quality of data. The atomic structure of AA bound to the COX-2 active site (PDB: 3HS5) low-pass filtered to 60 Å was used as an initial model for 3D refinement. The 3D refinement was performed without any symmetry and with C2-symmetry. An initial round of 3D refinement was performed using a downsampled (2.48 Å/pixel) dataset, aiming at low resolution. The final map of the first 3D refinement was used as a starting model for further 3D refinements, using the full-sized (1.24 Å/pixel) dataset as input, aiming at higher resolution.

#### *mPGES-1 expression and purification in E. Coli*

Initial kinetic studies with mPGES-1 were based on recombinant human enzyme expressed in *E. coli*. The human mPGES-1 gene with a C-terminal His<sub>6</sub>-tag was subcloned into a pET-21b expression vector. Silent mutations of the codons for Arg-40, Arg-74, and Arg-123 corrected for codon bias. The plasmid was transformed into Rosetta 2 (DE3) *E. coli* competent cells and transfected cells were cultured in a minimal medium (20 mM Na<sub>2</sub>HPO<sub>4</sub>, 20 mM KH<sub>2</sub>PO<sub>4</sub>, 90 mM NaCl, 200 mM NH<sub>4</sub>Cl, 130 μM CaCl<sub>2</sub>, 1 mM MgSO<sub>4</sub>, 0.4% glucose, 0.3% casamino acids). Cells were grown in an incubator shaker at 37 °C, 250 rpm. When an OD<sub>600</sub> of 0.7 was achieved, cell cultures were cooled to 18 °C, and protein expression was induced by the addition of 1 mM Isopropyl β-D-1-thiogalactopyranoside (IPTG). The cells were cultured further at 18 °C, 200 rpm for approximately 36 additional hours. Cells were harvested by centrifugation at 6,500 x g, 4 °C, 6 mins, and stored at -20 °C. Frozen cell pellets were resuspended in cold lysis buffer (50 mM KH<sub>2</sub>PO<sub>4</sub>, pH 8.0, 300 mM KCl, 1 mM GSH, 1 mM DTT, 1 mM EDTA, 10% glycerol). Lysozyme was added to a final concentration of 0.2 mg/mL, and cells were stirred for 2 h at 4 °C. Cells were sonicated on ice using a Qsonica Q500 sonicator (60% amplitude, 50% duty cycle, 2 mins on, 4 mins off) until the mixture was homogeneous. The cellular debris was cleared by centrifugation at 10,000 x g, 4°C, 30 mins. The membrane fractions from the cell lysate were isolated using ultracentrifugation at 100,000 x g, 4°C, 2 h. The supernatant was discarded, and membrane pellets were washed with cold 50 mM KH<sub>2</sub>PO<sub>4</sub>, pH 8.0. The membranes were solubilized in cold extraction buffer (50 mM KH<sub>2</sub>PO<sub>4</sub>, pH 8.0, 300 mM KCl, 1 mM

GSH, 5 mM imidazole, 10% glycerol, 0.5% n-Dodecyl- $\beta$ -D-maltoside ( $\beta$ -DDM)). The enzyme was solubilized by gentle stirring overnight at 4 °C. The solubilized enzyme was incubated with equilibrated Ni-NTA agarose and gently stirred at 4 °C for at least one hour. The resin was added to a gravity column for purification. Extraction buffer containing 35 mM imidazole was added to wash the non-specific proteins from the column, and the His<sub>6</sub>-tag mPGES-1 was eluted by adding extraction buffer containing 250 mM imidazole. The fractions were collected, and the presence of the protein was verified by SDS-PAGE. The eluted protein was concentrated using an Amicon pressure concentrator (MWCO = 10 kDa) to approximately 10 mL and dialyzed against 1 L of ion-exchange buffer (50 mM KH<sub>2</sub>PO<sub>4</sub>, pH 7.0, 1 mM GSH, 20% glycerol, 1% polyoxyethylene(10)dodecyl ether) at 4 °C, overnight. The dialyzed protein was then applied to sulfopropyl sepharose equilibrated with ion-exchange buffer in a gravity column. The protein was washed with a similar buffer containing 0.1% DDM, or 1% 3-[(3-Cholamidopropyl)dimethylammonio]-1-Propanesulfonate (CHAPS), and then eluted with a similar buffer containing 100 mM KCl and 0.05% DDM, or 0.5% CHAPS. The eluted protein was concentrated using an Amicon pressure concentrator (MWCO = 10 kDa) until the A<sub>280</sub> was approximately 1.2, giving a final concentration of approximately 1 mg/mL. The enzyme was then dialyzed overnight at 4 °C in a buffer containing 50 mM KH<sub>2</sub>PO<sub>4</sub>, pH 7.0, 300 mM KCl, 1 mM GSH, 1 mM DTT, 7.5% glycerol, 1% CHAPS. Protein was aliquoted and stored at -20 °C for future use. In alternate enzyme preparations and purifications, the final purification step with ion-exchange and final dialysis replaced 1 mM GSH with 1 mM of various GSH analogues, GSO<sub>3</sub><sup>-</sup>,  $\gamma$ -L-Glu-L-SerGly (GOH), or  $\gamma$ -L-Glu-L-AlaGly (GH). The purification of each enzyme preparation was verified by SDS-PAGE and Western blotting using a QIAexpress Anti-His antibody for the detection of His<sub>6</sub> tagged proteins. Since mPGES-1 is unstable when the cofactor-binding site is unoccupied, apo-mPGES-1 experiments were not possible. Therefore, all experiments described herein are with mPGES-1 complexed with either GSH or one of its analogues.

### *mPGES-1 expression and purification optimization in Sf9 cells*

To enhance the expression of recombinant human mPGES-1, a baculovirus expression system for the infection of Sf9 cells similar to that described above for murine COX-2 was utilized. Briefly, the cDNA of recombinant human mPGES-1 containing a C-terminal His<sub>6</sub>-tag was cloned into a pVL-1392 transfer vector and co-transfected with linearized baculovirus DNA (*Autographa californica* nuclear polyhedrosis virus). The virus containing the mPGES-1 gene was amplified in *Spodoptera frugiperda* Sf9 cells and the amplified virus stocks were subsequently used to infect larger Sf9 cell cultures. Cell cultures at a density of  $1.2 \times 10^6$  cells/mL were infected with amplified virus and grown in an incubator shaker at 27°C, 140 rpm for 72 h. Cells were harvested by centrifugation and purified using the aforementioned purification procedure of human mPGES-1 expressed in *E. coli*. Slight modifications were implemented to increase the yield of pure, homogeneously folded enzyme. Following the second purification step with ion-exchange chromatography, fractions were pooled, concentrated to approximately 2 mL, and purified with gel filtration on a HiLoad 16/600 Superdex 200 pg column in size-exclusion buffer containing 50 mM KH<sub>2</sub>PO<sub>4</sub>, pH 7.0, 300 mM KCl, 1 mM GSH, 1 mM DTT, 7.5% glycerol, 0.05% β-DDM. Fractions (5 mL) were collected, pooled, and concentrated in small aliquots and frozen at -20 °C for future use.

### *mPGES-1 Site-Directed Mutagenesis*

For preparing the Asp-49-Ala, Arg-126-Ala, Ser-127-Ala, and Ser-127-Cys mutants, the wild-type human mPGES-1 gene in the pVL-1392 transfer vector was used as a template for standard site-directed mutagenesis with PCR. The following primers were used for each mutant:

Mutant	Primer
Asp-49-Ala (Forward)	GCCAACCCCGAGGCTGCCCTGAGACAC
Asp-49-Ala (Reverse)	GTGTCTCAGGGCAGCCTCGGGTTGGC
Arg-126-Ala (Forward)	GCGTGCACCCATCGCCTCCGTGACCTAC
Arg-126-Ala (Reverse)	GTAGGTCACGGAGGCGATGGGTGCACGC
Ser-127-Ala (Forward)	TGCACCCATCCGCGCCGTGACCTACAC
Ser-127-Ala (Reverse)	GTGTAGGTCACGGCGCGGATGGGTGCA
Ser-127-Cys (Forward)	TGCACCCATCCGCTGCGTGACCTACAC
Ser-127-Cys (Reverse)	GTGTAGGTCACGCAGCGGATGGGTGCA

Mutated plasmids were transfected into XL1 Blue supercompetent cells and plasmid sequences were verified with sequencing (GenHunter, Nashville, TN).

*Synthesis of  $\gamma$ -L-Glu-L-SerGly (GOH) and  $\gamma$ -L-Glu-L-AlaGly (GH)*

Both analogues of GSH, GOH and GH, were synthesized according to a published method (142). Briefly, the protected active  $\gamma$ -ester of L-glutamic acid was prepared by the reaction of N-t-BOC-L-glutamic acid  $\alpha$ -benzyl ester and 4-nitrophenol, followed by glacial acetic acid. The dicyclohexylurea was removed by vacuum filtration, and solvent was evaporated from the filtrate to leave an oily residue. The oil was dissolved in hot ethanol, and the product crystallized upon cooling overnight. The needles formed from precipitation were the protected active  $\gamma$ -ester, which was then coupled to either L-serylglycine or L-alanylglycine in 33% pyridine/H<sub>2</sub>O. Following stirring overnight, NaHCO<sub>3</sub> in H<sub>2</sub>O was added, and the reaction mixture was extracted with ethyl acetate. The organic layer was back-extracted with additional H<sub>2</sub>O. The aqueous fractions were pooled together, lowered to pH 2.5 with 3 M HCl, and stored at 4 °C. The granulated oily product contained the protected peptide, which was then deprotected by dissolving in anhydrous trifluoroacetic acid. Anhydrous HBr gas was bubbled through the solution for 30 mins on ice, then at room temperature for 2 h. Excess solvent was removed by flash evaporation and the remaining tan oil was washed with diethyl ether and dried in a vacuum desiccator. The product was purified by anion-exchange with BioRad AG1-X2 acetate beads. The product was added to the beads in a gravity column and the beads were then washed with 50 mM acetic acid. The product was eluted from the beads by flowing through a linear gradient of 50 mM to 1 M acetic acid. Fractions containing the purified product were pooled and lyophilized three times with H<sub>2</sub>O to yield a white hygroscopic powder. Final purified product was characterized using both <sup>1</sup>H-NMR and <sup>13</sup>C-NMR at the Vanderbilt Small Molecule NMR Facility. <sup>1</sup>H-NMR and <sup>13</sup>C-NMR spectra revealed that the chemical shifts corresponded to literature values.

### *Glutathione Transferase Activity Assays*

A glutathione transferase assay of recombinant human mPGES-1 activity was based on a previously published method (116). Briefly, a reaction mixture containing 100 mM  $\text{KH}_2\text{PO}_4$ , pH 6.5, 4 mM GSH, 1  $\mu\text{M}$  purified mPGES-1, and 0.1%  $\beta$ -DDM was mixed and brought to a volume of 990  $\mu\text{L}$ . The absorbance at 340 nm was recorded as a blank measurement. The conjugation of GSH to the substrate CDNB was initiated by the addition of 10  $\mu\text{L}$  of 200 mM CDNB in ethanol. The reaction mixture was quickly mixed, and the absorbance at 340 nm was monitored at 22 °C for 20 mins. The background reaction contained the same mixture without the addition of enzyme and was subtracted from the activity in the presence of enzyme.

### *Prostaglandin E Synthase Activity Assay by Mass Spectrometry*

The isomerization of  $\text{PGH}_2$  to  $\text{PGE}_2$  was detected with LC-MS/MS, with the method being modified from a previously published procedure (143).  $\text{PGH}_2$  in acetone was distributed in small aliquots and kept on dry ice until use in each reaction. To initiate isomerization, 100  $\mu\text{L}$  of a 100 nM purified mPGES-1 enzyme stock solution in reaction buffer (100 mM  $\text{KH}_2\text{PO}_4$ , pH 7.5, 1 mM GSH, 1% glycerol and 0.05%  $\beta$ -DDM) was added to each  $\text{PGH}_2$  aliquot. Each sample was reacted for one min on ice, and unreacted  $\text{PGH}_2$  was decomposed to 12-HHT and malondialdehyde (MDA) by the addition of 400  $\mu\text{L}$  of quench buffer (25 mM  $\text{FeCl}_2$ , 50 mM citric acid, pH 3.0, and 0.5  $\mu\text{M}$  11 $\beta$ - $\text{PGE}_2$  as an internal standard). Each sample was purified using disposable C18 solid-phase extraction columns and eluted in 100% methanol. Methanol was evaporated under  $\text{N}_2$  gas, and samples were resuspended in 20% acetonitrile/ $\text{H}_2\text{O}$  and analyzed by LC-MS/MS with a Phenomenex Luna 3.0  $\mu$ , C18(2), 100 Å column (150 x 2.00 mm) equipped with a Phenomenex Security Guard Cartridge Kit, eluting at a flow rate of 350  $\mu\text{L}/\text{min}$  using mobile phase A ( $\text{H}_2\text{O}$  + 0.1% formic acid) and mobile phase B ( $\text{CH}_3\text{CN}$  + 0.1% formic acid). A gradient of 31.2 to 42.5% B was run over 14.3 minutes. Using negative electrospray ionization, the detection of

PGE<sub>2</sub>, 11β-PGE<sub>2</sub>, and PGD<sub>2</sub> was confirmed by the SRM of the transition  $m/z$  351.2 → 271.2 on a ThermoFinnigan TSQ triple-quadrupole mass spectrometer.

#### *Prostaglandin E Synthase Activity Assay by Fluorescence*

An alternative method for assessing mPGES-1 activity examined the degradation of the PGH<sub>2</sub> substrate as opposed to observing the formation of the PGE<sub>2</sub> product. Similar to the LC-MS/MS-based method, PGH<sub>2</sub> substrate was distributed in small aliquots in tubes on dry ice. To initiate the reaction, 100 μL of a 100 nM purified mPGES-1 enzyme stock solution in reaction buffer (100 mM KH<sub>2</sub>PO<sub>4</sub>, pH 7.5, 1 mM GSH, 1% glycerol, and 0.05% β-DDM) were added to each PGH<sub>2</sub> aliquot. Each sample was reacted for one min on ice, and unreacted PGH<sub>2</sub> was decomposed to 12-HHT and MDA by the addition of 100 μL of quench buffer (100 mM FeCl<sub>2</sub>, 500 mM citric acid, pH 2.0). To each sample, 100 μL of a solution containing 15 mM thiobarbituric acid (TBA) in 80 mM KH<sub>2</sub>PO<sub>4</sub>, pH 2.0 was added and heated to 80 °C for 30 mins. Precipitate from each sample was removed by centrifugation. A 200 μL aliquot of each reaction mixture was transferred to a 96-well plate, and fluorescence of the resulting MDA-TBA complex was recorded in a BioTek Synergy MX plate reader. Samples were excited at 485 nm, and emissions were observed at a wavelength of 545 nm.

#### *Stopped-flow Kinetics of mPGES-1 Thiolate Formation*

Stopped-flow kinetic experiments were performed in collaboration with the laboratory of Dr. Ralf Morgenstern at the Karolinska Institutet in Stockholm, Sweden. Initially, a solution of 50 μM of purified mPGES-1 was rapidly injected in an Applied Photophysics SX20 stopped-flow cell against a solution of the same buffer containing 20 mM GSO<sub>3</sub><sup>-</sup>. With a 1:1 mixing ratio, the final concentrations of the enzyme and competitor were 25 μM and 10 mM, respectively. The change in absorbance at 239 nm was observed for various time points ranging from 5 seconds to 300 seconds to observe any potential drift that might occur. Recombinant enzyme was also injected against a stock solution of 20 mM GOH to observe any

potential competition of the thiolate with the oxygen analogue in the active site of the enzyme. Further stopped-flow experiments were performed following the concentration of enzyme to a final concentration of 150  $\mu\text{M}$ . The enzyme was rapidly mixed against  $\text{GSO}_3^-$  or GOH, each at a final concentration of 10 mM.

#### *Peptide Sequencing of mPGES-1 by Tandem Mass Spectrometry*

The peptides of purified mPGES-1 were sequenced using a previously published method with modifications (138). Purified mPGES-1 was dialyzed into a buffer containing 50 mM  $\text{KH}_2\text{PO}_4$ , pH 7.0), 200 mM KCl, 1 mM GSH (or GOH, GH), 7.5% glycerol, and 0.5% CHAPS. The enzyme solution was initially brought to a concentration of approximately 0.2 mg/mL (12  $\mu\text{M}$ ) in  $\text{H}_2\text{O}$  at 0  $^\circ\text{C}$ . Enzymatic digestion of the enzyme was performed on ice for seven minutes by adding 580  $\mu\text{M}$  pepsin in  $\text{H}_2\text{O}$ . The digested peptides were separated by reversed-phase HPLC on a Phenomenex Aeris Peptide 3.6  $\mu\text{m}$  XB-C18 column (50 x 2.1 mm) submerged in an ice bath and eluted at a flow rate of 300  $\mu\text{L}/\text{min}$  with a 30 min gradient of 5-50%  $\text{CH}_3\text{CN}$  and 0.4% formic acid. The peptides were analyzed on a LTQ tandem mass spectrometer using positive electrospray ionization, with scans of  $m/z$  300 to 1500. Peptides were sequenced with data-dependent tandem MS/MS by collision-induced dissociation (CID). The identity of each peptide was verified using the computational program PEAKS Client 7 (Bioinformatics Solutions Inc.), which determines the identity of peptide fragments based on raw data acquisition. PEAKS then predicts peptide fragmentation based on the protease used for digestion, the FASTA sequence for the protein, and the MS instrument and parameters used. Experimental fragmentation patterns were matched with predicted peptide fragmentation. Selected peptides were further verified using MassXpert MS analysis software which compares experimental peptide parent masses with all possible peptides within the protein. Experimental fragmentation spectra were then compared to theoretical fragmentation patterns of all possible peptides by the ProteinProspector program MS-Product. Verified peptides were then compiled to generate a peptide coverage map.



## CHAPTER III

### MOLECULAR BASIS OF CYCLOOXYGENASE-2 INHIBITION BY MEFENAMIC ACID AND IBUPROFEN

NSAIDs inhibit the COX enzymes by binding in the COX active site of the catalytic subunit, the allosteric subunit, or both and preventing the oxygenation of substrates. Numerous NSAIDs have been developed, including nonspecific inhibitors of both COX-1 and COX-2, as well as coxibs that selectively inhibit COX-2. Some NSAIDs inhibit COX by binding rapidly and reversibly to the enzyme. Others bind rapidly to the enzyme in an initial step followed by one or more slower steps to form a tight enzyme-inhibitor complex. Furthermore, some inhibitors of the COX enzymes are substrate-selective, in that they are rapidly reversible, weak inhibitors of AA oxygenation, but potent, time-dependent inhibitors of endocannabinoid oxygenation. Presumably, the substrate-selective inhibitors bind in the allosteric subunit of the enzyme and induce a conformational change in the catalytic subunit that prevents the oxygenation of endocannabinoids but not AA. Inhibition of AA oxygenation requires lower affinity binding of the inhibitor in the catalytic subunit (88).

Ibuprofen and mefenamic acid were both reported to be rapid, reversible inhibitors of AA oxygenation, but potent, tight-binding inhibitors of endocannabinoid oxygenation. Although their inhibitory mechanisms were initially thought to be similar, the potency and mode of binding of each inhibitor appear to differ from those of the other (88). In the crystal structure of mCOX-2 with a racemic mixture of ibuprofen, only the (*S*)-enantiomer of the inhibitor was bound, consistent with its having higher affinity for the enzyme. The carboxylate of (*S*)-ibuprofen forms interactions with the constriction site residues, Arg-120 and Tyr-355, and mutation of these residues affects inhibitor binding (144). The inhibitor mefenamic acid has been shown to bind in the COX active site in an inverted orientation, similar to that of diclofenac and lumiracoxib, in that its carboxylate forms interactions with Tyr-385 and Ser-530. Flurbiprofen and meclofenamic acid are structurally similar inhibitors to ibuprofen and mefenamic acid,

respectively. However, flurbiprofen and meclofenamic acid are both slow, tight-binding inhibitors and are not substrate-selective (89,91). The differences in the substrate-selectivity of these structurally similar inhibitors have not yet been explained. The studies herein seek to further understand the molecular mechanisms of substrate-selective inhibition by inhibitors such as mefenamic acid and ibuprofen.

## Results

### *Substrate-Selective Inhibition of Cyclooxygenase-2 by Mefenamic Acid and Ibuprofen*

In order to assess the substrate-selective inhibition of ibuprofen and mefenamic acid, activity assays were conducted, and product formation was quantified by LC-MS/MS. For all assays presented here, 15 nM mCOX-2 was reconstituted with 2 equivalents of heme in each reaction mixture. Reactions were initiated with the addition of 5  $\mu$ M of either AA or 2-AG and allowed to proceed for 10 s before being quenched with organic solvent containing deuterated internal standards. The short reaction time was chosen in order to minimize the total amount of substrate turnover and limit enzyme self-inactivation.

Other experimental parameters were varied to investigate the substrate selectivity of inhibition. Since inhibition of 2-AG oxygenation has been reported to be time-dependent whereas inhibition of AA oxygenation is not, assays were conducted both with and without a 15 min preincubation of inhibitor and enzyme. Another experimental variable that was evaluated was the absence or presence of the hydroperoxide activator PPHP. The presence of inhibitors can theoretically increase the enzyme lag phase by slowing the reaction or directly interfering with enzyme activation. Since a short reaction time of 10 s was used, a significant lag phase would produce misleading kinetic data. This effect would be expected to be greater for 2-AG than AA inhibition, as higher peroxide concentrations are required to activate the enzyme when 2-AG is the substrate (90). A concentration of 1  $\mu$ M PPHP was reported to be sufficient to maximize substrate oxygenation of either AA or 2-AG by COX-2 in *in vitro* kinetic assays (64). When included, PPHP was added simultaneously with each substrate.

As indicated in Figures 17 and 18 and Table 3, both inhibitors were more potent for inhibiting 2-AG oxygenation than AA oxygenation under all conditions tested except one (ibuprofen yielded the same  $IC_{50}$  for inhibition of 2-AG and AA oxygenation in the presence of PPHP following preincubation of inhibitor with the enzyme). This result was consistent with a previous report in which the substrate selectivity of the inhibitors was evaluated in the absence of added hydroperoxide using an oxygraph instrument (88). In the case of ibuprofen, preincubation of the inhibitor with the enzyme increased potency for 2-AG oxygenation by  $\sim 7$ -fold regardless of the presence or absence of PPHP, and addition of PPHP reduced inhibitor potency by  $\sim 1.5$ -fold with or without preincubation (based on  $IC_{50}$  values). In contrast, preincubation increased inhibitor potency for AA oxygenation to a much greater extent ( $>200$ -fold and  $>1,400$ -fold in the absence or presence of PPHP, respectively). For AA oxygenation, inclusion of PPHP had no significant effect on the potency of ibuprofen in the absence of preincubation, but it increased inhibitor potency  $\sim 5$ -fold when preincubation was included in the assay (Figure 17, Table 3).

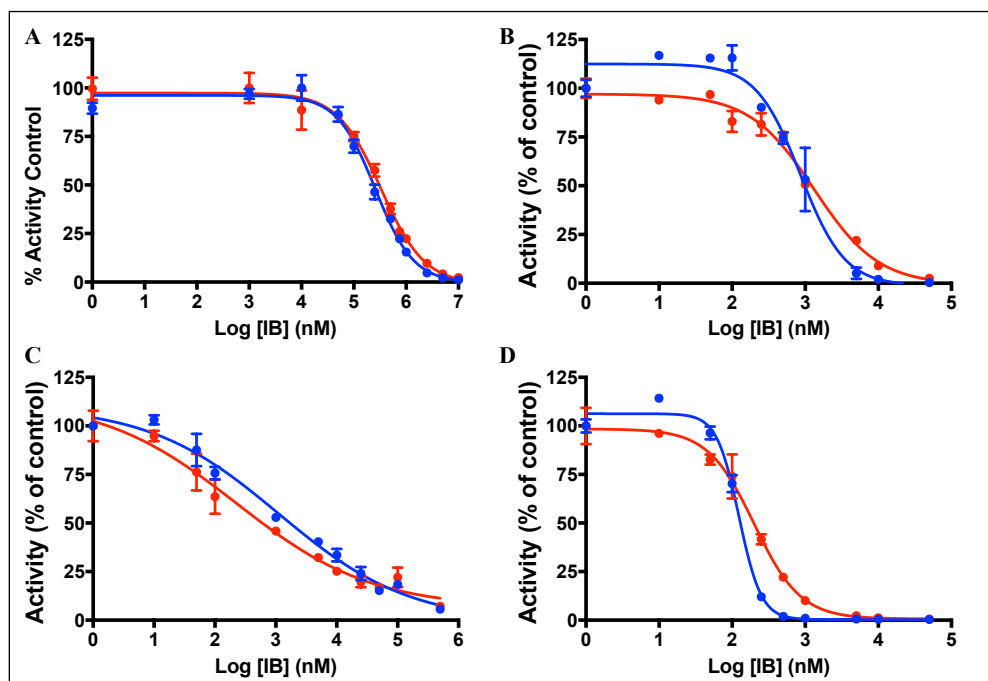


**Figure 17.**  $IC_{50}$  curves for mCOX-2 inhibition by ibuprofen (IB). In each experiment, 15 nM mCOX-2 was reconstituted with 30 nM heme and used for oxygenation of 5  $\mu$ M substrate. Substrate oxygenation was tested in the absence (blue) or presence (red) of 1  $\mu$ M of the hydroperoxide activator PPHP. Inhibition of AA oxygenation was observed with no pre-incubation of ibuprofen with COX-2 (A) or a 15 min pre-incubation of ibuprofen with COX-2 (C). Inhibition of 2-AG oxygenation was observed with no pre-incubation of ibuprofen with COX-2 (B) or a 15 min pre-incubation of ibuprofen with COX-2 (D).

**Table 3.** IC<sub>50</sub> values (μM) (95% confident range) for AA and 2-AG oxygenation in the presence of ibuprofen and mefenamic acid. For each substrate with or without pre-incubation, IC<sub>50</sub> values (μM) are listed in the absence (blue) or presence (red) of 1 μM PPHP.

<b>Ibuprofen</b>			
	No pre-incubation		No pre-incubation
5 μM AA	260 (220-300)	5 μM 2-AG	0.86 (0.69-1.1)
5 μM AA	330 (280-400)	5 μM 2-AG	1.3 (1.0-1.8)
	15 min pre-incubation		15 min pre-incubation
5 μM AA	1.1 (0.61-2.3)	5 μM 2-AG	0.12 (0.12-0.13)
5 μM AA	0.23 (0.07-0.53)	5 μM 2-AG	0.20 (0.17-0.23)
<b>Mefenamic acid</b>			
	No pre-incubation		No pre-incubation
5 μM AA	100 (89-120)	5 μM 2-AG	0.05 (0.04-0.06)
5 μM AA	110 (100-120)	5 μM 2-AG	0.53 (0.41-0.71)
	15 min pre-incubation		15 min pre-incubation
5 μM AA	0.12 (0.08-0.18)	5 μM 2-AG	0.01 (0.01-0.01)
5 μM AA	88 (43-180)	5 μM 2-AG	0.07 (0.04-0.10)

For mefenamic acid using 2-AG as the substrate, preincubation of the enzyme with inhibitor resulted in an increase in potency similar to what was seen with ibuprofen (~5-fold and ~8-fold in the absence and presence of PPHP, respectively). In the absence of PPHP, preincubation caused a much greater (>800-fold) increase in potency for AA oxygenation than 2-AG oxygenation as was seen for ibuprofen, but in the presence of PPHP, preincubation did not alter mefenamic acid potency when AA was the substrate. When 2-AG was the substrate, PPHP had a greater effect on mefenamic acid potency (~7 to 10-fold increase in IC<sub>50</sub>) than was observed for ibuprofen. In the case of AA oxygenation, PPHP had no effect on mefenamic acid potency in the absence of a preincubation, as was observed for ibuprofen. However, PPHP produced a >700-fold decrease in mefenamic acid potency for AA oxygenation when the enzyme was preincubated with the inhibitor (Figure 18, Table 3).

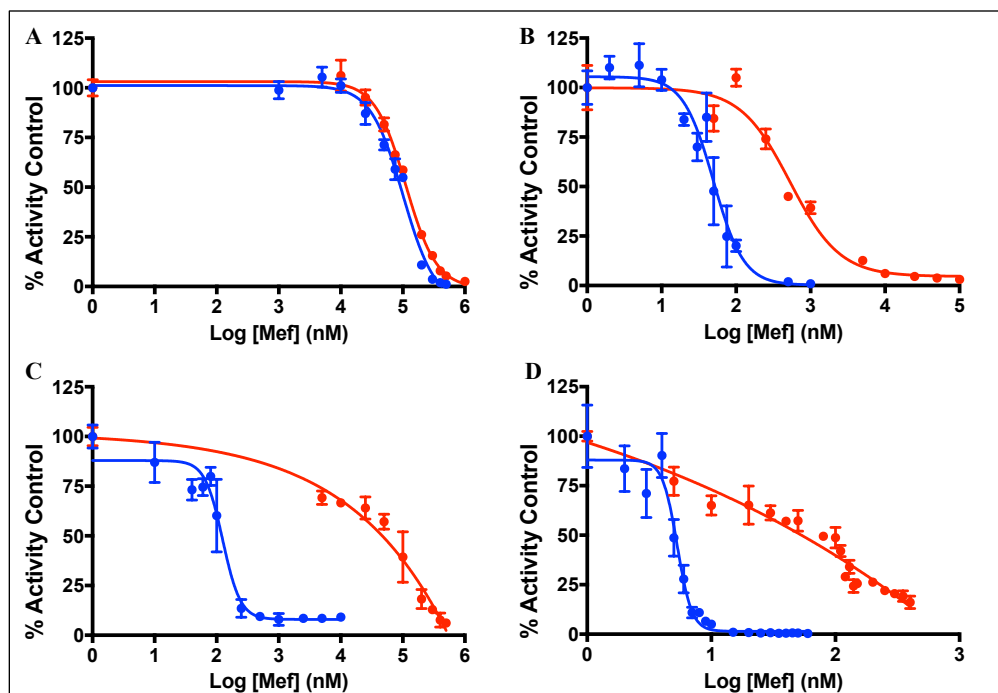


**Figure 18.** IC<sub>50</sub> curves for mCOX-2 inhibition by mefenamic acid (MEF). In each experiment, 15 nM mCOX-2 was reconstituted with 30 nM heme and used for oxygenation of 5  $\mu$ M substrate. Substrate oxygenation was tested in the absence (blue) or presence (red) of 1  $\mu$ M of the hydroperoxide activator PPHP. Inhibition of AA oxygenation was observed with no pre-incubation of mefenamic acid with COX-2 (A) or a 15 min pre-incubation of mefenamic acid with COX-2 (C). Inhibition of 2-AG oxygenation was observed with no pre-incubation of mefenamic acid with COX-2 (B) or a 15 min pre-incubation of ibuprofen with COX-2 (D).

In summary, the results for 2-AG inhibition were consistent for the two inhibitors with some quantitative differences. Both inhibitors were more effective following preincubation with the enzyme, and both were less effective in the presence of PPHP, with the reduction in potency being substantially greater for mefenamic acid than for ibuprofen. These findings are consistent with past reports that inhibition of 2-AG oxygenation by these inhibitors is time-dependent (88). They also suggest that the mechanism of inhibition by both inhibitors is dependent to some degree on suppression of peroxide-dependent enzyme activation, and this appears to be more important for mefenamic acid than for ibuprofen. In the case of AA, both inhibitors are more potent following preincubation with the enzyme, a result that contradicts prior reports that both are rapidly reversible inhibitors of AA oxygenation (88). The effects of PPHP were also harder to explain in the case of AA oxygenation than 2-AG oxygenation. PPHP increased the potency of ibuprofen following preincubation of the inhibitor with the enzyme, an unexpected finding, as eliminating

an artificially extended lag phase by adding peroxide would be expected to reduce, rather than increase, apparent inhibitor potency. In contrast, PPHP had the opposite effect on the potency of inhibition by mefenamic acid, suggesting a significant difference between the two inhibitors with regard to their effects on enzyme activation when AA is the substrate.

Since the experiments investigating inhibitor potency in the absence or presence of PPHP suggested that mefenamic acid strongly affects enzyme activation when the enzyme is preincubated with the inhibitor, an additional experiment was performed to evaluate substrate oxygenation differences in the absence or presence of mefenamic acid (100 nM), with or without PPHP, at various reaction times following a 15 min preincubation (Figure 19). For the DMSO control samples, PPHP appeared to slightly suppress enzyme activity, likely due to the promotion of enzyme suicide inactivation from an increased peroxide concentration. However, there does not appear to be a lag phase in product formation in the absence of inhibitor or PPHP, indicating that there is likely an adequate level of peroxide contamination in both substrates to rapidly activate the enzyme. In contrast, in the absence of PPHP, mefenamic acid appears to cause a lag in AA oxygenation since less product is made in the first 10 s than is made in the 5 s period between 10 and 15, or in the 10 s period between 20 and 30. In fact, less product is made in the absence of PPHP in the first 10 s than in the presence of PPHP even though PPHP seems to suppress the reaction by itself. Therefore, at this concentration, mefenamic acid extends the lag phase for AA oxygenation, and the effect is so severe for 2-AG that no product is formed at all. However, increasing the lag phase is not the only mechanism for inhibition, as less product is formed from both substrates when PPHP is added to each reaction and the lag phase is eliminated.

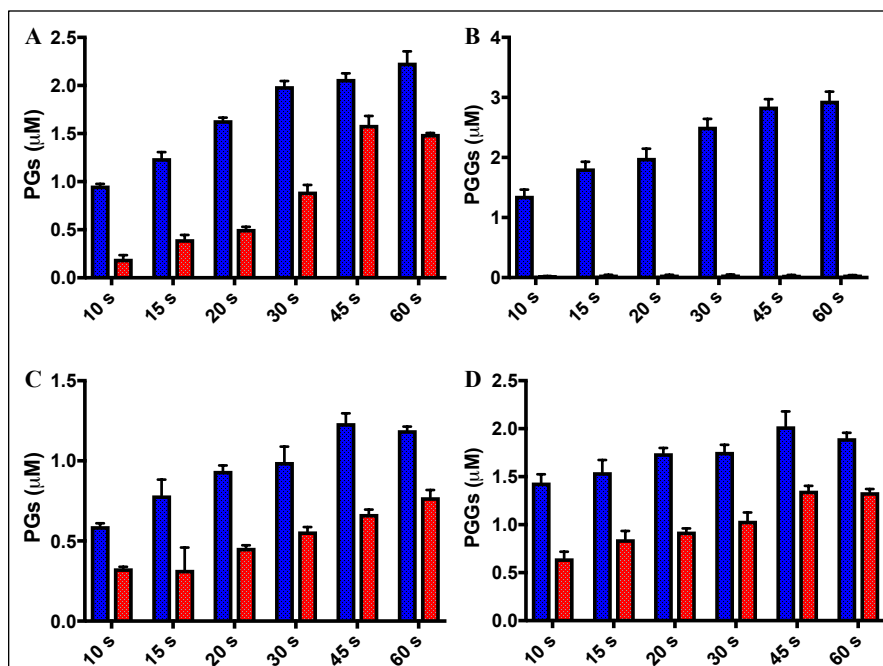


**Figure 19.** Time course assay for COX-2 substrate oxygenation in the presence of 100 nM mefenamic acid (MA) (red) or DMSO (blue). 15 nM mCOX-2 was reconstituted with 30 nM heme and pre-incubated at 37 °C for 15 mins in the absence or presence of inhibitor. (A) AA oxygenation in the absence of PPHP. (B) 2-AG oxygenation in the absence of PPHP. (C) AA oxygenation in the presence of PPHP. (D) 2-AG oxygenation in the presence of PPHP.

#### *Mefenamic Acid Acts as a Reducing Co-substrate of COX-2 Heme*

Based on the previous experiments, it appeared that mefenamic acid affects the lag phase of the enzymatic reaction, and that it does so by a mechanism in addition to simply slowing the rate of the reaction, as indicated by the fact that PPHP has a much greater effect on the potency of mefenamic acid than ibuprofen. One possibility is that mefenamic acid acts as a reducing co-substrate of the oxidized heme prosthetic group. Mefenamic acid's susceptibility to oxidation has been illustrated by its cytochrome P450-mediated conversion to quinoneimines (145). In fact, Malkowski and co-workers determined that mefenamic acid and other fenamate inhibitors can act as reducing co-substrates that reset the heme of activated COX-2 to its resting ferric state, and they can destabilize the catalytic tyrosyl radical that connects the enzyme's peroxidase activity to its cyclooxygenase activity. Their experiments determined that the fenamates bind in an inverted orientation in the COX active site, forming interactions with Tyr-385, and they hypothesized that these interactions could facilitate tyrosyl radical destabilization. Due to the greater

hydroperoxide tone required to activate COX-2 for 2-AG oxygenation than AA oxygenation, they further proposed that mefenamic acid-mediated substrate-selective inhibition could be explained by its ability to suppress peroxide-dependent enzyme activation (91). To further explore this hypothesis and to test its applicability to other classes of inhibitors, additional experiments were performed to observe the oxidation state of the heme in the presence of mefenamic acid or ibuprofen.

In order to investigate whether mefenamic acid or ibuprofen could function as a co-substrate to reduce the heme back to its resting state, the Soret peak absorbance of the heme moiety was monitored with UV-Visible spectroscopy. When heme is oxidized by the peroxide, there is a shift in absorbance from 409 to 415 nm. If the heme is returned to its reduced ferric state, a stronger absorbance at 409 nm will be observed. To initially test the effect of inhibitors on the heme oxidation state, various concentrations of either ibuprofen or mefenamic acid were pre-incubated with 1  $\mu\text{M}$  mCOX-2 and 2  $\mu\text{M}$  heme. The oxidation of the heme was initiated by adding 15  $\mu\text{M}$   $\text{H}_2\text{O}_2$ , and the absorbance at 409 nm was recorded. Every 20 s thereafter, the absorbance at 409 nm was recorded again. The incubation of ibuprofen with COX-2 elicited no increase in absorbance at 409 nm, indicating that it was unable to reduce the heme back to its ferric state. Similarly, incubating either 100 nM or 1  $\mu\text{M}$  mefenamic acid with the enzyme had no effect on absorbance at 409 nm. However, increasing the concentration of inhibitor to 10  $\mu\text{M}$  or higher resulted in net heme reduction (Figure 20). This result is not surprising, as an excess of peroxide concentration in comparison to mefenamic acid concentration can reoxidize the heme.



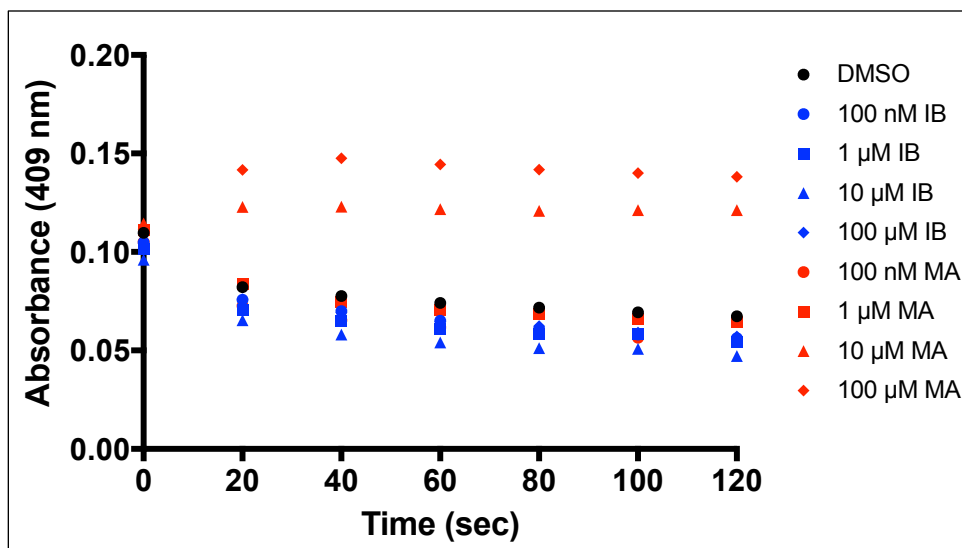


**Figure 20.** Heme oxidation in the presence of either ibuprofen (IB) or mefenamic acid (MA) and 1  $\mu$ M COX-2 and 2  $\mu$ M heme. Soret peak absorbance at 409 nm was recorded as a function of time following addition of 15  $\mu$ M  $H_2O_2$ .

A similar experiment continuously monitored absorbance at 409 nm following heme oxidation with an increased concentration of  $H_2O_2$  (50  $\mu$ M) and concentrations of each inhibitor up to 500  $\mu$ M. Ibuprofen still showed no ability to reduce the heme back to its resting state, whereas higher concentrations of mefenamic acid (100 and 500  $\mu$ M) increased the soret peak absorbance at 409 nm.

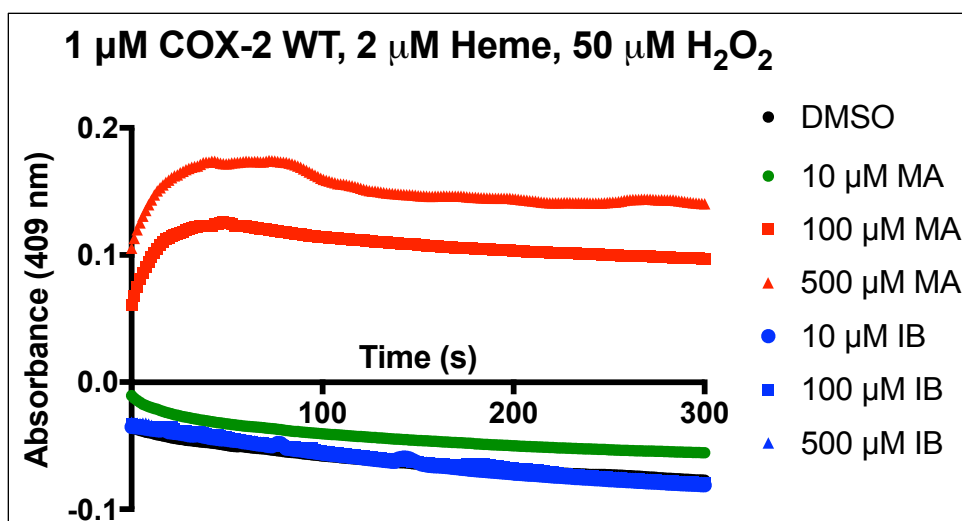


**Figure 21.** Heme oxidation in the presence of either ibuprofen (IB) or mefenamic acid (MA) and 1  $\mu$ M COX-2 and 2  $\mu$ M heme. Soret peak absorbance at 409 nm was recorded as a function of time following addition of 50  $\mu$ M  $H_2O_2$ .

## Discussion

Even though the concept of substrate-selective inhibition of COX-2 by various NSAIDs has been well studied, there are underlying mechanistic properties that are still unclear. As noted above, the original model proposed to explain substrate-selective inhibition of COX-2 is that high affinity, time-dependent binding of inhibitor to the allosteric site blocks 2-AG oxygenation whereas lower affinity, rapidly reversible binding of inhibitor to the catalytic site is required to block AA oxygenation (88). That model was called into question, at least in the case of fenamic acid inhibitors, when Orlando et al. proposed that substrate-selective inhibition could be explained on the basis of the fenamates' ability to act as reducing co-substrates for the enzyme (144). The requirement for higher peroxide tone to sustain 2-AG oxygenation would make it more susceptible than AA oxygenation to this mechanism of inhibition (90). This model predicts that addition of exogenous hydroperoxide should reduce inhibitor potency, and that the effect should be greater for 2-AG oxygenation than for AA oxygenation, thus reducing or eliminating the differential potency of inhibition for 2-AG versus AA. The experiments performed here were designed to further explore these distinct, but not mutually exclusive models.

### *Mefenamic Acid Acts as a Reducing Co-substrate of COX-2 Heme*

The model proposed by Orlando et al. depends on the ability of the fenamates to act as reducing co-substrates for the enzyme. To determine if this mechanism applies to other substrate-selective inhibitors, the abilities of mefenamic acid and ibuprofen to serve as co-reductants of COX-2 were compared. The POX and COX reactions are chemically linked together through the heme prosthetic group, which is oxidized by peroxides and reduced by the abstraction of an electron from Tyr-385 to initiate the COX reaction. A subsequent one electron reduction by the reducing co-substrate returns the heme back to its resting ferric state. To investigate the oxidation state of the heme moiety in the POX active site in the presence of each inhibitor, UV-Visible spectroscopy was utilized to observe the soret peak of the heme prosthetic group. The pre-incubation of the enzyme with ibuprofen did not affect the soret peak absorbance shift after the addition of peroxide. However, the addition of mefenamic acid elicited an increase in the soret peak absorbance at

409 nm, indicating that the inhibitor was acting as a co-substrate to reduce the heme back to its ferric state. As could be predicted, only concentrations of mefenamic acid in excess of peroxide concentration were able to achieve net reduction of the heme. Therefore, mefenamic acid functions as a reducing co-substrate of the heme, which likely plays a role in its mechanism of inhibition, in agreement with previous experiments (91). The mechanism by which mefenamic acid disrupts the activation state of COX-2 certainly depends on its susceptibility to oxidation. In addition, mefenamic acid binds to COX-2 in an inverted orientation with its carboxylate forming interactions with Ser-530 and the catalytic Tyr-385. It is possible that this proximity to Tyr-385 enables mefenamic acid to directly interfere with tyrosyl radical formation or to promote radical quenching. Ibuprofen shares neither of these traits, and consistently, does not act as a COX-2 co-reductant. Thus, these experiments confirm the original reports of Orlando et al. that mefenamic acid can reduce the heme of COX-2, but they also demonstrate that this mechanism does not apply to all substrate-selective inhibitors. It is also important to note that COX-2 activity is typically measured in the presence of excess phenol, which serves as reducing co-substrate for the enzyme. Consequently, it is not clear to what degree mefenamic acid or any other inhibitor usurps this function under standard assay conditions.

#### *Substrate-Selective Inhibition of Cyclooxygenase-2 by Mefenamic Acid and Ibuprofen*

The experiments that gave rise to the data in Table 3 were designed to more thoroughly evaluate the original model of substrate-selective inhibition in the context of a potential role for peroxide tone. The data support some, but not all of the original model. In the absence of preincubation, there is a marked difference in potency for inhibition of AA versus 2-AG oxygenation for both ibuprofen and mefenamic acid whether or not PPHP is present. This suggests that, consistent with the model, each inhibitor is interacting with the enzyme at different sites to block oxygenation of AA versus 2-AG. However, the data also reveal a significant time-dependency for AA oxygenation that is not in agreement with prior reports. An understanding of this discrepancy, obviously of concern, may lie in the different methods used to assay enzyme activity. In the current study, COX-2 activity was measured on the basis of product formation at a

fixed time point using a relatively short reaction time of 10 s. The addition of PPHP was used to eliminate the lag phase of the reaction, so that full enzyme activity would be achieved throughout that 10 s period. Previous experiments that were used to develop the original model of substrate-selective inhibition quantified AA oxygenation from O<sub>2</sub> uptake using an oxygen electrode, a method that monitors reaction progress on a continuous basis. As no hydroperoxide was included in the reaction mixtures in these studies, reaction rate was quantified on the basis of the most rapidly descending portion of the O<sub>2</sub> concentration curve following the lag phase. This method, which has been widely used to assay COX activity, suffers from the fact that no effort is made to control for variation in enzyme activation or inactivation rates. Thus, there is no way to know whether or not the measured rate is a true reflection of the initial rate of the enzymatic reaction, and one cannot be assured that steady state is ever approximated. The assay used here attempted to eliminate some of these variables, but it is not currently known if this difference in methodology can explain the discrepant results. Regardless of the source of the differences, however, the current data suggest that for both AA and 2-AG inhibition and for both ibuprofen and mefenamic acid, the enzyme forms a more tightly bound complex upon preincubation with the enzyme. Ironically, this effect (increase in potency) was greater for inhibition of AA than for 2-AG, so that preincubation reduced, to some extent, the differential observed between the IC<sub>50</sub> values for inhibition of the two substrates for both inhibitors. In other words, substrate-selectivity was reduced by preincubating enzyme with inhibitor for both ibuprofen and mefenamic acid.

PPHP had a significant effect on the potencies of both inhibitors when the enzyme had been preincubated with the inhibitors before adding substrate. Presumably, this corresponds to the most potent enzyme-inhibitor complex that can be formed. In the case of 2-AG, inhibitor potency was always lower in the presence of PPHP, and the effect was greater for mefenamic acid than for ibuprofen. These results are consistent with the ability of inhibitors to impede peroxide-dependent enzyme activation as proposed by Orlando, et al (144). In the case of ibuprofen, the effect of the inhibitor is likely due to its ability to slow activation simply by slowing the reaction, whereas mefenamic acid can also directly interfere with activation by serving as a reducing co-substrate. In contrast, the effects of PPHP on inhibition of AA

oxygenation are not straight-forward. PPHP increased the potency of ibuprofen when AA was the substrate, so inclusion of PPHP essentially eliminated the differential in  $IC_{50}$  between AA and 2-AG oxygenation for ibuprofen, thus apparently eliminating substrate-selective inhibition. This would appear to support the hypothesis of Orlando, et al, that substrate-selective inhibition is dependent on peroxide tone. However, the PPHP-mediated increase in potency of ibuprofen for AA oxygenation is totally inconsistent with this model. In the case of mefenamic acid, PPHP decreased the potency of inhibition of AA oxygenation, as would be expected, but that decrease (>700-fold) was greater than the decrease observed for 2-AG oxygenation (~7-fold). Thus, PPHP actually increased the differential in  $IC_{50}$  values between AA and 2-AG oxygenation rather than decreasing it, as the model proposed by Orlando, et al would predict.

### Conclusions

Kinetic evaluation of the COX reaction is complicated by the requirement for product-dependent activation, suicide inactivation, and the presence of two functionally distinct binding sites that can accommodate both inhibitors and substrates. From the experiments described here, preincubation time-dependence and peroxide tone affected the differences in potency for AA versus 2-AG, and this was true for both ibuprofen and mefenamic acid. The results both partially support and call into question prior models of substrate-selective inhibition. Notably, inhibition of AA oxygenation by both ibuprofen and mefenamic acid was found to be time-dependent to a greater degree than inhibition of 2-AG oxygenation. Furthermore, although a role for peroxide tone in substrate-selective inhibition was confirmed, the effects of PPHP on the potencies of each inhibitor were not totally consistent with expectations, and the importance of this mechanism varies between inhibitors. Thus, these experiments have raised as many questions as they have answered, and further work will be required to fully explain the mechanism(s) of substrate-selective inhibition.

## CHAPTER IV

### DUAL CYCLOOXYGENASE-FATTY ACID AMIDE HYDROLASE INHIBITOR EXPLOITS NOVEL BINDING INTERACTIONS IN THE CYCLOOXYGENASE ACTIVE SITE

Numerous inhibitors have been developed for the COX enzymes to inhibit oxygenation of their substrates. The inhibition of COX-1 prevents the formation of PGs, which are primarily pro-inflammatory mediators. Moreover, the inhibition of COX-2 prevents formation of PGs, and prevents the oxygenation of 2-AG, which is an endogenous agonist for the CB<sub>1</sub> and CB<sub>2</sub> receptors. More recently, dual inhibitors of the COX-2 enzyme and other enzymes that metabolize bioactive lipids to pro-inflammatory mediators have been developed. These inhibitors target COX-2 and 5-LOX, COX-2 and sEH, and COX-2 and fatty acid amide hydrolase (FAAH) (146-148). The use of NSAIDs like flurbiprofen can often cause undesirable side effects, particularly gastrointestinal toxicity. By inhibiting both COX-2 and FAAH, it is possible to circumvent this toxicity by preventing the producing of PGs, while preventing the hydrolysis of AEA to AA and ethanolamide. AEA, like 2-AG, is an endogenous agonist of the cannabinoid receptors and exhibits analgesic effects *in vivo*. The data presented herein described the inhibition of COX-2 by ARN2508, a dual COX-2•FAAH inhibitor. Based on structural and kinetic data, it was determined that ARN2508 adopts a unique binding pose in the COX-2 active site which has not been observed for other NSAIDs. Ser-530 and Gly-533 in the active site are also key determinants in its inhibitory kinetics.

## Results

### *Structural analysis of COX-2 with (S)-ARN2508*

To investigate the structural characteristics of ARN2508 in complex with mCOX-2, a crystal structure with the (*S*)-enantiomer was solved at a resolution of 2.27 Å by molecular replacement using the high-resolution monomer model of mCOX-2 in complex with naproxen (PDB: 3NT1). The potency of the (*R*)-enantiomer for mCOX-2 inhibition is low, similarly to (*R*)-flurbiprofen. Hence, a crystal structure for (*R*)-ARN2508 was not solved. ARN2508 is a compound consisting of a common biphenyl core, a part of

the NSAID flurbiprofen for COX inhibition and a part of the FAAH inhibitor, URB597 (Figure 22). The propionic acid group needed for COX inhibition is attached to one side of the biphenyl core, whereas a carbamate substituent necessary for FAAH inhibition is attached to the opposite side of the central core. Various hydrophobic substituents were also attached to the distal carbamate nitrogen and tested for their ability to inhibit COX-2.

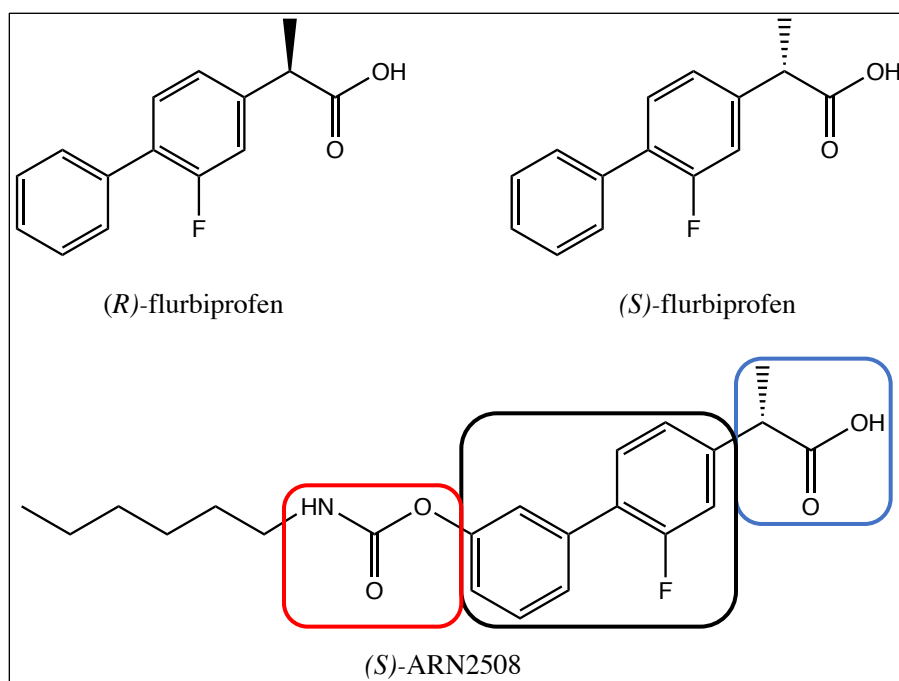


**FIGURE 22.** Chemical structures of (*R*)- and (*S*)-flurbiprofen and (*S*)-ARN2508. The alkyl carbamate substituent of ARN2508 is needed for FAAH inhibition (red box). The propionic acid moiety is needed for COX inhibition (blue box). ARN2508 also contains a common biphenyl core for inhibition of both enzymes (black box).

From the crystal structure of (*S*)-ARN2508 in complex with mCOX-2, it was observed that the flurbiprofen moiety of ARN2508 sits in the hydrophobic channel of the enzyme's active site with the same binding mode that is adopted by flurbiprofen in COX-1 and COX-2 (51,89,149). Thus, the carboxylate moiety of ARN2508 lies at the constriction of the active site, ion-pairing to Arg-120 and hydrogen-bonding to Tyr-355, and the aromatic rings project upwards toward Tyr-385. However, hydrogen bond formation with ARN2508's carbamate group requires an upward displacement of the side chain of Ser-530 in the COX-2•(*S*)-ARN2508 complex relative to its position in the COX-2•flurbiprofen complex. Additional hydrogen bonds form between Tyr-385 and the oxygen atoms of ARN2508's carbamate group. The alkyl

chain of ARN2508 reaches deeply into the distal portion of the cyclooxygenase channel between helices 2 and 17, making hydrophobic interactions with various residues including Phe-205, Phe-209, Phe-210, Val-228, Ile-341, Val-344, Ile-377, Phe-381, and Leu-534 (Figure 23).

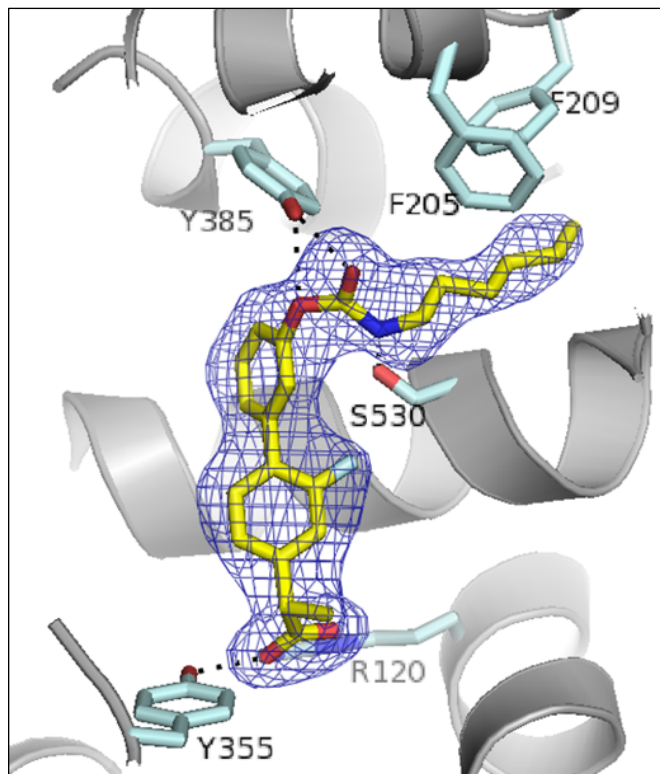


**Figure 23.** Crystal structure of (*S*)-ARN2508 in the COX-2 channel. The OMIT  $F_o-F_c$  map is contoured at  $3\sigma$ ; the inhibitor is colored in yellow sticks and the interacting residues of COX-2 are illustrated in light cyan. Potential H-bonds are presented with dashed lines.

#### *Potency, isoform-selectivity, and substrate-selectivity of ARN2508 enantiomers*

It was previously reported that racemic ARN2508 has an  $IC_{50}$  value of approximately 12 nM for COX-1 and 430 nM for COX-2 (147). To further assess the potency of the inhibitor, each enantiomer was individually tested for both ovine COX-1 (oCOX-1) and COX-2 inhibition. The results (Figure 24) indicated that the potency of the (*S*)-enantiomer of ARN2508 ( $IC_{50} = 7.0$  nM) for COX-1 inhibition is much greater than that of the (*R*)-enantiomer ( $IC_{50} = 4.6$   $\mu$ M). Similarly, using 5  $\mu$ M AA as substrate, the (*S*)-enantiomer was the more potent of the two against COX-2, achieving complete inhibition of AA oxygenation with an  $IC_{50}$  of approximately 39 nM (Figure 25A), whereas the (*R*)-enantiomer inhibited the



enzyme by ~50% at 10  $\mu\text{M}$  and failed to reach complete inhibition at the highest concentration tested (100  $\mu\text{M}$ ). Thus, as previously reported for the racemic mixture, each enantiomer of ARN2508 exhibits a small degree of COX-1 selectivity. The potency of the (*S*)-enantiomer for 2-AG oxygenation by COX-2 ( $\text{IC}_{50} = 21 \text{ nM}$ ) was greater than that for AA oxygenation, but only by approximately two-fold (Figure 25B). In contrast, (*R*)-ARN2508 exhibited an ~30-fold higher inhibitor potency for 2-AG ( $\text{IC}_{50} = 0.34 \mu\text{M}$ ) versus AA oxygenation and completely blocked 2-AG oxygenation. These results indicate that the (*R*)-enantiomer is a substrate-selective COX-2 inhibitor.

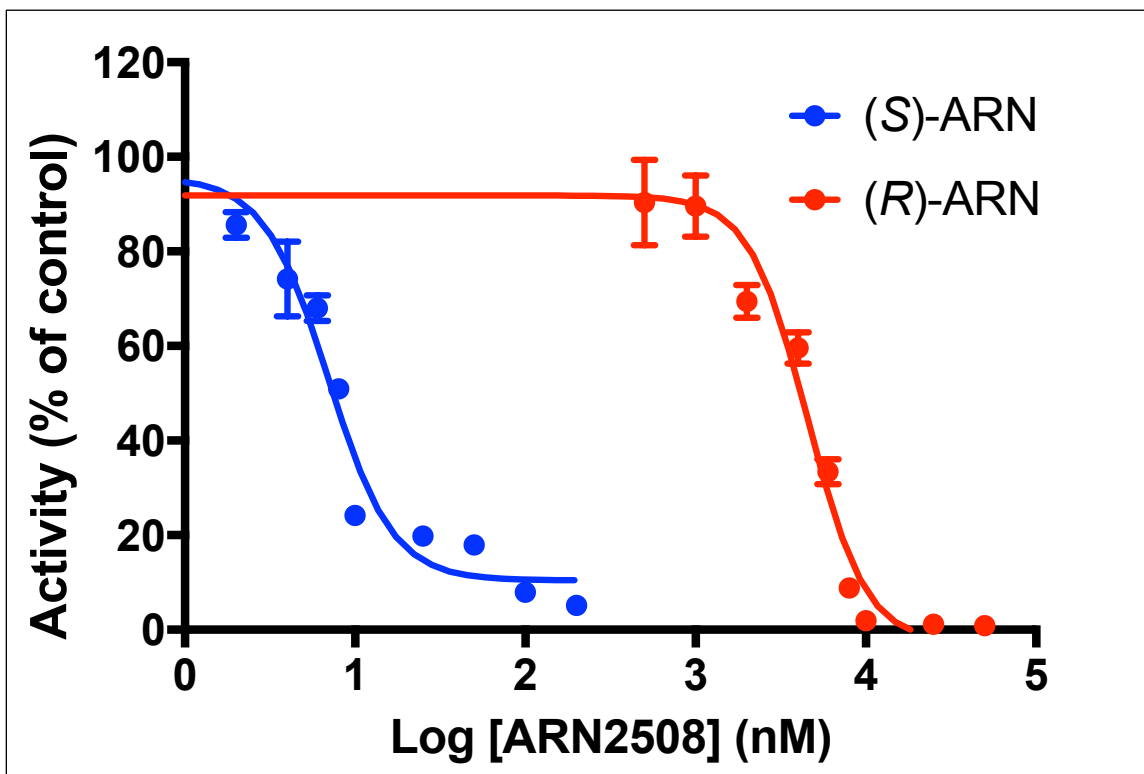


**Figure 24.** Inhibition of oCOX-1 with ARN2508. Oxygenation of 5  $\mu\text{M}$  AA by oCOX-1 was assessed by quantification of enzymatic product formation utilizing LC-MS/MS. Enzyme was preincubated with each enantiomer of ARN2508 for 10 min. AA (5  $\mu\text{M}$ ) was allowed to react for 10 s before quenching with organic solvent containing deuterated internal standards. Results are the mean  $\pm$  S.D. of triplicate determinations.

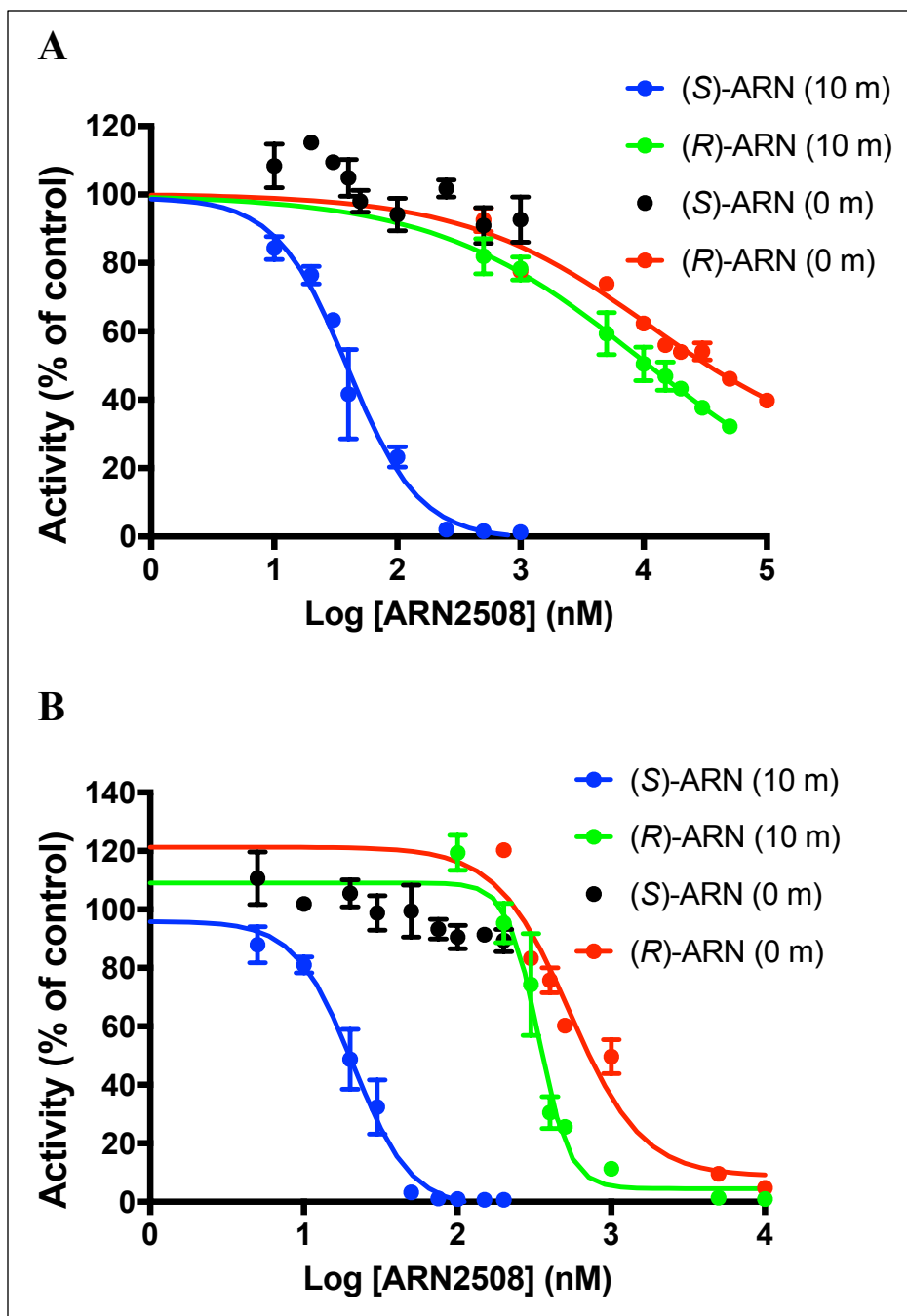


**FIGURE 25.** Inhibition of mCOX-2 with ARN2508, with or without pre-incubation. Oxygenation of 5  $\mu$ M AA (A) or 5  $\mu$ M 2-AG (B) by mCOX-2 was assessed by quantification of enzymatic product formation utilizing LC-MS/MS. Each enantiomer of ARN2508 was pre-incubated for 10 min (10 m) or added simultaneously (0 m) with substrate. Each substrate was allowed to react for 10 s before quenching with organic solvent containing deuterated internal standards. Results are the mean  $\pm$  S.D. of triplicate determinations.

### *Time-dependency of AA and 2-AG oxygenation inhibition by ARN2508 enantiomers*

As most highly potent COX inhibitors are time-dependent, initial experiments included an arbitrarily chosen 10 min preincubation period prior to substrate addition. To further explore the time-dependency of ARN2508, various concentrations of each enantiomer were added simultaneously with either AA or 2-AG to COX-2, reactions were quenched after 10 s, and products were analyzed using LC-MS/MS. The data indicate that COX-2 inhibition by the (*R*)-enantiomer is essentially time-independent for both AA and 2-AG oxygenation, as preincubation had minimal effect on the observed IC<sub>50</sub> values or extent of inhibition observed. In contrast, COX-2 inhibition by the (*S*)-enantiomer is strongly time-dependent, as indicated by IC<sub>50</sub> values in the nM range for both AA and 2-AG oxygenation following preincubation, but failure to reach even 50% inhibition in the absence of preincubation at the concentrations tested. (Figure 25).

To further assess the kinetic mechanism of ARN2508-mediated COX-2 inhibition, various concentrations of the (*S*)-enantiomer were preincubated with wild-type COX-2 for different time periods, and the activity of the enzyme was measured. A plot of enzyme activity versus time for each inhibitor concentration exhibited pseudo-first order kinetics (Figure 26A), and the observed first order rate constants for each curve ( $k_{obs}$ ) were plotted against inhibitor concentration. The resulting data (Figure 26B) failed to yield the hyperbolic curve that is expected from the two-step model. A possible explanation is that the two-step model is correct, but insufficient concentrations of inhibitor were used to fully delineate the hyperbola. Indeed, fitting of the data to this model yields a first step dissociation constant of 220  $\mu\text{M}$  and inhibition rate constant of 41  $\text{min}^{-1}$ , corresponding to an overall kinetic efficiency ( $k_{on}/K_1$ ) of 0.18  $\text{min}^{-1}\cdot\mu\text{M}^{-1}$ . These values are, at best, only estimates, as evaluation of much higher inhibitor concentrations is necessary to fully define the curve. Unfortunately, solubility limitations prevented this evaluation. An alternative explanation is that the plot is linear rather than hyperbolic, suggesting that ARN2508 does not follow the typical two-step kinetic mechanism. In this case, the binding process would more likely occur in a single step, or if multistep, the first step is rate-limiting. The slope of the line (0.11  $\text{min}^{-1}\cdot\mu\text{M}^{-1}$ ) provides an estimate of the second order rate constant for the binding of inhibitor to enzyme in this model. Regardless

of which model is correct, the formation of the inhibitory (S)-ARN2508•COX-2 complex occurs substantially more slowly than formation of the inhibitory complex of (S)-flurbiprofen with COX-2, which exhibits a reported overall kinetic efficiency of  $6 \text{ min}^{-1} \cdot \mu\text{M}^{-1}$  (150).

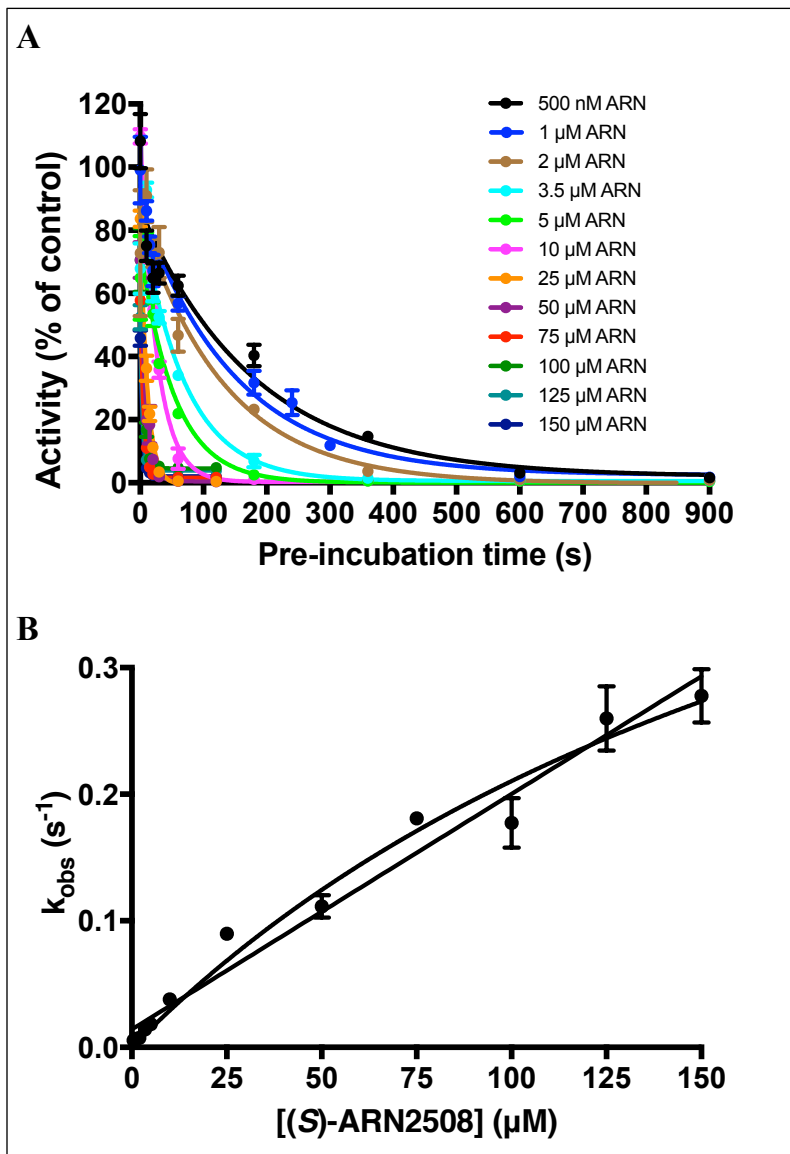


**FIGURE 26.** Kinetics of the time-dependent inhibition of mCOX-2 by (S)-ARN2508. (A) Various concentrations of (S)-ARN2508 were incubated with wild-type mCOX-2 for the indicated preincubation times before the addition of 5  $\mu\text{M}$  AA. Each enzymatic reaction proceeded for 10 s before being quenched with organic solvent containing deuterated internal standards. Oxygenation of AA was assessed by quantification of enzymatic product formation utilizing LC-MS/MS. (B) Observed first order rate constants were plotted against inhibitor concentration to obtain the kinetic parameters for the enzyme-substrate interaction. Both linear and hyperbolic fits are shown. Results are the mean  $\pm$  S.D. of triplicate determinations.

### Importance of Tyr-355 in determining the potency of ARN2508

The Tyr-355 residue of COX-2 is within hydrogen-bonding distance of the carboxylate group of ARN2508. To evaluate the importance of this interaction, ARN2508 was tested for its ability to inhibit AA oxygenation by Y355F. As seen in Figure 27, the Y355F mutation had only modest effects on the kinetics of the enzyme with AA as substrate. The potency of (*S*)-ARN2508 decreased slightly for the Y355F mutant, as indicated by an approximately 2.5-fold increase in IC<sub>50</sub>. The potency of the (*R*)-enantiomer decreased more substantially; failure to achieve more than 50% inhibition at the highest inhibitor concentration tested (50 μM) precluded determination of an IC<sub>50</sub> value. These findings differ significantly from those obtained with other previously reported carboxylate-containing NSAIDs, including indomethacin, meclofenamic acid, and ibuprofen which exhibit substantially reduced potency against the COX-2 Y355F enzyme, and they support the hypothesis that hydrogen bond formation with Tyr-355 contributes only modestly to the binding affinity of (*S*)-ARN2508.

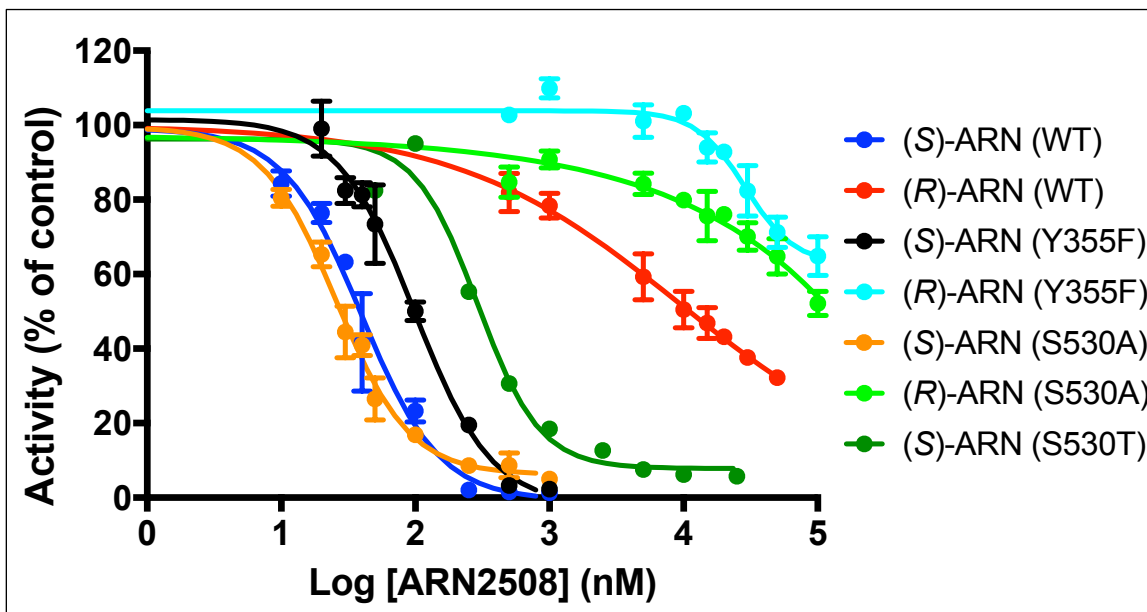


**FIGURE 27.** Inhibition of mCOX-2 mutants with ARN2508. Oxygenation of 5 μM AA by wild-type, Y355F, S530A, or S530T mCOX-2 enzymes was assessed by quantification of enzymatic product formation utilizing LC-MS/MS. Each enzyme was preincubated with the indicated enantiomer of ARN2508 for 10 min. AA was allowed to react for 10 s before quenching with organic solvent containing deuterated internal standards. Results are the mean ± S.D. of triplicate determinations.

### Role of Ser-530 in ARN2508 binding to COX-2

The presence of a reactive carbamoyl group and the known ability of ARN2508 to covalently modify FAAH suggested the possibility that the inhibitor also covalently modifies COX-2. The proximity of the carbamoyl group of ARN2508 to Ser-530 observed in the crystal structure led to the hypothesis that a covalent modification might occur at that residue in solution. However, LC-MS/MS analysis of the tryptic peptides of COX-2 that had been incubated with the inhibitor failed to reveal the mass shift expected from the addition of ARN2508 to Ser-530. Despite obtaining ample sequence coverage (84%) that includes Ser-530, no detectable modifications were observed (Figure 28). These results do not support covalent bond formation between the inhibitor and Ser-530.

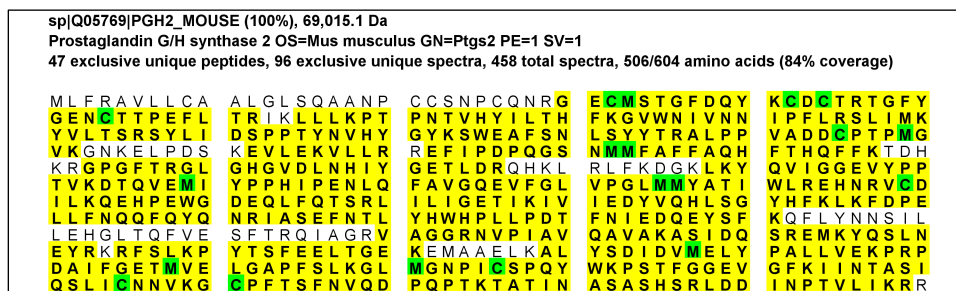


**FIGURE 28.** Peptide coverage of digested wild-type COX-2 following incubation with (*S*)-ARN2508. Peptide coverage of 84% was obtained from trypsin digestion of wild-type COX-2 following incubation with (*S*)-ARN2508. The peptide containing Ser-530 (PRPD AIFGETMVELGAPFSLK) was identified, but no mass shift of the peptide as would be expected from covalent modification by inhibitor was observed.

Although the data did not support covalent bond formation between the carbamoyl group of (*S*)-ARN2508 and Ser-530 of COX-2, the crystal structure revealed the presence of a hydrogen bond between these moieties. To determine the importance of this interaction to ARN2508's potency and to further rule out a covalent interaction, the ability of each enantiomer to inhibit a COX-2 S530A mutant enzyme was evaluated. As in the case of Y355F, the S530A mutation had minimal effect on enzymatic activity using AA as substrate. Furthermore, this mutation did not have a major effect on the potency of (*S*)-ARN2508 and caused only a mild reduction in the potency of the (*R*)-enantiomer using AA as substrate and a 10 min preincubation (Figure 27). These findings do not support the hypothesis that an interaction (covalent or noncovalent) with the hydroxyl group of Ser-530 plays a significant role in ARN2508's potency.

Although the potency of (*S*)-ARN2508 (as measured by IC<sub>50</sub> values) was nearly identical for wild-type and S530A COX-2 following our standard 10 min preincubation time, the position of S530A at the bend of the active site suggested that this residue might interfere with the insertion of ARN2508's hydrophobic tail into the upper part of the channel. To test this hypothesis, the rate of inhibition of the mutant to that of the wild-type enzyme at two concentrations of (*S*)-ARN2508 was compared (Figure 29A). The data clearly showed a much higher rate of inhibition in the case of the mutant enzyme. Unfortunately, the very rapid rates at high (*S*)-ARN2508 concentrations precluded a full kinetic analysis.

For a time-dependent inhibitor, the measured IC<sub>50</sub> value is dependent on the length of the preincubation period. Longer preincubations provide time for the enzyme-inhibitor complex to form, making the inhibitor appear more potent and reducing the IC<sub>50</sub>. Consistently, when the potency of (*S*)-ARN2508 was determined for S530A and wild-type COX-2 following a 30 s preincubation period, the IC<sub>50</sub> values obtained for both enzymes were substantially higher (0.31 μM for S530A and 4.51 μM for wild-type) than those obtained following a 10 min preincubation. Notably, at this short preincubation time, (*S*)-ARN2508 is significantly more potent against the mutant than the wild-type enzyme. This is due to the much more rapid development of inhibition with the mutant (Figure 30).

Since the S530A mutant decreases steric bulk from the bend in the COX-2 active site and eliminates hydrogen bonding with the inhibitor, we evaluated the effects of a COX-2 S530T mutation on inhibitor potency to observe how additional steric bulk in that region might alter the rate or potency of inhibition. This mutation had substantial effects on enzyme activity, both raising the K<sub>M</sub> (3-fold) and lowering the V<sub>max</sub> (3-fold). The mutation was also associated with a reduction in potency of (*S*)-ARN2508. Somewhat unexpectedly, however, the rate of inhibition of S530T observed with two concentrations of (*S*)-ARN2508 was faster than that of the wild-type enzyme (Figure 29B). These results suggest that the larger threonine residue does not substantially impede the inhibitor's access to the top channel of the COX-2 active site.

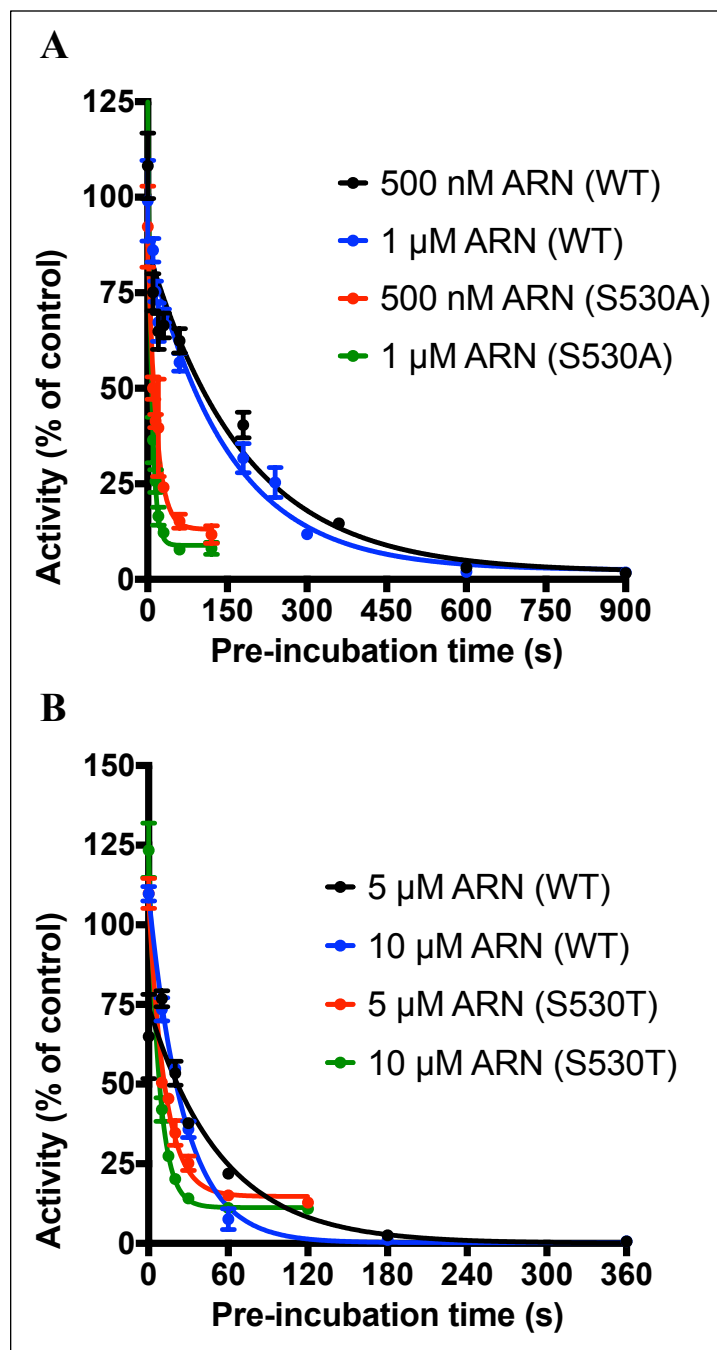


**FIGURE 29.** Kinetics of the time-dependent inhibition of S530A and S530T mCOX-2 by (*S*)-ARN2508. (A) Two concentrations of (*S*)-ARN2508 were incubated with wild-type or S530A mCOX-2 for the indicated preincubation times before the addition of 5  $\mu$ M AA. Each enzymatic reaction proceeded for 10 s before being quenched with organic solvent containing deuterated internal standards. Oxygenation of AA was assessed by quantification of enzymatic product formation utilizing LC-MS/MS. (B) Two concentrations of (*S*)-ARN2508 were incubated with wild-type or S530T mCOX-2 for the indicated preincubation times before the addition of 5  $\mu$ M AA. Results are the mean  $\pm$  S.D. of triplicate determinations.



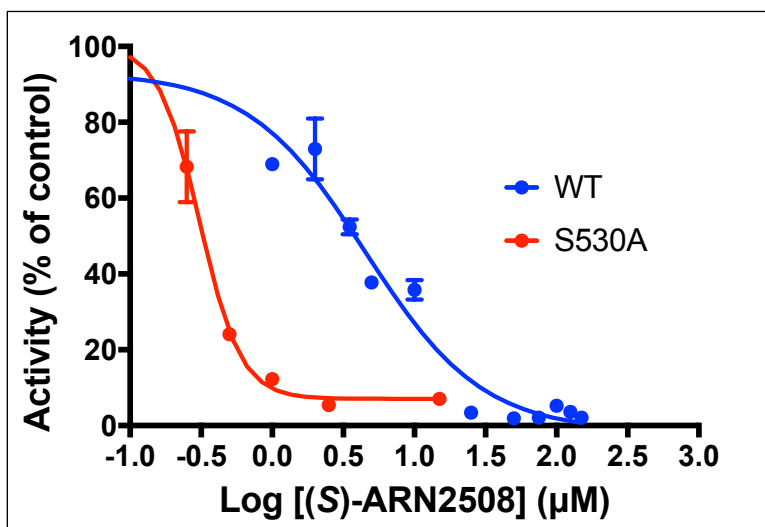


**FIGURE 30.** Dose response of (*S*)-ARN2508 with 30 s preincubation. Indicated concentrations (*S*)-ARN2508 were preincubated with either wild-type or S530A mCOX-2 for 30 s before the addition of 5 µM AA. Each enzymatic reaction proceeded for 10 s before being quenched with organic solvent containing deuterated internal standards. Oxygenation of AA was assessed by quantification of enzymatic product formation utilizing LC-MS/MS. Results are the mean ± S.D. of triplicate determinations.

#### *Inhibition of COX-2 Gly-533 mutants by (S)-ARN2508*

As observed from the crystal structure, AA binds in an L-shaped conformation with its omega tail inserted into the top channel of the COX-2 active site. Gly-533 lies near the end of the channel, and mutations of this residue to bulkier side chains inhibit the oxygenation of AA. However, Gly-533 mutants including G533A, G533V, and G533L can oxygenate the 18-carbon fatty acid  $\alpha$ -LNA (46). One of the major products formed from this reaction is 12-hydroxy-octadecatrienoic acid (12-HOTrE) (58), which contains a conjugated double bond that can be detected by UV-visible spectroscopy at 235 nm. The oxygenation of  $\alpha$ -LNA by wild-type mCOX-2 and the mutant G533L in the presence of (*S*)-ARN2508 or (*S*)-flurbiprofen was evaluated to determine if disruption of the structure of the top channel would significantly impact ARN2508's potency, due to the extension of the inhibitor's hydrophobic tail to the end of the upper active site channel. Differences were observed between the wild-type enzyme and the G533L mutant with respect to inhibition by (*S*)-ARN2508 versus (*S*)-flurbiprofen. In Figure 31, oxygenation of  $\alpha$ -

LNA by wild-type mCOX-2 is shown to be completely inhibited by 10  $\mu$ M of both (*S*)-ARN2508 and (*S*)-flurbiprofen following a preincubation of 3 min or greater. With a 1 min preincubation, there was slight substrate oxygenation in the presence of (*S*)-ARN2508, but not (*S*)-flurbiprofen. In contrast, although (*S*)-flurbiprofen completely inhibited mCOX-2 G533L following a 3 min preincubation, (*S*)-ARN2508 was only partially effective. Even following a 15 min preincubation, (*S*)-ARN2508 inhibited oxygenation by G533L COX-2 less efficiently than did (*S*)-flurbiprofen preincubated for just 1 min (Figure 31). These findings suggest that the bulky side chain of G533L interferes with the binding of (*S*)-ARN2508's side chain in the active site channel and that this binding interaction is important to the inhibitor's potency.

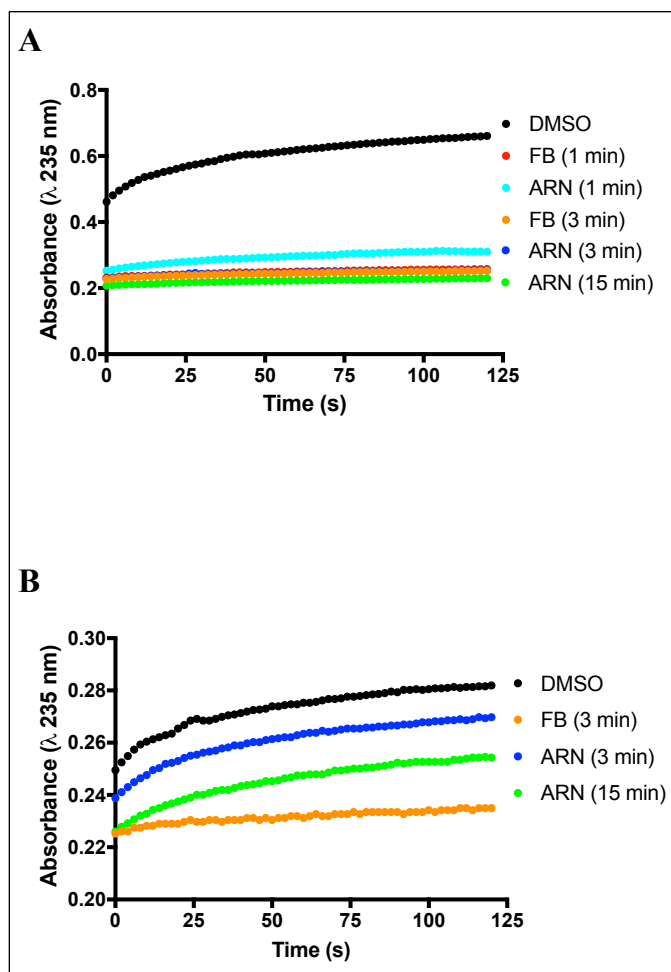


**FIGURE 31.** Kinetics of LNA inhibition by (*S*)-ARN2508 and (*S*)-flurbiprofen. (A) Wild-type mCOX-2 (200 nM monomer) with 30 nM of heme was used to oxygenate 50  $\mu$ M LNA. 10  $\mu$ M (*S*)-ARN2508 (ARN) or (*S*)-flurbiprofen (FB) from a DMSO stock were preincubated with enzyme for the indicated time before the addition of substrate. (B) G533L mCOX-2 (200 nM monomer) with 30 nM of heme was used to oxygenate 50  $\mu$ M LNA. Reactions were monitored by increasing absorbance at 235 nm.

## Discussion

ARN2508 is a designed dual inhibitor of COX enzymes and FAAH. Herein, it was shown that each enantiomer of the compound exhibits distinct kinetics of inhibition of substrate oxygenation by both COX isoforms. (*S*)-ARN2508 is a time-dependent, highly potent, tightly bound inhibitor that is slightly more potent against COX-1 than COX-2. In contrast, (*R*)-ARN2508 is a weak, rapidly reversible inhibitor of AA oxygenation that is slightly more potent against COX-1 than COX-2 and a substrate-selective inhibitor for COX-2-dependent 2-AG oxygenation. This kinetic behavior of the two ARN2508 enantiomers is similar to that of the enantiomers of its parent compound, flurbiprofen (89,150-152).

The identical enantioselectivity of ARN2508 and flurbiprofen is not surprising, as the orientation of (*S*)-ARN2508's flurbiprofen moiety in the COX-2 active site (Figure 23) is nearly identical to that observed for (*S*)-flurbiprofen in complex with COX-1 and COX-2. The  $\alpha$ -methyl group of the flurbiprofen core of ARN2508 is adjacent to Tyr-355, which forms part of the constriction at the entrance into the active site. A similar binding interaction is observed for flurbiprofen, and previous studies have indicated that Tyr-355 is involved in flurbiprofen's time-dependent inhibition (80). A clash between Tyr-355 and the  $\alpha$ -methyl group of the (*R*)-enantiomer of profen-class inhibitors has been predicted to interfere with binding, thus explaining the poor potency of these compounds (79). However, a crystal structure of (*R*)-flurbiprofen complexed with COX-2 revealed a shift in the inhibitor's carboxylate group,  $\alpha$ -carbon, and fluorophenyl ring that enables accommodation of the  $\alpha$ -methyl group with retention of polar interactions with both Arg-120 and Tyr-355. Nevertheless, the overall result is a reduction in total enzyme-inhibitor contacts that likely explains the (*R*)-enantiomer's lower potency (89). It is likely that a similar conformational change is required to accommodate the (*R*)-methyl group of (*R*)-ARN2508, providing an explanation for its reduced potency relative to that of the (*S*)-enantiomer. However, as a crystal structure of (*R*)-ARN2508 complexed with COX was not obtained, this hypothesis could not be confirmed.

Despite its structural and kinetic similarities to flurbiprofen, the alkyl carbamate substituent of ARN2508 imparts to it properties that are not observed in any other previously reported NSAID. These

include FAAH inhibition and utilization of the upper portion of the cyclooxygenase active site channel. Indeed, the crystal structure data reveal a number of interesting aspects to the binding interactions of ARN2508 in the active site of COX-2. The catalytic Tyr-385 residue forms hydrogen bonds with both oxygen atoms of the carbamate moiety of ARN2508 reminiscent of the hydrogen bond formed between Tyr-385 and the carbonyl oxygen of aspirin. This interaction places the aspirin carbonyl in a position that is hypothesized to be favorable for nucleophilic attack by the oxygen of Ser-530 and stabilizes the negatively charged tetrahedral intermediate formed in the transition state (70). However, in the COX-2•(*S*)-ARN2508 complex crystal structure, an additional interaction is observed between the amide nitrogen of ARN2508 and Ser-530, thus making a nucleophilic attack by the Ser-530 hydroxyl group on the carbonyl carbon of the inhibitor less favorable. This is consistent with previous molecular modeling and simulation studies that predicted unfavorable geometry for covalent modification of COX by ARN2508 (153) and with site-directed mutagenesis data and tryptic peptide analysis by LC-MS/MS shown here, which do not support covalent modification of Ser-530 by the inhibitor. In fact, there is no major loss of (*S*)-ARN2508 potency for S530A COX-2, suggesting that the hydrogen bond between the inhibitor and Ser-530 also plays a minimal role in inhibitor potency. Nevertheless, the S530A mutation clearly exerts a subtle effect on the enzyme-inhibitor interaction. Specifically, (*S*)-ARN2508 inhibits the S530A mutant more rapidly than the wild-type enzyme.

Although slow-binding COX inhibitors have consistently been seen to exhibit multi-step kinetic mechanisms in which one or more rapidly reversible steps is/are followed by the rate-limiting formation of a much more tightly bound enzyme-inhibitor complex (84), the structural basis for the initial enzyme-inhibitor interaction in most cases is poorly understood. For some NSAIDs, such as indomethacin and the diarylheterocycle class of COX-2-selective inhibitors, the slow step has been attributed to insertion of a portion of the molecule into a specific binding pocket in the enzyme active site (84). Such mechanistic data are not available for flurbiprofen or ARN2508. Clearly, however, the alkyl side chain of ARN2508 impacts its binding kinetics in that a longer preincubation period is required for (*S*)-ARN2508 than for (*S*)-flurbiprofen to reach the same level of inhibition. Although kinetic analysis failed to clearly delineate the

mechanism of (*S*)-ARN2508-mediated inhibition of COX-2, the available data suggest that if a classic two-step mechanism is applicable, much higher inhibitor concentrations are needed to form the initial complex for (*S*)-ARN2508 ( $K_I \approx 220 \mu\text{M}$ ) than (*S*)-flurbiprofen ( $K_I = 0.17 \mu\text{M}$ ) (150). Alternatively, the (*S*)-ARN2508-COX-2 complex may form in a single slow step or in multiple steps of which the first one is rate-limiting. The only structural difference between flurbiprofen and ARN2508 is the presence of the alkyl carbamate side chain on the latter. Thus, it is reasonable to hypothesize that insertion of ARN2508's alkyl chain into its position in the active site is responsible for their kinetic differences. Our data also support the hypothesis that Ser-530, which is present at the bend of the channel plays a role in the insertion process. Mutation of Ser-530 to Ala shortens the time required for (*S*)-ARN2508 to inhibit COX-2, whereas it does not affect the rate of binding of flurbiprofen. Hydrogen bond interactions between Ser-530 and the carbamoyl group of the inhibitor may also contribute to its COX-2 binding interaction, although removal of this hydrogen bond does not substantially alter potency as measured in our standard  $\text{IC}_{50}$  assay.

To further investigate the effects of Ser-530, we mutated it to a bulkier threonine residue. This mutation resulted in a 90% reduction in catalytic efficiency ( $k_{\text{cat}}/K_M$ ), suggesting that the added bulk significantly impairs active site structure and/or dynamics. It also resulted in a mild reduction in potency of (*S*)-ARN2508 although the rate of inhibition was, surprisingly, slightly higher than that of the wild-type enzyme (Figure 29A). Structural studies have shown that the threonine side chain of the mutant overlays one of several alternative conformations adopted by serine in the wild-type enzyme (154). This orientation must provide sufficient room for the  $\omega$ -end of the substrate to access the hydrophobic top channel. The hydroxyl group of threonine can also hydrogen bond to the inhibitor, as does that of the serine residue, based on an assessment of the previously deposited S530T crystal structure.

Our data suggest substantial importance of the nonpolar interactions established between the alkyl chain of ARN2508 and the top channel of COX-2, which is lined with hydrophobic residues. This region of the active site, where the  $\omega$ -tail of AA normally binds, has not previously been reported as the site of a COX protein-inhibitor interaction. The interactions observed in our crystal structure are consistent with

previous structure-activity relationship (SAR) studies (155), and in accordance with those predicted by molecular simulations that showed a nearly identical statistical distribution of hydrophobic contacts between COX-1 and AA when compared to COX-1 and ARN2508 (153). In the SAR studies, increasing the length of the alkyl chain up to eight carbons correlated with an increase in potency toward FAAH. However, the trend differed with respect to inhibition of COX-1 and COX-2. Short alkyl chains with two or three carbons exhibited low inhibitor potency. Increasing chain length resulted in an increase, followed by a decrease in potency for both isoforms. Inhibition of COX-1 was maximized at a chain length of six carbons, whereas that for COX-2 was optimal and similar for chain lengths of five to seven carbons. The current crystal structure revealed that the additional steric bulk of longer alkyl chains cannot be accommodated in the hydrophobic channel. Kinetic experiments with the G533L mutant of COX-2 further support the hypothesis that the alkyl chain of ARN2508 binds in the top channel and that this interaction is important to inhibitory kinetics in a way that is specific to ARN2508. In particular, a G533L mutation markedly reduces the potency of ARN2508 while having little effect on the potency of flurbiprofen. Mutation of this residue to valine is known to abolish oxygenation of AA due to the inability of the substrate to access the top channel and bind close enough to Tyr-385 to initiate the enzymatic reaction (156).

### Conclusions

COX-2 and FAAH are critical enzymes in the inflammatory response; they regulate the presence of pro-inflammatory eicosanoids and degrade endocannabinoids that have analgesic and anti-inflammatory effects. ARN2508 is a pharmacologically distinctive compound in that it can simultaneously block the activity of both enzymes. Here, it was shown that the *in vitro* efficacy of ARN2508 for inhibition of PG synthesis is primarily attributable to the (*S*)-enantiomer, whereas both enantiomers may effectively block COX-2-dependent oxygenation of endocannabinoids. In contrast, ARN2508-mediated inhibition of FAAH is not affected by the orientation of the compound's  $\alpha$ -methyl group. Rather, ARN2508 irreversibly blocks FAAH through covalent modification of the enzyme via a reaction between the carbamate moiety of the inhibitor and the catalytic Ser-241 of FAAH (157). Here, it is also shown that a covalent modification of

COX-2 by ARN2508 does not occur based on crystal structure, site-directed mutagenesis, and analysis of digested peptides by mass spectrometry. Although their mechanisms of inhibition differ, FAAH and COX enzymes both contain long, hydrophobic channels, allowing favorable binding of ARN2508 (158). In conclusion, ARN2508 inhibits COX via structural determinants contributed primarily by its flurbiprofen moiety, whereas the alkyl carbamate substituent, which is required for FAAH inhibition, imparts distinct attributes to its COX inhibitor kinetics and binding interactions.

## CHAPTER V

### EFFORTS TOWARD INVESTIGATING THE STRUCTURAL DYNAMICS OF CYCLOOXYGENASE-2 WITH CRYO ELECTRON MICROSCOPY

Multiple X-ray crystal structures of COX-2 in complex with various substrates and inhibitors have been deposited in the PDB. Although these structures have provided invaluable insight into the structural characteristics of the enzyme, X-ray crystallography is limited as a biophysical technique since it gives a more static snapshot of a molecule bound in a particular conformation to a protein. Since COX-2 is a membrane-bound enzyme, it must be initially solubilized in detergent for crystallization. Therefore, the conformational dynamics of the enzyme in a detergent solution might differ from its native membrane environment. In recent years, Cryo-electron microscopy (Cryo-EM) has improved significantly in its capability to determine the molecular structures of larger proteins and protein complexes at high resolution. This is due, in part, to the utilization and improvement of the direct electron detector and advancements in image processing (159). Cryo-EM is advantageous in that protein structures can be studied in their native or nearly native environment (160). Cryo-EM data analysis of a protein can also be combined with X-ray structures for initial modeling to generate valuable biophysical information.

Nanodiscs are lipid bilayer mimetics which have gained significant utilization in recent years for various biochemical studies. Nanodiscs consist of a bilayer of synthetic phospholipids encircled by variants of the apolipoprotein A1, also known as membrane-scaffold proteins (MSPs). Within the assembled phospholipid bilayer, membrane proteins with TM helices can embed or membrane binding domains can attach to the phospholipid head groups, similarly to their assembly in a native membrane bilayer (161). COX-2 has been reconstituted into nanodiscs to assess its biochemical function and negative stain EM confirmed that a single homodimer of COX-2 associated with one leaflet of a single nanodisc (162). To further assess the structural dynamics of COX-2, recombinant purified enzyme was reconstituted into nanodiscs and investigated using Cryo-EM in collaboration with the laboratory of Hans Hebert at the Karolinska Institutet in Huddinge, Sweden.



## Results

To prepare the COX-2-containing nanodiscs, recombinant His<sub>6</sub>-tagged enzyme was mixed with an excess of POPC phospholipids and MSP1E3D1 scaffold protein. The components were mixed at 4 °C for at least one hour. Hydrophobic Bio-beads were added to the reaction mixture to absorb detergent from the solution and initiate the self-assembly of the nanodiscs. The mixtures were stirred overnight and purified with size-exclusion chromatography. Following purification, fractions were assessed for their purity by SDS-PAGE. In Figure 32, it can be seen that two prominent bands are present from each fraction, as expected. The top band corresponds to a molecular weight of approximately 72 kDa, representing a monomer of COX-2. The bottom band corresponds to a molecular weight of approximately 30 kDa, representing the non-tagged MSP1E3D1 scaffold protein. The intensity of the MSP band is greater than that of COX-2, most likely indicative of excess nanodiscs.

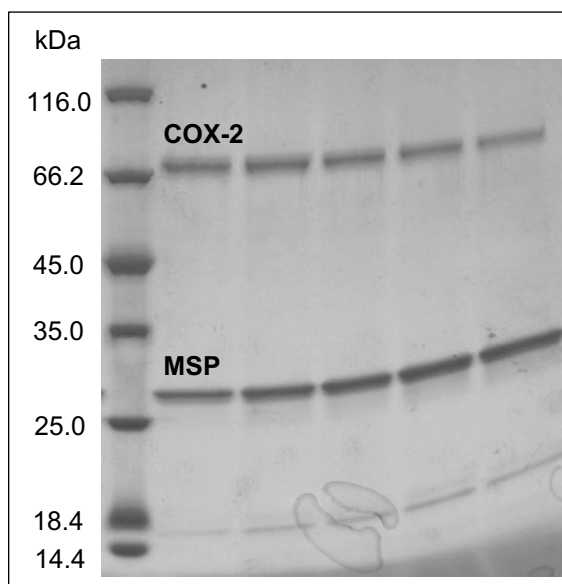


**Figure 32.** SDS-PAGE gel of COX-2 reconstituted nanodiscs with an excess of empty nanodiscs.

To initially assess the assembled nanodiscs, negative stain EM was utilized. This technique relies on a heavy metal contrasting agent to enable the visualization of protein particles by the electron microscope. Following the purification of COX-2 reconstituted nanodiscs using size-exclusion chromatography, an

aliquot was diluted to a final total protein concentration of approximately 300 ng/mL. 3  $\mu$ L of the solution was added to a glow-discharged carbon-coated copper grid. 3  $\mu$ L of a buffer containing 1% uranyl formate was subsequently added to the grid and analysis of the sample was completed using a transmission electron microscope at room temperature. Upon the investigation of the particles, most appeared to be uniform in shape, resembling empty nanodiscs (Figure 33).

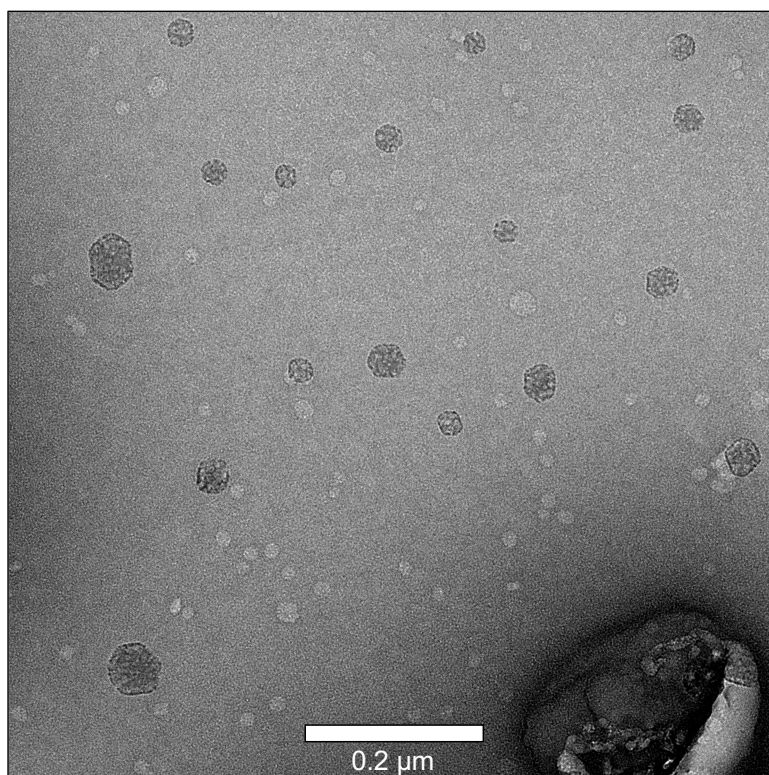


**Figure 33.** Negative stain EM of COX-2 reconstituted nanodiscs following size-exclusion chromatography. Larger, dark circles are stain contaminants, whereas smaller light circles represent nanodisc particles. An excess of empty nanodiscs was present after initial purification.

An additional COX-2 nanodisc preparation was completed utilizing an additional IMAC purification step before the final size-exclusion purification step. Again, purified COX-2 was mixed with an excess of POPC phospholipids and detergent was removed from the solution with the addition of Bio-beads. Following the self-assembly of the nanodiscs, the sample was buffer exchanged to remove excess EDTA in solution, which can affect IMAC purification. The sample was then incubated with Ni-NTA resin for at least one hour at 4  $^{\circ}$ C. Empty nanodiscs with the non-tagged MSP were washed from the resin with a similar buffer

containing 50 mM imidazole. His<sub>6</sub>-tagged COX-2 reconstituted into nanodiscs was eluted from the resin with a similar buffer containing 200 mM imidazole. Fractions including the flow-through, wash, and elution were collected and analyzed by SDS-PAGE. A majority of the excess empty nanodiscs did not bind to the resin and were found in the flow-through fraction, as well as the first wash fraction. Additional wash fractions contained very small amounts of protein. The elution fraction displayed both expected bands from COX-2 and the MSP. Therefore, the elution fraction contained purified nanodiscs containing COX-2 (Figure 34).

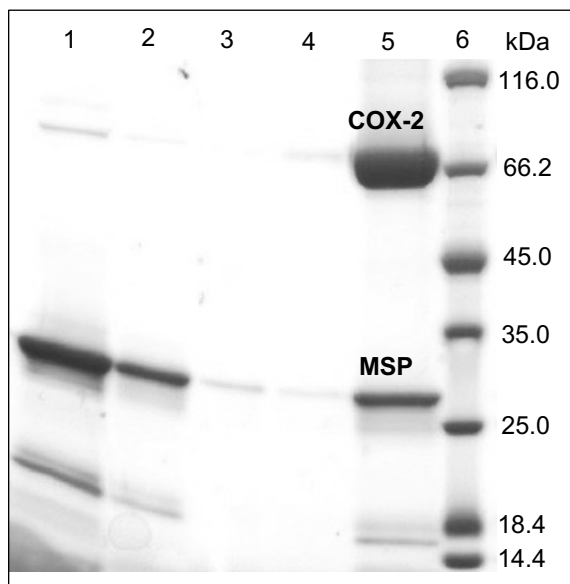


**Figure 34.** SDS-PAGE gel of purified COX-2 reconstituted nanodiscs following IMAC and size-exclusion purifications. Lanes from left to right: 1: Flow-through. 2: Wash 1. 3: Wash 2. 4: Wash 3. 5: Elution 1. 6: MW marker.

To further assess the incorporation of COX-2 into the nanodisc bilayer, a Native PAGE gel was utilized to observe the migration of the nanodisc complex under non-denaturing conditions. For the native gel, 1  $\mu$ g of total protein in each sample was loaded and analyzed with Coomassie blue staining. One sample contained recombinant COX-2 solubilized in detergent, another sample contained empty nanodiscs, and the final sample contained COX-2 reconstituted nanodisc complexes. The native gel revealed a sharp band for detergent-solubilized COX-2. However, nanodisc samples exhibited smearing in the gel due to an excess of phospholipids. A shift can be observed between the empty nanodisc sample to a higher molecular weight

in the sample consisting of the COX-2 nanodisc complex. The approximate molecular weight of the complex based on the molecular weight marker was approximately 400 kDa, thus indicating the incorporation of one COX-2 dimer into one leaflet of a single nanodisc (Figure 35).

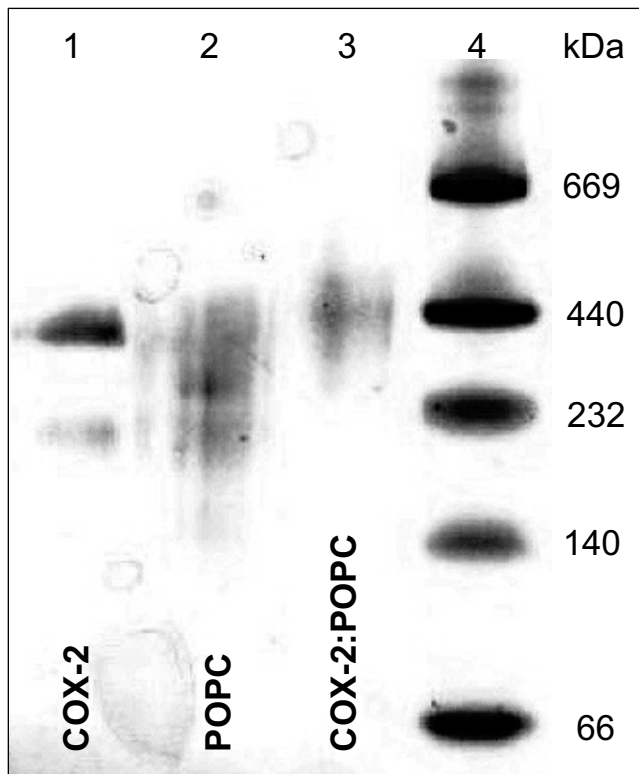


**Figure 35.** Native PAGE gel of COX-2 nanodiscs. 1  $\mu\text{g}$  of total protein was loaded in each sample. Samples from left to right include: 1: Detergent-solubilized COX-2. 2: Empty POPC nanodiscs. 3: COX-2 nanodiscs. 4: MW Marker.

Following the purification of COX-2 nanodiscs with both IMAC and size-exclusion purification, samples were initially assessed with negative stain EM. The nanodisc sample following the final purification was diluted to a concentration of approximately 7  $\mu\text{g}/\text{mL}$ , added to a carbon grid as described above, and analyzed with the electron microscope. Upon analysis, it was observed that the particles were more irregular in shape, indicating that a majority of the particles were nanodiscs containing COX-2 (Figure 36).

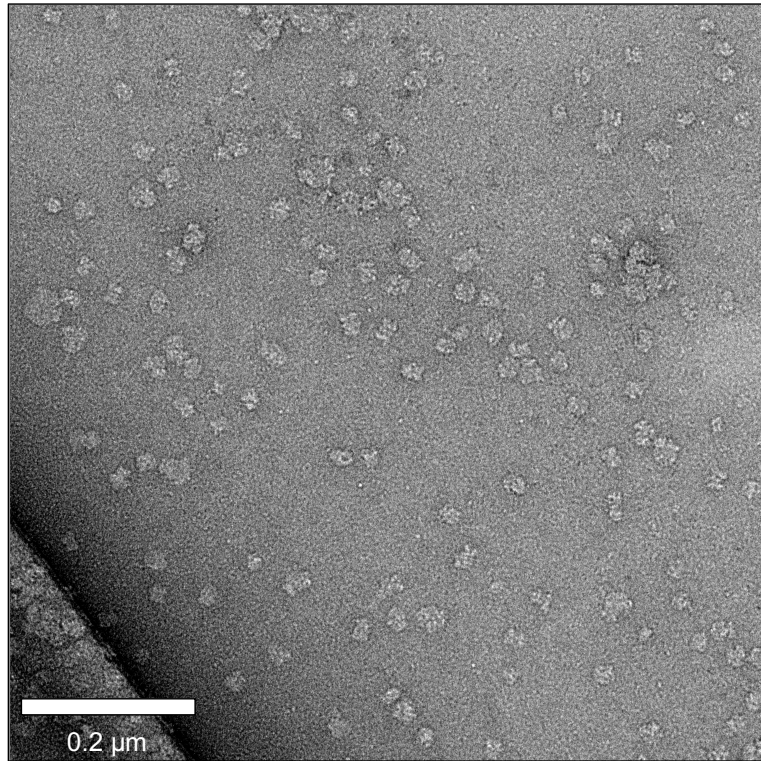


**Figure 36.** Negative stain EM of COX-2 reconstituted nanodiscs following IMAC and size-exclusion chromatography. Particles are indicative of COX-2 reconstituted nanodisc complexes.

Cryo-EM was subsequently utilized to assess the COX-2 nanodiscs following negative stain EM. Similarly to negative stain, the COX-2 nanodisc sample was diluted to either approximately 35  $\mu\text{g/mL}$  or 14  $\mu\text{g/mL}$  and a 3  $\mu\text{L}$  aliquot was added to a glow-discharged Quantifoil holey carbon grid. Grids were plunge-frozen in liquid ethane and subsequently stored frozen in liquid nitrogen. The initial dataset from Cryo EM analysis consisted of 244 images and 65,164 particles. 2D class averages were calculated from a smaller set of particles to assess the quality of the data set. The two-fold symmetry of the COX-2 dimer can be clearly distinguished in many of the image averages (Figure 37).

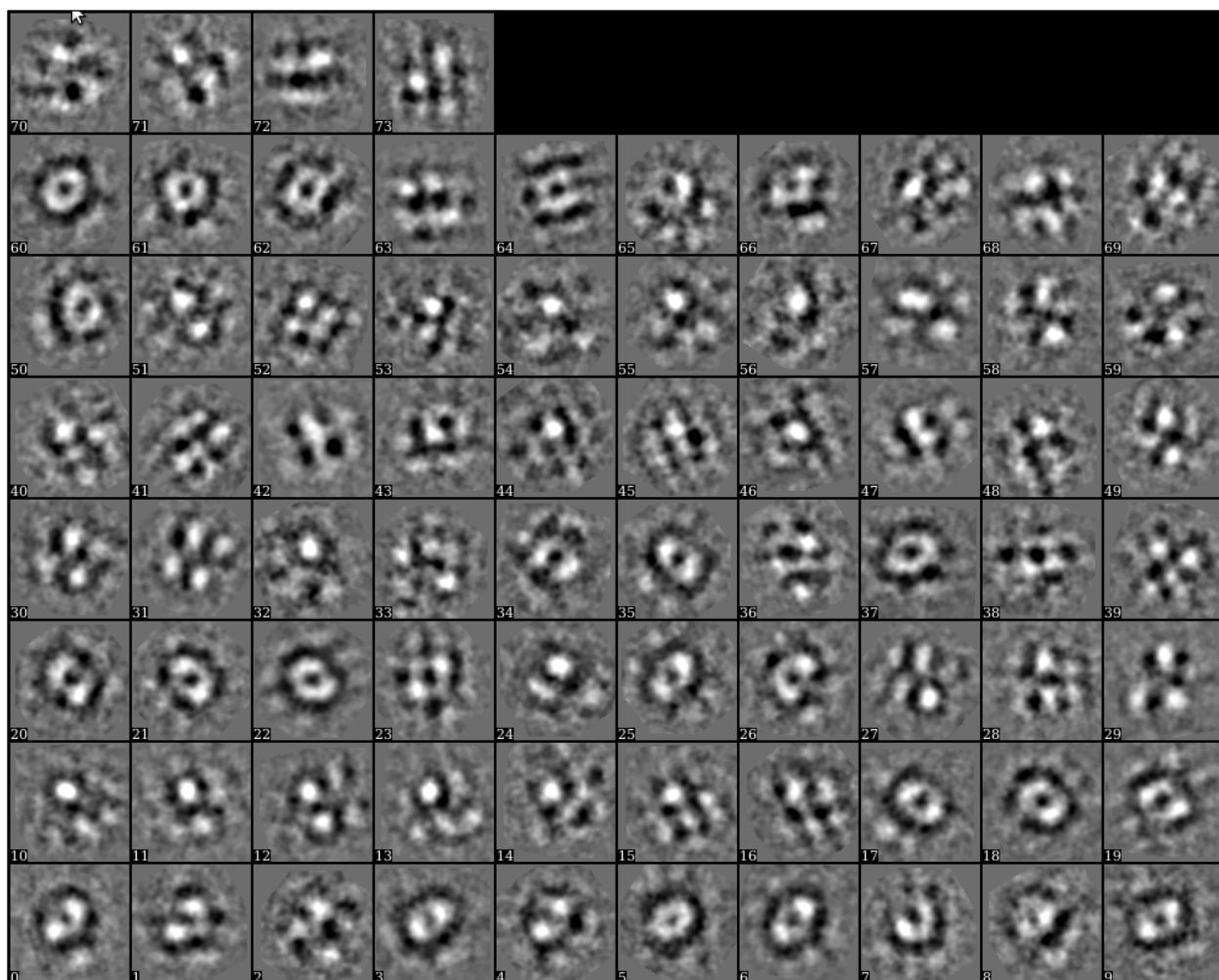


**Figure 37.** 2D class averages of COX-2 nanodisc particles from Cryo-EM. Each class average box measures approximately  $238 \text{ \AA}^2$  ( $23.8 \text{ nm}^2$ ).

The atomic structure of AA bound to the COX-2 active site (PDB: 3HS5)(48) was low-pass filtered to  $60 \text{ \AA}$  and used to generate an initial model for 3D refinement (Figure 38).

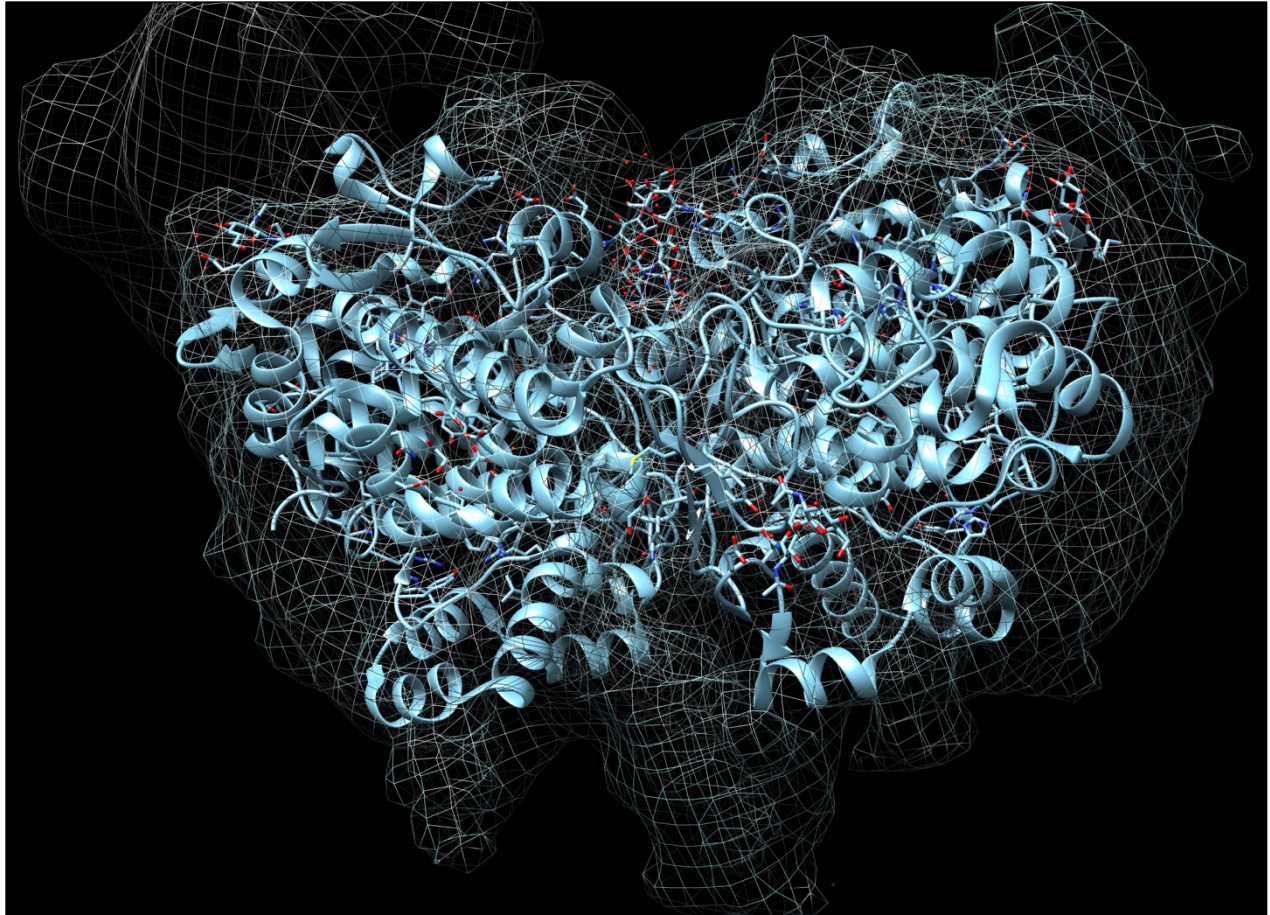


**Figure 38.** 3D model of electron density from COX-2 nanodiscs generated based on the atomic structure of AA bound to COX-2 (PDB: 3HS5).

### Discussion

The reconstitution of recombinant wild-type mCOX-2 into nanodiscs was successfully completed. The initial nanodiscs were produced exclusively utilizing POPC phospholipids. The formed nanodiscs were purified with size-exclusion chromatography. Since an excess of phospholipids and MSP was added relative to COX-2, an excess of empty nanodiscs were formed. Unfortunately, size-exclusion chromatography was not efficient at separating the empty nanodiscs from the COX-2:nanodisc complexes. Therefore, initial investigation with negative stain EM revealed that a majority of the empty nanodiscs were, in fact, present in the solution.

The next nanodisc preparation proceeded similarly but was followed with an additional IMAC purification step, utilizing the His<sub>6</sub>-tag of COX-2. Again, an excess of POPC phospholipids and MSP were

added relative to the COX-2 dimer for preparation of the nanodiscs. The mixture was incubated with Ni-NTA resin in order to separate the COX-2-reconstituted nanodiscs and empty nanodiscs. Analysis with SDS-PAGE indicated that a majority of the empty nanodiscs did not bind to the resin and were found in the flow-through. The COX-2-reconstituted nanodiscs were eluted from the resin with a high imidazole concentration and subsequently purified with size-exclusion chromatography. Following purification, the COX-2:nanodisc sample was analyzed with negative stain EM, revealing particles which contrasted those from the initial nanodisc preparation. A majority of the particles were observed to be more irregular in shape, whereas the initial preparation produced more uniformly circular particles. Thus, the additional IMAC purification was sufficient for yielding COX-2 reconstituted into POPC nanodiscs that could be identified with EM.

The COX-2:nanodisc solution was further diluted to approximately 35  $\mu\text{g}/\text{mL}$  and investigated using Cryo-EM. Multiple images were collected and averaged into multiple 2D images. In many of the 2D class averages, the two-fold symmetry of the COX-2 dimer can be observed, including less electron density at the dimer interface. The electron density was modeled into three dimensions using the X-ray crystal structure of COX-2 with AA in the active site (PDB: 3HS5) and clearly overlapped most of the residues. Unfortunately, most of the electron density of the nanodisc could not be observed from the initial 3D model, most likely due to increased molecular motion relative to the more static COX-2 dimer.

## Conclusions

The work presented here showed that recombinant COX-2 can be reconstituted into nanodiscs and analyzed with EM. Although electron density of the COX-2 dimer was seen in the reconstructed 3D model, resolution was relatively low and most of the electron density from the nanodisc components was absent. Future experiments will optimize buffer conditions as well as the incorporation of alternative phospholipids in the nanodisc bilayer. In addition to POPC, other phospholipids such as phosphatidylserine (PS) or PI can be incorporated into the nanodisc complex to more closely mimic the cellular membrane bilayer composition.



## CHAPTER VI

### ELUCIDATION OF THE CHEMICAL MECHANISM OF HUMAN INDUCIBLE MICROSOMAL PROSTAGLANDIN E<sub>2</sub> SYNTHASE 1

In 2013, a high-resolution crystal structure of recombinant human mPGES-1 was solved and revealed that a Ser-127 residue was in close proximity to the thiolate of the GSH cofactor in the active site (123). Asp-49 and Arg-126 are additional residues in the active site and were proposed to be essential for catalysis. Although a chemical mechanism for the mPGES-1 reaction was proposed based on these structural data, it was not confirmed with site-directed mutagenesis activity assay studies. In this work, projects were completed in collaboration with laboratories at the Karolinska Institutet in Stockholm, Sweden to further elucidate the catalytic mechanism of mPGES-1 and if other GSH analogues are sufficient for substrate isomerization.

#### Results

##### *Protein expression and purification optimization in Sf9 cells*

In order to complete initial kinetic and inhibitory studies, recombinant human mPGES-1 enzyme was overexpressed in an *E. coli* system. Typically, approximately 500 µg of purified enzyme was obtained from 9 liters of cell culture. The low enzyme yield was not sustainable for multiple kinetic assays, especially when larger volumes of concentrated enzyme are required for stopped-flow spectroscopy studies. To increase the yield of recombinant enzyme, a baculovirus expression system was utilized. Amplified baculovirus stocks containing the human mPGES-1 gene were used to infect large cultures of *Spodoptera frugiperda* Sf9 cells and cultured for overexpression of the enzyme. Typically, from 2 liters of cell culture, approximately 2.5 mg of purified enzyme was obtained following protein expression and purification. Utilizing purification with IMAC, cation-exchange, and size-exclusion chromatography, homogeneously folded enzyme was obtained with a purity of ≥ 95% (Figure 39).

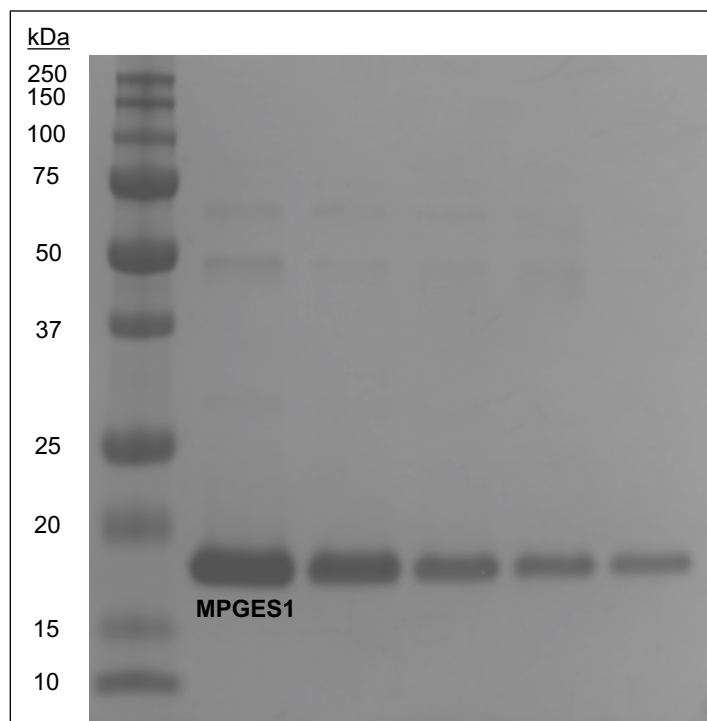


**Figure 39.** SDS-PAGE gel of wild-type human mPGES-1.

#### *Glutathione Transferase Assay*

Following recombinant mPGES-1 purification, enzyme activity was initially assessed by observing the conjugation of GSH to CDNB. mPGES-1 was reported to catalyze this reaction, although it is much less efficient than other MAPEG proteins such as MGST1. The specific activity of this reaction at 30 °C was reported to be 0.8  $\mu\text{mol min}^{-1} \text{mg}^{-1}$  (116). For the assay reported here, reactions were performed at room temperature, and specific activity was slightly lower than but comparable to the literature value, at 0.6  $\mu\text{mol min}^{-1} \text{mg}^{-1}$  (Figure 40).

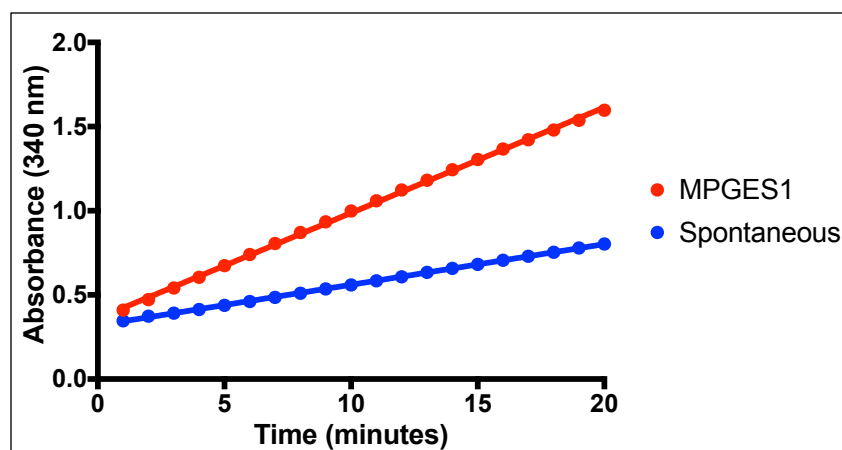


**Figure 40.** GST activity assay in the presence of wild-type mPGES-1.

#### *mPGES-1 activity with glutathione analogues*

Based on previously reported structural and kinetic data, it was known that GSH is a required cofactor for the isomerization of PGH<sub>2</sub> by mPGES-1. To initiate catalysis, the thiolate of GSH is activated, enabling it to exert a nucleophilic attack on the oxygen of carbon-9 of the cyclopentane ring, forming a sulfenic acid ester intermediate (126). Nucleophilic attack by an activated thiolate is a common mechanism for initiating catalysis by other MAPEG proteins as well as GSTs. In fact, the isozymes 3-3 and 4-4 of rat liver GST were inhibited by two GSH analogues, including the replacement of the more reactive thiol with a hydroxyl group in the serine analogue (GOH) or substitution of the thiol with a methyl group in the alanine analogue (GH). These analogues are competitive inhibitors of GSH in the presence of varying concentrations of the CDNB substrate (142). Both the serine and alanine analogues of GSH were synthesized and utilized to investigate the activity of purified mPGES-1. The purity of each analogue was verified with <sup>1</sup>H-NMR (Figure 41) as well as <sup>13</sup>C-NMR. Chemical shifts corresponded to the reported literature values.

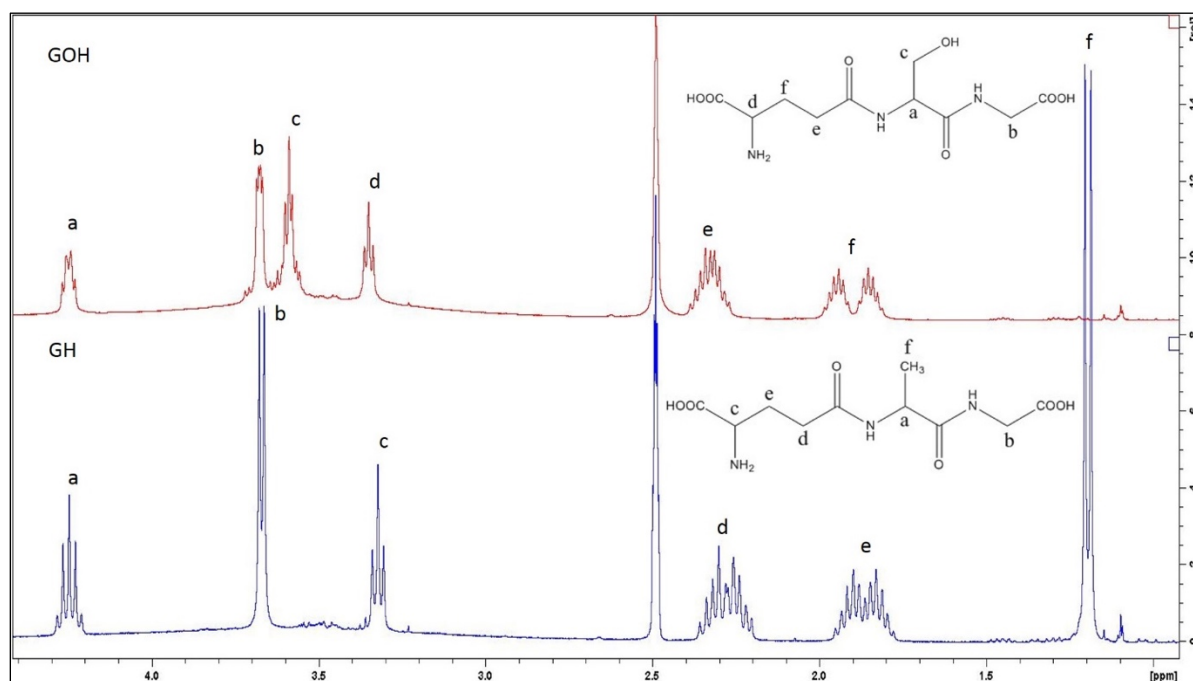


**Figure 41.**  $^1\text{H-NMR}$  spectra of the oxygen analogue  $\gamma\text{-L-Glu-L-SerGly}$  (GOH) and the desthio analogue of glutathione,  $\gamma\text{-L-Glu-AlaGly}$  (GH).

The enzymatic activity of mPGES-1 purified in the presence of 1 mM GSH was compared with that of mPGES-1 purified in the presence of 1 mM GOH or GH and to the spontaneous reactions with either 1 mM GSH, GOH, or GH. For each enzymatic reaction (mPGES-1-GSH, mPGES-1-GOH, mPGES-1-GH), 1 mM of the corresponding cofactor was added to the reaction buffer, in addition to the enzyme-cofactor complex, and the isomerization of 25  $\mu\text{M}$   $\text{PGH}_2$  to  $\text{PGE}_2$  was observed by LC-MS/MS. The amount of  $\text{PGE}_2$  was quantified from its peak area in each chromatogram relative to the peak area of the internal standard  $11\beta\text{-PGE}_2$ . In Figure 42, it can be observed that approximately 5-10% of  $\text{PGH}_2$  spontaneously isomerized to  $\text{PGE}_2$  in the presence of 1 mM GSH, GOH, or GH and the absence of any enzyme (red bars). This result is not surprising, as  $\text{PGH}_2$  is unstable in aqueous buffer, isomerizing to both  $\text{PGE}_2$  and  $\text{PGD}_2$ . In the presence of 100 nM wild-type mPGES-1 purified in the presence of 1 mM GSH and 1 mM added GSH, approximately 30% of  $\text{PGH}_2$  substrate was isomerized to  $\text{PGE}_2$  in a 1 min reaction. However, the same reaction in the presence of wild-type mPGES-1 purified in the presence of either 1 mM GOH or 1 mM GH

plus 1mM of added GOH or GH, respectively, had comparable substrate isomerization to those of the corresponding the spontaneous reactions, thus indicating that GSH is an essential cofactor, and the activated thiolate is crucial for catalysis.

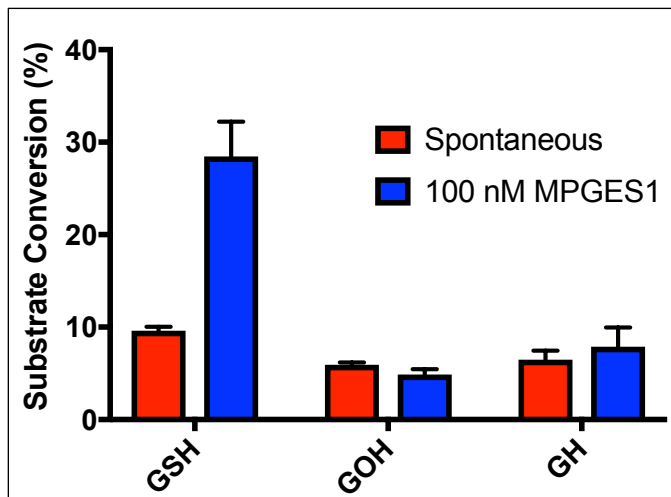


**Figure 42.** PGH<sub>2</sub> isomerization with GSH, GOH, and GH. The formation of the PGE<sub>2</sub> product was quantified by LC-MS/MS and quantified relative to the internal standard, 11 $\beta$ -PGE<sub>2</sub>.

To further investigate the activity of enzyme in complex with the GOH analogue, experiments were performed to see if varying concentrations of exogenously provided GOH could compete with GSH for binding to the enzyme and subsequently inhibit isomerization. Moreover, experiments were performed to see if GSH could compete with GOH for binding to the enzyme and rescue substrate isomerization. In Figure 43, the enzymatic isomerization of PGH<sub>2</sub> is represented by the blue bar. For this particular condition, 100 nM wild-type mPGES-1 purified with 1 mM GSH, plus 1mM of added GSH, and no GOH analogue, catalyzed substrate isomerization. The green bars represent the same reaction conditions with 100 nM enzyme and 1 mM GSH, but with increasing concentrations of GOH. Even up to a concentration of 10 mM GOH, a significant reduction in substrate isomerization was not observed. An opposite effect was observed when 100 nM wild-type mPGES-1 purified with 1 mM GOH, plus 1mM of added GOH, and no GSH was utilized for catalysis. As seen in Figure 44, substrate isomerization with only GOH was comparable to spontaneous isomerization. However, the addition of 0.5 mM GSH to the reaction mixture was able to completely rescue substrate isomerization.

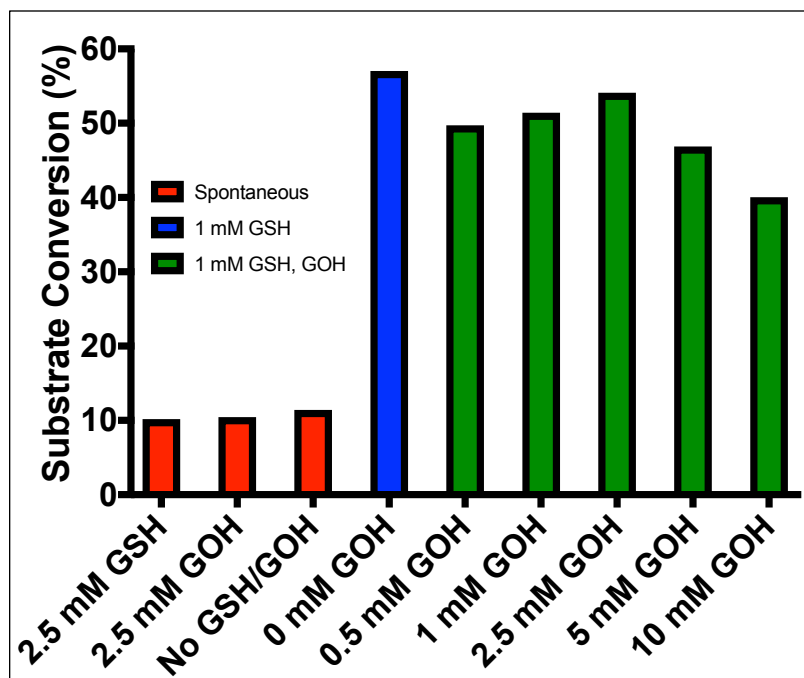


**Figure 43.** PGH<sub>2</sub> isomerization with GSH and competition with increasing concentrations of GOH. The formation of the PGE<sub>2</sub> product was quantified by LC-MS/MS.

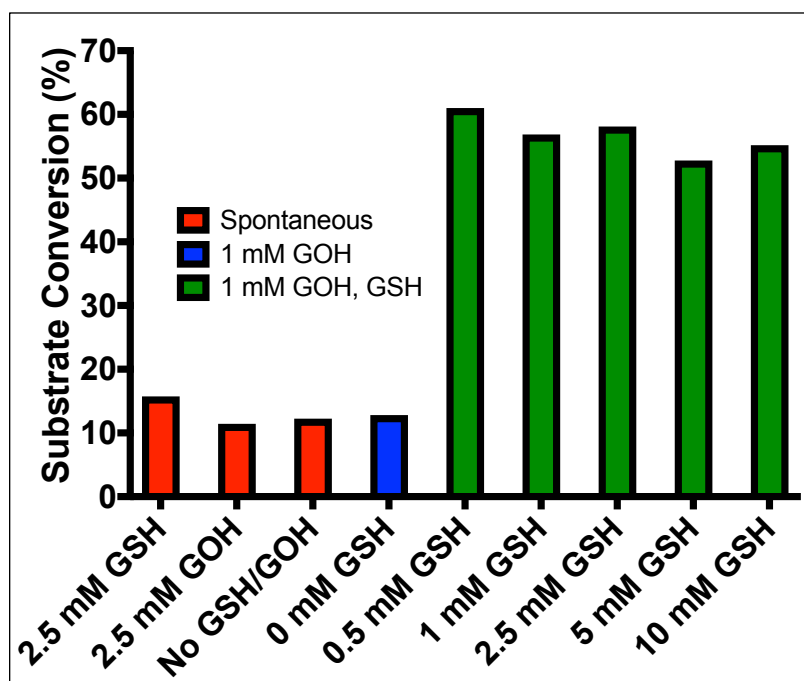


**Figure 44.** PGH<sub>2</sub> isomerization with GOH and competition with increasing concentrations of GSH. The formation of the PGE<sub>2</sub> product was quantified by LC-MS/MS.

Similar results were observed for PGH<sub>2</sub> isomerization in the presence of mPGES-1 purified with GOH in collaborative experiments performed by the laboratory of Jesper Haeggström at the Karolinska Institutet (126).

#### *Stopped-flow kinetics of mPGES-1 thiolate formation*

Stopped-flow is a spectroscopic technique used for investigating rapid reaction mechanisms in a solution over the course of about 1 millisecond to hundreds of seconds. The change in the fluorescence signal or absorbance at a particular wavelength can then be recorded as a function of time. Assuming that one-third the sites of the mPGES-1 trimer contain an activated thiolate at one time, one equivalent of the thiolate of GSH can be observed by difference spectroscopy since thiolates have an absorption band at 239 nm ( $\epsilon_{239} = 5000 \text{ M}^{-1} \text{ cm}^{-1}$ ). The mPGES-1-GSH complex was mixed rapidly with GOH to observe if there was a loss of the absorbance at 239 nm. Initially, 50  $\mu\text{M}$  of wild-type mPGES-1 in complex with GSH was mixed with 20 mM GOH in a stopped-flow cell, giving final concentrations of 25  $\mu\text{M}$  and 10 mM, respectively. The absorbance at 239 nm was recorded for up to 300 s. A distinct change in absorbance at 239 nm could not be observed (Figure 45A).

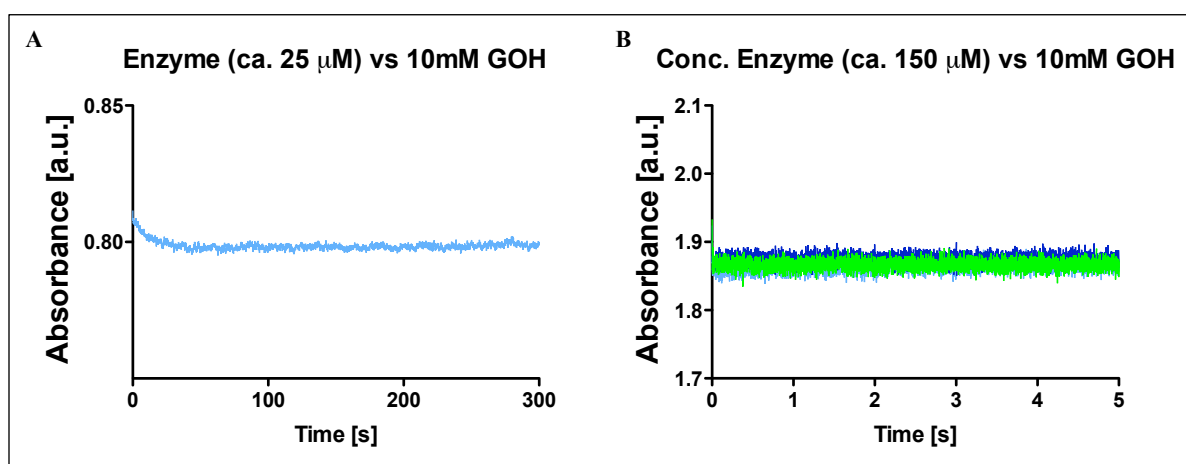


**Figure 45.** (A) Stopped-flow chromatogram monitoring absorbance at 239 nm with 25  $\mu\text{M}$  mPGES-1 and 10 mM GOH. (B) Stopped-flow chromatogram monitoring absorbance at 239 nm with 150  $\mu\text{M}$  mPGES-1 and 10 mM GOH.

Therefore, the enzyme was concentrated to approximately 300  $\mu\text{M}$  and injected into the stopped-flow cell against 20 mM GOH. The overall absorbance was increased, but an expected change in absorbance at 239 nm corresponding to the transient loss of the thiolate was not observed (Figure 45B). Similar experiments were also performed the mPGES-1-GSH complex was mixed rapidly with  $\text{GSO}_3^-$  but an observable change in absorbance at 239 nm was not detected (data not shown).

#### *mPGES-1 Peptide Mapping by Mass Spectrometry*

The conformational dynamics of proteins can be monitored with HDX-MS more effectively than with other biophysical techniques such as X-ray crystallography, which gives a more static snapshot of the structural components. HDX-MS revealed that the competitive inhibitor  $\text{GSO}_3^-$  causes changes in the structure of mPGES-1 due to the presence of additional electron density from the oxygen atoms of the sulfonate group (138). With the replacement of GSH with GOH or GH, structural dynamics are likely to be unchanged, but this can be verified with HDX-MS. In order to investigate mPGES-1 conformational dynamics using HDX-MS, it was necessary to initially map the peptide elution patterns using LC-MS/MS. mPGES-1 storage buffer was optimized to include the minimum amount of salts, glycerol, and detergent in order to keep the enzyme stable, yet minimally suppress the ionization signal from the mass spectrometer. Various experimental parameters, including mobile phase gradients, enzyme concentrations, and pepsin concentrations and incubation times, were initially optimized to give the most complete peptide coverage of the enzyme. The mPGES-1 enzyme in complex with GSH was mapped with approximately 83% of peptide sequences identified in the proteomics software PEAKS 7. After verifying the fragmentation patterns of these peptides, approximately 81% of peptide sequences were successfully confirmed and mapped (Figure 46). Many of the amino acid residues that have been proposed to form hydrogen bonds with the GSH cofactor were identified and mapped. Although peptides of mPGES-1 were sufficiently mapped, subsequent HDX-MS studies with the enzyme in complex with each analogue were not completed due to the transition of laboratories and initiating projects with COX-2.



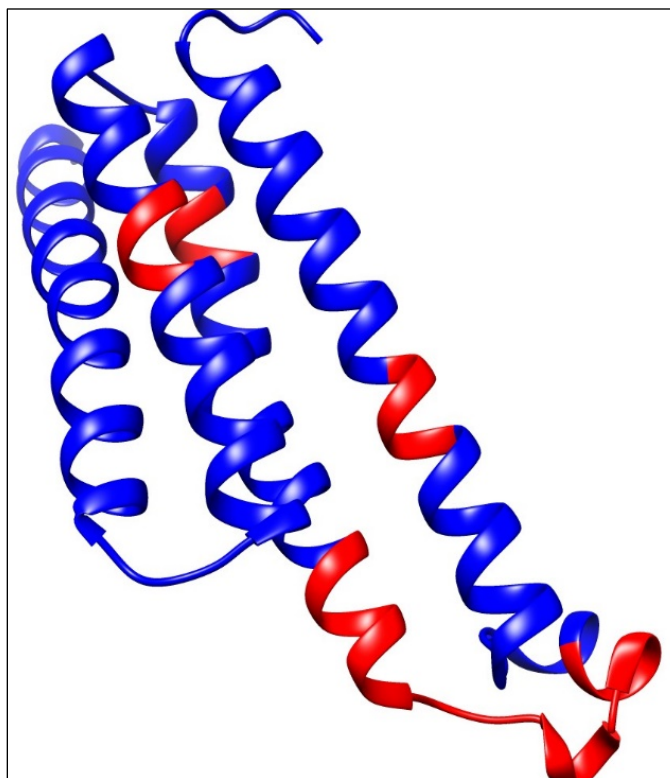


**Figure 46.** Confirmed peptide coverage of mPGES-1 using LC-MS/MS. Blue indicates peptide coverage and red indicates no peptide coverage.

#### *Role of Serine 127 in mPGES-1 Catalysis*

Ser-127 of mPGES-1 was proposed to act as a hydrogen bond donor to stabilize and activate the thiolate of GSH, thus enabling nucleophilic attack on PGH<sub>2</sub> (123). Site-directed mutagenesis of Ser-127 as well as other possible residues involved in the catalytic mechanism, Asp-49 and Arg-126, was not completed along with the structural analysis. To further investigate the proposed chemical mechanism, Asp-49, Arg-126, and Ser-127 mutant sequences were separately prepared by site-directed mutagenesis of the wild-type recombinant mPGES-1 gene sequence in the baculovirus transfer vector. Initially, the Ser-127-Ala mutant was expressed and purified in Sf9 cells and used to assess the isomerization of PGH<sub>2</sub>. Unexpectedly, the isomerization of PGH<sub>2</sub> in the presence of 100 nM Ser-127-Ala mPGES-1 was comparable to that of the wild-type control (Figure 47).

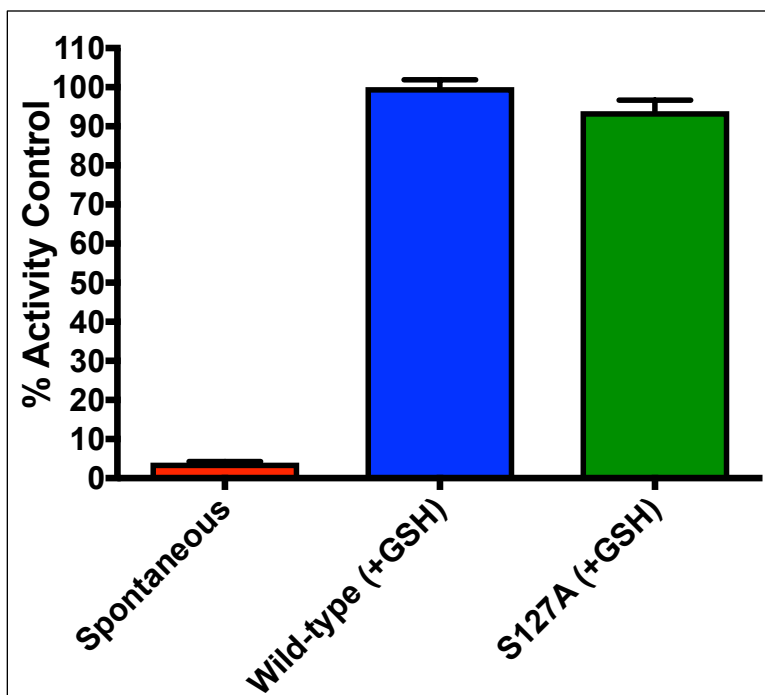


**Figure 47.** PGH<sub>2</sub> isomerization in the presence of wild-type and S127A mPGES-1. The formation of the PGE<sub>2</sub> product was quantified by LC-MS/MS.

As previously mentioned, GSO<sub>3</sub><sup>-</sup> acts a competitive inhibitor which cannot initiate catalysis due to the lack of the nucleophilic thiolate. Moreover, the additional electron density from the sulfonate oxygens alters the conformation of the mPGES-1 active site. Since Ser-127 is approximately 3.2 Å from the thiol of GSH in the mPGES-1 active site, additional steric bulk at that position could possibly disrupt catalysis. Therefore, Ser-127 was mutated to a residue with an additional electron shell. The Ser-127-Cys mutation was expressed and purified similarly to the wild-type and S127A enzymes. The isomerization of PGH<sub>2</sub> to PGE<sub>2</sub> in the presence of the S127C was initially observed by fluorescence (Figure 48) and additionally by mass spectrometry (Figure 49). Based on 1 min reaction times with 100 nM enzyme, a significant reduction in activity was observed for the S127C mutant as compared to both the wild-type and S127A enzymes.

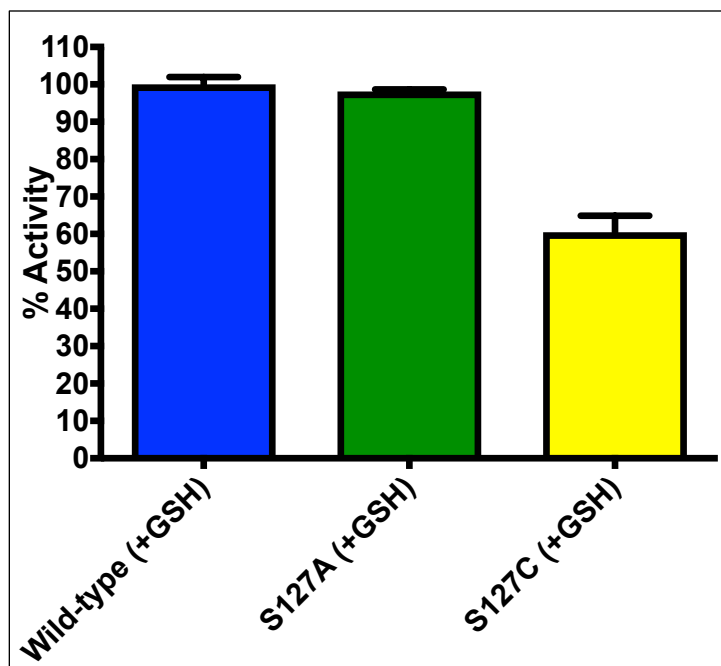


**Figure 48.** MDA fluorescence assay to assess the activity of wild-type, S127A, and S127C mPGES-1 enzymes. Fluorescence was observed for the MDA-TBA complex, formed from the degradation of unreacted PGH<sub>2</sub> substrate.

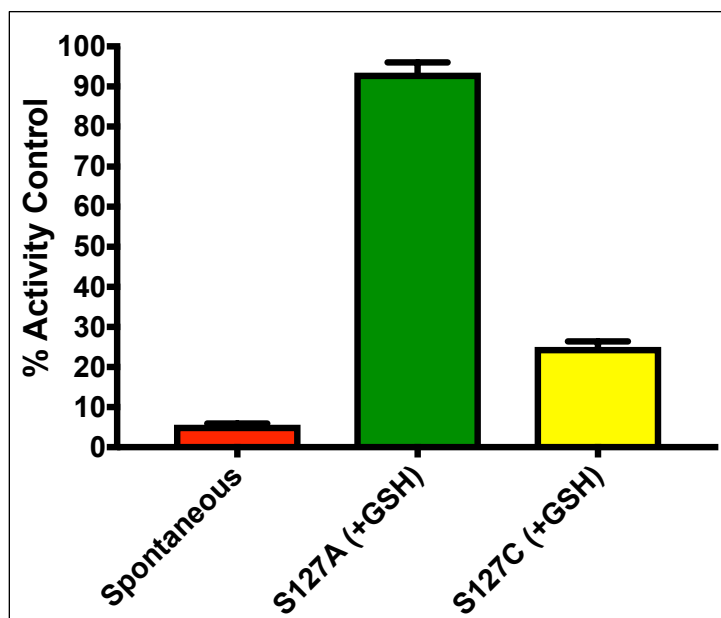


**Figure 49.** PGH<sub>2</sub> isomerization to assess the activity of S127A and S127C mPGES-1 enzymes in the presence of 1 mM GSH. The formation of the PGE<sub>2</sub> product was quantified by LC-MS/MS.

An additional assay investigated the isomerization of  $\text{PGH}_2$  in the presence of Ser-127-Cys mPGES-1 purified in the presence of 1 mM GSH or 1 mM  $\text{GSO}_3^-$  in order to determine if the cysteine residue could potentially function as a nucleophile and initiate catalysis in the active site. However, mPGES-1 Ser-127-Cys purified with  $\text{GSO}_3^-$  had comparable activity to the spontaneous reaction and lower than that of mPGES-1 Ser-127-Cys purified with GSH (Figure 50).

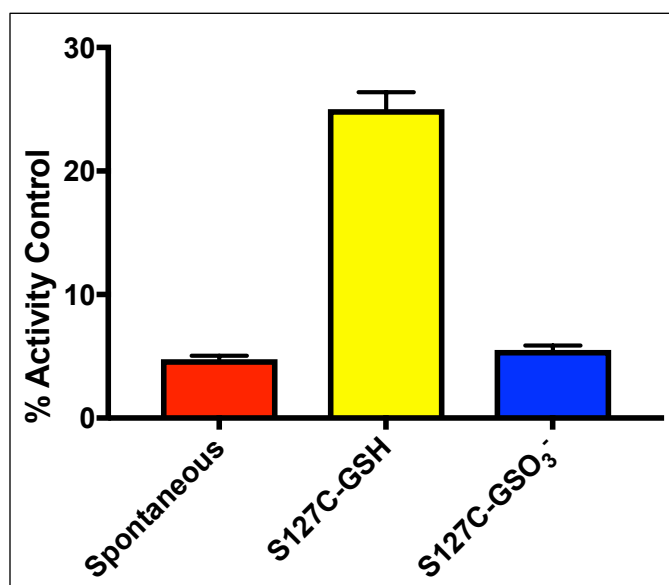


**Figure 50.**  $\text{PGH}_2$  isomerization to assess the activity of 100 nM mPGES-1 S127C purified with either GSH or purified with 1 mM  $\text{GSO}_3^-$ . The formation of the  $\text{PGE}_2$  product was quantified by LC-MS/MS.

## Discussion

### *mPGES-1 activity with glutathione analogues*

GSH analogues including the oxygen analogue (GOH) and the desthio analogue (GH) were previously shown to be inhibitors of two isozymes of GST from rat liver (142). Both of these analogues were synthesized and used to assess if they could promote the mPGES-1-catalyzed isomerization of  $\text{PGH}_2$ . GSH is a cofactor that is crucial for mPGES-1 enzyme activity and structural stability. GSH hydrogen bonds to amino acid residues from two individual subunits of the mPGES-1 trimer, forming part of the active site in the cavity between them. Although GSH is known to bind between the subunit interfaces of the enzyme, less is known about the binding affinity of GSH in all three subunits at any given time. However, molecular

dynamic simulations and hybridization experiments suggested that the enzyme exhibits one-third-sites reactivity (124). Since GSH is known to catalyze substrate isomerization, both GOH and GH analogues were separately purified with mPGES-1 to investigate their effects on enzyme activity. As expected, the rate of substrate isomerization by the enzyme purified with the desthio analogue (GH) was comparable to that of the spontaneous reaction. This was not a surprising result, as a nucleophilic compound is needed to initiate catalysis. A similar absence of catalytic activity was observed in the case of mPGES-1 complexed with GOH indicating that its nucleophilic hydroxyl group lacks sufficient reactivity to catalyze the isomerization reaction. Since both analogues failed to substitute for GSH to form active mPGES-1, a competition experiment was completed to investigate whether the GOH analogue could displace GSH in the active site and inhibit activity or if GSH could displace GOH and thus rescue activity. Surprisingly, GOH was unable to significantly inhibit mPGES-1 activity in complex with GSH, even when 10 mM GOH was added to the reaction. This finding contrasts with results of earlier experiments with  $\text{GSO}_3^-$ , a known competitive inhibitor of mPGES-1 with an  $\text{IC}_{50}$  value of 1.8 mM (138). Note that, for assessing  $\text{GSO}_3^-$ -mediated inhibition, the final concentration of GSH in each reaction was 0.4 mM. The  $K_M$  of GSH for mPGES-1 is 0.71 mM (116). In the studies reported here, a final GSH concentration of 1 mM was used, so one would expect higher concentrations of competitor to be required to observe inhibition. However, the absence of significant effect at a GOH/GSH ratio of 10:1 suggests that the affinity of GOH for the enzyme is much lower than that of GSH. In a similar assay, mPGES-1 purified with GOH was added to reaction mixtures containing a final GOH concentration of 1 mM. In the absence of any GSH, no activity was observed. However, adding only 0.5 mM GSH was sufficient to completely rescue enzymatic activity. This result was rather surprising as GSH and GOH are structurally similar, yet it appears that mPGES-1 has a strong preference for GSH binding in the active site.

Stopped-flow kinetic experiments were utilized to spectroscopically detect the thiolate from mPGES-1 complexed with GSH. One equivalent of the thiolate of GSH, based on one-third of sites occupancy, can be observed by difference spectroscopy from the thiolate absorption band at 239 nm. Since the mPGES-1 enzyme is unstable in the absence of GSH, simple difference spectroscopy experiments using

the apo-enzyme are not possible. The loss of the absorbance at 239 nm will correlate with the replacement of the GSH thiolate and indicate its rate of dissociation from the enzyme. Based on the observed first-order rate constant, it can be determined whether or not GSH is bound tightly to the enzyme. To determine if the sulfenic acid ester intermediate is present in the chemical mechanism of mPGES-1, stopped-flow spectroscopy experiments can also be utilized. If the proposed intermediate were indeed formed, it would result in the transient loss of the thiolate signal at 239 nm immediately followed by a recovery of the signal if the formation of the intermediate is faster than its decomposition. For a 25  $\mu\text{M}$  enzyme solution in the stopped-flow cell, the expected absorbance for the thiolate at 239 nm would be approximately 0.125. That absorbance would be lowered to approximately 0.04, assuming that one-third of the trimer interfaces contain a thiolate at one time, as was observed for the structurally related enzyme, MGST2 (109). In the experiments completed here, the change in absorbance was only approximately 0.01 for the 25  $\mu\text{M}$  enzyme injection, much weaker than expected for the replacement of the thiolate in the active site. Similar results were also observed when 25  $\mu\text{M}$  enzyme was injected against  $\text{GSO}_3^-$ . When the enzyme concentration was increased to 150  $\mu\text{M}$  in the stopped-flow cell, an absorbance change of approximately 0.25 was expected. However, no observable change in absorbance corresponding to the loss of the thiolate occurred after the enzyme was rapidly mixed against GOH. Further optimization of the stopped-flow experiments is necessary to observe the potential thiolate signal in the presence of mPGES-1. Moreover, further kinetic studies in addition to structural dynamic investigations with HDX-MS would be needed to assess the enzyme's preference in binding GSH in its active site. The presence of either GOH or GH bound to the enzyme could cause the solvent accessibility for active site peptides to be different compared to solvent accessibility when the enzyme is bound to GSH. The differences would likely be minimal since the hydroxyl of GOH and the methyl of GH occupy smaller areas compared to the thiol of GSH.

#### *Role of Serine 127 in mPGES-1 Catalysis*

mPGES-1 mutants, including Asp-49-Ala, Arg-126-Ala, Ser-127-Ala, and Ser-127-Cys, were prepared by mutating the wild-type mPGES-1 gene sequence in a baculovirus transfer vector. Initially, the

Ser-127-Ala mutant enzyme was tested for its ability to isomerize  $\text{PGH}_2$  in the presence of GSH. Surprisingly, the enzymatic activity of the mutant was comparable to that of the wild-type enzyme. An additional mutant, Ser-127-Cys, interestingly showed decreased enzyme activity compared to that of the wild-type control. Since the thiol of Cys possesses a larger electron radius compared to the hydroxyl of Ser, this result suggested that it might disrupt the conformation of the GSH thiolate in the active site. Therefore, catalysis is still possible, but its rate might be impaired by a reduced rate of substrate binding into or product exit from the active site. An additional assay tested the activity of the Ser-127-Cys mutant in the presence of the  $\text{GSO}_3^-$  inhibitor. The Ser-127-Cys mutant complexed with  $\text{GSO}_3^-$  could presumably catalyze substrate isomerization by a nucleophilic attack exerted by the Cys thiol. However, isomerization in the presence of the mutant and  $\text{GSO}_3^-$  was comparable to spontaneous isomerization, thus indicating a Cys thiol in the mPGES-1 active site cannot act as a nucleophile to initiate catalysis. It is also possible that  $\text{GSO}_3^-$  inhibits substrate binding to Ser-127-Cys mPGES-1. Therefore, additional experiments investigating substrate isomerization with Ser-127-Cys purified in the presence of either GOH or GH need to be performed. Further structural dynamic analysis of the mPGES-1 crystal structure from 2013 as well as site-directed mutagenesis revealed that Ser-127 is not necessary for catalysis, but an interaction between Asp-49 and Arg-126 is crucial for enzymatic activity (126). Catalysis is proposed to be mediated through stabilization of the thiolate of GSH by Arg-126 and a crystallographic water to function as a proton shuttle to transfer the proton from the thiol of GSH to protonate the oxygen of carbon-11 on the substrate cyclopentane ring (126). Additional mutagenesis studies of mPGES-1 also confirmed that Ser-127 does not function to activate the thiolate of GSH for catalysis, yet mutation of either Asp-49 or Arg-126 residues is detrimental to enzyme activity (127).

## Conclusions

Although a high-resolution crystal structure of mPGES-1 was solved, its catalytic mechanism was still not completely elucidated. In order to develop better therapeutic inhibitors, a further understanding of the enzyme's mechanistic properties is needed. By synthesizing GSH analogues, enzyme activity was

shown to be completely dependent on the GSH thiolate to exert a nucleophilic attack on the PGH<sub>2</sub> substrate. Furthermore, site-directed mutagenesis studies completed herein and by labs at the Karolinska Institutet determined that thiolate activation was mediated by a crucial interaction between the Asp-49 and Arg-126 residues as well as a water molecule in the enzyme active site. Stopped-flow spectroscopic studies were insufficient to observe the transient loss of the thiolate in the active site in the presence of enzyme inhibitors. The physical observation of the thiolate could further verify the enzymatic mechanism and potentially identify rate-limiting steps in catalysis. These studies are valuable for future kinetic and inhibitory studies of the mPGES-1 enzyme.



## CHAPTER VII

### CONCLUSIONS

#### Discussion

Inflammation is a biological process that protects an organism from chemical or physical injury. Activated immune cells release a plethora of reactive chemical species in the affected area to ultimately repair tissue damage and resolve the initial causative agent of injury. The acute inflammation typically lasts for a short time period but if not resolved, can evolve to a chronic state. The continuous generation of reactive chemical mediators can damage not only the affected site of injury, but cellular macromolecules from healthy tissue including proteins, lipids, carbohydrates, and nucleic acids. Metabolites of PUFAs are potent lipid mediators that function as autocrine or paracrine signaling molecules to regulate many processes in the inflammatory pathway. AA is hydrolyzed from the membrane bilayer of cells and subsequently metabolized to various classes of eicosanoids that have diverse functions including PGs that are primarily pro-inflammatory compounds. The increased production of PGE<sub>2</sub> arises from the induced expression of the enzymes COX-2 and mPGES-1 which are co-localized in the ER lumen and perinuclear region of the cell. COX-2 is inhibited by many NSAIDs which decreases the production of multiple PGs that regulate cardiovascular and gastrointestinal processes. mPGES-1 has more recently become a therapeutic target for the selective inhibition of PGE<sub>2</sub> production, but no inhibitor has yet reached the market.

The studies in this dissertation investigated the molecular properties of both COX-2 and mPGES-1. Although many NSAIDs have been developed for COX-2 inhibition, there is still much unknown about how they inhibit enzyme activity. Different classes of NSAIDs bind to the COX-2 active site in various orientations and exhibit distinct inhibitory kinetics. Some NSAIDs are substrate-selective, in that they are more potent for inhibiting the oxygenation of substrates over others. One inhibitor may be substrate-

selective, whereas another inhibitor from the same class may not be. Although they bind to the enzyme in a similar orientation, their molecular basis for substrate selectivity is elusive.

mPGES-1 was discovered in the late 1990s by Bengt Samuelsson and collaborators. Since that time, the structural and functional properties of the enzyme have been investigated and enzyme inhibitors have also been developed. Unfortunately, species differences between the human and rat enzyme isoforms and the lipophilic properties of inhibitors have made subsequent *in vivo* testing challenging. In 2013, a high-resolution crystal structure was solved of the human mPGES-1 enzyme and a chemical mechanism of substrate isomerization was proposed. Unfortunately, no mutagenesis studies were completed and did not further support the structural data. The studies herein were completed to further elucidate the chemical mechanism of mPGES-1, eventually leading to the design and development of more efficacious inhibitors for therapeutic treatment of inflammation.

#### *Molecular Basis of Cyclooxygenase-2 Inhibition by Ibuprofen and Mefenamic Acid*

The experiments completed here sought to determine the molecular mechanisms of substrate-selective inhibition of COX-2 by the inhibitors of ibuprofen and mefenamic acid. It is hypothesized that substrate-selective inhibitors potentially inhibit 2-AG oxygenation by binding in the allosteric subunit of COX-2. To inhibit AA oxygenation, a higher concentration of the inhibitor must also bind in the catalytic subunit. For ibuprofen inhibition, an apparent dependence on time-dependence was observed for AA oxygenation. This result was unexpected as ibuprofen typically rapidly binds to the enzyme and forms a weak inhibitor-enzyme complex. Another observation from the experiments completed here was the greater effect of peroxide tone on mefenamic acid inhibition of AA and 2-AG oxygenation. In contrast to ibuprofen, mefenamic acid is more potent in the absence of a peroxide activator, indicating that the interaction of the inhibitor and the catalytic Tyr-385 residue is likely affected. Mefenamic acid can also act as a reducing co-substrate to reduce the heme, essentially resetting the enzyme to its resting state. Therefore, 2-AG oxygenation is more dependent on the presence of peroxide whether or not the inhibitor is preincubated with the enzyme. For AA oxygenation, however, a striking difference was observed for peroxide

dependence and whether or not mefenamic acid was preincubated with the enzyme. This effect could be due to the formation of a low-affinity complex that is not affected by enzyme activation, but a preincubation period could form a tighter complex that is more dependent on enzyme activation by peroxide.

*Dual Cyclooxygenase-Fatty Acid Amide Hydrolase Inhibitor Exploits Novel Binding Interactions in the Cyclooxygenase Active Site*

NSAIDs effectively inhibit the COX enzymes, thus reducing pain and inflammation. However, the drugs exhibit cardiovascular and gastrointestinal side effects. ARN2508 is a dual inhibitor of the COX enzymes as well as FAAH, thus reducing the production of PGs while concomitantly increasing the intracellular concentration of the endocannabinoid AEA. The inhibitor exhibits high potency, target selectivity, and decreased gastrointestinal toxicity in mouse models, presumably due to its ability to increase levels of AEA and other fatty acyl ethanolamides (FAEs). Herein, the mechanism of COX inhibition by ARN2508 was investigated. A 2.27 Å resolution X-ray crystal structure of the COX-2•(*S*)-ARN2508 complex reveals that ARN2508 adopts a binding pose similar to that of its parent NSAID flurbiprofen. However, ARN2508's alkyl tail is inserted deep into the top channel, an active site region not exploited by any previously reported NSAID. As for flurbiprofen, ARN2508's potency is highly dependent on the configuration of the  $\alpha$ -methyl group. Thus, (*S*)-ARN2508 is more potent than (*R*)-ARN2508 for inhibition of AA oxygenation by both COXs and 2-AG oxygenation by COX-2. Also, similarly to (*R*)-flurbiprofen, (*R*)-ARN2508 exhibits substrate-selectivity for inhibition of 2-AG oxygenation. Site-directed mutagenesis confirms the importance of insertion of the alkyl tail into the top channel for (*S*)-ARN2508's potency and suggests a role for Ser-530 as a determinant of the inhibitor's slow rate of inhibition compared to that of (*S*)-flurbiprofen. The Gly-533 residue at the COX upper channel terminus also affects the binding of the  $\omega$ -tail of ARN2508. Mutating Gly to a bulkier hydrophobic residue slows binding of the inhibitor in the active site.

## *Efforts Toward Investigating the Structural Dynamics of Cyclooxygenase-2 With Cryo-Electron Microscopy*

Numerous X-ray crystal structures of COX-2 in complex with substrates and inhibitors have been solved. The structural data of these compounds in the enzyme active site has provided valuable insights into the molecular mechanisms of enzyme. However, X-ray crystallography is limited as a biophysical technique as it does not reveal information about enzyme molecular dynamics in the presence of a ligand. COX-2 functions as a heterodimer and the binding of one molecule in the allosteric subunit can affect the binding of a second substrate or inhibitor in the catalytic subunit. Based on limited information from X-ray crystallography, partial occupancy of an NSAID in one subunit reveals a change in the conformation of peptides within a loop region of the enzyme dimer interface(65). COX-2 heterodimers with one subunit containing a Tyr-385-Phe mutation display similar kinetic parameters as the COX-2 heterodimer with two native subunits. In fact, the heme cofactor binds with even higher affinity to the native subunit in the presence of the Tyr-385-Phe mutant subunit (62). Multiple amino acid residues form interactions at the dimer interface of the enzyme and most likely affect the cross-talk between each subunit. However, conformational differences of many of these residues has not been observed by biophysical experiments. Here, recombinant COX-2 was reconstituted into membrane mimetics, or nanodiscs, for observation using EM. COX-2 nanodiscs were purified with IMAC and size-exclusion chromatography. The nanodiscs complexes were initially analyzed using negative stain EM. Cryo-EM was also utilized to investigate the structure of the nanodisc complexes. From the acquisition of multiple 2D class averages from the nanodisc particles and the atomic structure of AA bound to the COX-2 active site (PDB: 3HS5), a 3D model of the COX-2 nanodisc complex was generated for refinement. Although electron density was clearly observed for the enzyme homodimer, electron density for the nanodisc bilayer could not be observed, possibly due to increased molecular dynamics.

### *Elucidation of the Chemical Mechanism of Human Inducible Microsomal Prostaglandin E<sub>2</sub> Synthase 1*

Based on structural data, the isomerization of PGH<sub>2</sub> to PGE<sub>2</sub> by mPGES-1 was proposed to be initiated by the thiolate of GSH. It was hypothesized that Ser-127 was essential for catalysis by functioning as a hydrogen bond donor and stabilizing the thiolate. The studies presented here sought to investigate the role of Ser-127 in the chemical mechanism of mPGES-1. Site-directed mutagenesis was utilized to determine if Ser-127 was crucial for catalysis. The mutation of Ser-127 to Ala revealed similar enzymatic activity to the wild-type enzyme. However, mutation of Ser-127 to Cys reduced enzymatic activity. The Ala residue would be unable to act as a hydrogen bond donor to stabilize the thiolate, thus another residue in the active site is responsible for its activation. A Cys in the active site most likely reduces activity due to the presence of an additional electron shell that might affect the rate of substrate entrance into or product exit from the active site cavity. GSO<sub>3</sub><sup>-</sup> is an inhibitor of mPGES-1 and was purified with the Ser-127-Cys to determine if the Cys residue could function as a nucleophile to initiate substrate isomerization. However, the mutant enzyme had comparable isomerization to that of the spontaneous reaction, indicating that Cys can not initiate catalysis. To further assess the role of the GSH thiolate, GSH analogues were synthesized and purified with mPGES-1. The oxygen analogue (GOH) and desthio analogue (GH) were unable to catalyze substrate isomerization, confirming the thiolate of GSH is essential and must be activated by a residue other than Ser-127. Additional collaborative studies with labs at the Karolinska Institutet revealed that two additional residues in the active site, Asp-49 and Arg-126, are crucial for activity. With mutations of the two residues, it was observed that substrate isomerization to PGE<sub>2</sub> was inhibited but the enzyme retained reductase activity, producing PGF<sub>2α</sub>. Further molecular refinement of the crystal structure also revealed a water molecule in the active site can function to transfer a proton from GSH to the oxygen of carbon-11 of PGH<sub>2</sub> (126,127).

#### Future Studies

Although the studies presented here reveal additional information about the mechanisms and inhibition of both COX-2 and mPGES-1, many experiments will need to be completed in the future to

further advance the field of therapeutic treatment of inflammation. Further understanding the heterodimeric properties and substrate-selective inhibition by particular NSAIDs, including ibuprofen and mefenamic acid, is critical for developing more effective drugs with fewer side effects. Ibuprofen and mefenamic acid can be used in additional experiments for further assessing their dependence on a preincubation period and peroxide activation. Although the fixed time point mass spectrometry analysis presented here is an accurate method for minimizing substrate turnover and enzyme self-inactivation, longer reaction time points could provide additional information regarding inhibitor properties under various experimental parameters. A time course experiment with one concentration of mefenamic acid was completed here but completing a similar experiment with ibuprofen would be beneficial. Additional inhibition assays could be performed with COX-2 reconstituted into nanodiscs to assess if a more native-like environment could possibly affect inhibitory kinetics relative to a detergent-solubilized solution. Another valuable experiment to complete would be to assess inhibition kinetics in the presence of both AA and 2-AG substrates in the same reaction mixture. Since one substrate can affect the oxygenation of the other substrate, the addition of a substrate-selective inhibitors like ibuprofen or mefenamic acid could provide further information about the allosteric behavior of COX-2.

Additional studies with ARN2508 will also be valuable for further understanding the molecular and structural mechanisms of COX-2. Here, the (*S*)-enantiomer of the inhibitor was more potent for inhibition of both AA and 2-AG. However, the (*R*)-enantiomer was substrate-selective for 2-AG oxygenation. The crystal structure of wild-type COX-2 in complex with (*S*)-ARN2508 was solved, but diffraction quality crystals of wild-type COX-2 in complex with (*R*)-ARN2508 were not obtained. The crystal structure of its parent compound, (*R*)-flurbiprofen, in complex with COX-2 was previously solved and revealed that a conformational change of Tyr-355 at the constriction site allowed the (*R*)-enantiomer to bind in the active site (89). Therefore, it is likely a crystal structure of COX-2•(*R*)-ARN2508 can eventually be solved following optimization of crystallization conditions. In addition to the crystallization of wild-type COX-2•(*R*)-ARN2508, a crystal structure of S530A COX-2 or S530T COX-2 in complex with (*S*)-ARN2508 would provide further speculation about how Ser-530 dictates binding of the inhibitor in the

enzyme active site. Additional inhibition kinetics could also be completed with the addition of PPHP to determine if peroxide tone could exhibit an effect on the substrate-selectivity of (*R*)-ARN2508.

The initial structural investigations of COX-2 nanodiscs using EM provided a good starting point for further understanding the dynamics confirmations of the dimer interface. Obviously, additional EM data will need to be collected to obtain near atomic resolution of the complex. The initial nanodisc preparations indicated that particles can certainly be analyzed, but experimental parameters for the electron microscope and molecular refinement will need to be optimized for producing sufficient structural data. Various nanodisc complexes can also be formed using variants of the MSP to either increase or decrease the diameter of the nanodisc for the purpose of forming a more stable complex. In addition to incorporating POPC phospholipids, other phospholipids like PE, PI, and/or PS could be incorporated in various molecular ratios to more closely mimic the native membrane bilayer environment. Substrates and inhibitors can also be incubated with the COX-2 nanodisc complexes and analyzed with EM to determine if there could be conformational change at the dimer interface of the two enzyme subunits. Enzyme with mutations of residues at the interface could also be expressed and purified to determine if any conformational changes occur.

The chemical mechanism of mPGES-1 is now better understood based on mutagenesis studies and structural refinement. For future experiments, full enzyme kinetics need to be completed for the mutant enzymes to determine differences in substrate binding affinity and turnover compared to the wild-type enzyme. Although the Ser-127-Cys mutant was shown to have decreased enzyme activity, it will also be necessary to complete full enzyme kinetics in comparison to the wild-type enzyme. Comparing enzyme kinetics of Ser-127-Cys mPGES-1 to wild-type enzyme as well as the Ser-127-Ala will make it possible to better understand its mechanism of decreased substrate isomerization. HDX-MS might also be useful to determine if the presence of the Cys residue in the active site causes conformational changes of specific peptides. Since the sulfonate of  $\text{GSO}_3^-$  caused changes in solvent accessibility, it is possible that the larger thiol of Cys compared to the hydroxyl of the native Ser residue. Completing full kinetic analyses for these

mutants will further aid the development of more potent inhibitors of the enzyme. However, extensive work will need to be completed to make these inhibitors efficacious for *in vivo* inhibition.

Future experiments integrating COX-2 and mPGES-1 into a single nanodisc complex would be useful for understanding their molecular interactions. Kinetic analysis of the COX-2•mPGES-1 nanodisc complex would be useful for investigating substrate turnover and product release in a more native-like lipid environment.

### Concluding Remarks

Inflammation can lead to the progression of numerous debilitating diseases including cancers, neurodegeneration, arthritis, among others. For many years, inflammatory symptoms were treated with natural sources like willow bark. In 1828, the active anti-inflammatory compound of the bark, salicin, was isolated. Eventually, acetylsalicylic acid, or aspirin, was marketed in 1899 but its mechanism of action remained unknown for many years. Further studies in the 1960s and 1970s determined that eicosanoids are potent lipid mediators that regulate inflammatory processes and their production could be inhibited by the action of NSAIDs. These drugs have been very beneficial for the treatment of inflammation and one of their molecular targets, COX-2, has been extensively studied. In the late 1990s, mPGES-1 was discovered and proposed as a potential therapeutic target for the more selective treatment of inflammation with fewer side effects. It is my hope that the studies completed in this dissertation have contributed to the progress of understanding these enzymes involved in the inflammatory pathway for the ultimate purpose of developing more effective treatments in the future.



## APPENDIX A

### Curriculum Vitae Michael C. Goodman

#### ADDRESS

307 31st Ave. N., Apt. 2  
Nashville, TN 37203

Phone: 270-799-6957

Email: michael.c.goodman@vanderbilt.edu

#### EDUCATION

- 2012 – 2018                      Vanderbilt University, Nashville, TN  
Ph.D., Chemistry  
Cumulative GPA: 3.617  
Advisor: Richard N. Armstrong, Ph.D. (deceased June 2015)  
Advisor: Lawrence J. Marnett, Ph.D. (January 2016 – present)
- 2007 – 2011                      University of Kentucky, Lexington, KY  
B.S., Chemistry (Biochemistry option)  
Cumulative GPA: 3.598 (cum laude)  
Undergraduate research advisor: D. Allan Butterfield (2009 – 2011)

#### RESEARCH EXPERIENCE

- 2017                                      Department of Biosciences and Nutrition, Karolinska Institutet,  
Huddinge, Sweden  
Advisors: Hans Hebert, Caroline Jegerschöld  
Project: Cryo-Electron Microscopy of Cyclooxygenase-2 (COX-2)
- 2016 – 2018                      Department of Chemistry, Vanderbilt University  
Nashville, TN  
Graduate Research Assistant  
Advisor: Dr. Lawrence J. Marnett  
Project: Cyclooxygenase-2 (COX-2) substrate-selective inhibition kinetics
- 2015                                      Institute of Environmental Medicine, Karolinska Institutet  
Stockholm, Sweden  
Advisor: Dr. Ralf Morgenstern (in collaboration with Dr. Richard N. Armstrong)  
Project: Stopped-flow kinetics of microsomal prostaglandin E2 synthase 1 (mPGES-1)

- 2013 – 2015      Department of Chemistry, Vanderbilt University  
Nashville, TN  
Graduate Research Assistant  
Advisor: Dr. Richard N. Armstrong  
Project: Elucidation of the chemical mechanism and kinetics of microsomal prostaglandin E2 synthase 1 (mPGES-1)
- 2012              Department of Chemistry, Vanderbilt University  
Nashville, TN  
Graduate Research Assistant  
Advisor: Dr. Hassane S. Mchaourab  
Project: Binding of a spin-labeled substrate to the multidrug transporter protein NorM
- 2012              Department of Chemistry, Vanderbilt University  
Nashville, TN  
Graduate Research Assistant  
Advisor: Dr. Sandra J. Rosenthal  
Project: Investigation of neurotransmitter transporter proteins using Quantum dot labeling
- 2009 – 2012      Department of Chemistry, University of Kentucky  
Lexington, KY  
Undergraduate Research Assistant  
Advisor: Dr. D. Allan Butterfield  
Project: Identification of protein modifications from oxidative stress in the pathogenesis of Alzheimer's disease

### **TEACHING EXPERIENCE**

- 2012              Department of Chemistry, University of Kentucky  
Lexington, KY  
Organic Chemistry Workshop Leader  
CHE 232 – Organic Chemistry II
- 2011              Glasgow Independent Schools, Glasgow, KY  
Substitute Teacher
- 2010 – 2011      University of Kentucky, Lexington, KY  
Center for Academic Resources and Enrichment Services (CARES)  
Student Peer Tutor

### **STUDENT MENTORSHIP**

- 2017              James Bryson McCarthy (Undergraduate student)  
William Hiser (Undergraduate student)
- 2015              Clayton Wandishin (Graduate student)

## PEER-REVIEWED PUBLICATIONS

1. **Goodman MC**, Xu S, Rouzer C, Banerjee S, Ghebreselasie K, Migliore M, Piomelli D, Marnett LJ. Dual Cyclooxygenase-Fatty Acid Amide Hydrolase Inhibitor Exhibits a Unique Mechanism of Cyclooxygenase-2 Inhibition. *J. Biol Chem.* (2018) 293(9): 3028-38.
2. Raouf J, Rafique N, **Goodman MC**, Idbord H, Bergvist F, Armstrong RN, Jakobsson P, Morgerstern R, Spahiu L. Arg126 and Asp49 Are Essential for the Catalytic Function of Microsomal Prostaglandin E2 Synthase 1 and Ser127 Is Not. *PLoS One.* (2016) 11(9):e0163600.
3. Whitson J, Sell D, **Goodman MC**, Monnier V, Fan X. Evidence of Dual Mechanisms of Glutathione Uptake in the Rodent Lens: A Novel Role for Vitreous Humor in Lens Glutathione Homeostasis. *Invest. Ophthalmol. Vis. Sci.* (2016) 57(8): 3914-25.
4. Brock J, Hamberg M, Balagunaseelan N, **Goodman MC**, Morgenstern R, Strandback E, Samuelsson B, Rinaldo-Matthis A, Haeggström J. A dynamic Asp-Arg interaction is essential for catalysis in microsomal prostaglandin E2 synthase. *Proc. Natl. Acad. Sci.* (2016) 113(4): 972-7.
5. Thompson M, Keithly M, **Goodman MC**, Hammer N, Cook P, Jagessar K, Harp J, Skaar E, Armstrong RN. Structure and Function of the Genomically Encoded Fosfomycin Resistance Enzyme, FosB, from *Staphylococcus aureus*. *Biochemistry.* (2014) 53(4): 755-65.
6. Steed R, Mishra S, Stein R, **Goodman MC**, Mchaourab H. Na<sup>+</sup>-Substrate Coupling in the Multidrug Antiporter NorM Probed with a Spin-Labeled Substrate. *Biochemistry.* (2013) 52(34): 5790-9.
7. Yokel R, Au T, MacPhail R, Hardas S, Butterfield DA, Sultana R, **Goodman MC**, Tseng M, Dan M, Haghazari H, Unrine J, Graham U, Wu P, Grulke E. Distribution, elimination and biopersistence to 90 days of a systemically-introduced 30 nm ceria engineered nanomaterial in rats. *Toxicol. Sci.* (2012) 127(1): 256-68.

## PEER-REVIEWED PRESENTATIONS

### Oral Presentations:

1. February 2018  
Department of Biochemistry Symposium  
Vanderbilt University, Nashville, TN  
Title: Dual cyclooxygenase-fatty acid amide hydrolase inhibitor exploits novel binding interactions in the cyclooxygenase active site
2. March 2017  
Chemical Biology Association of Students Seminar Series  
Vanderbilt University, Nashville, TN  
Title: Substrate Selectivity and Time Dependence of a COX-2/FAAH dual inhibitor

Poster Presentations:

1. October 2017  
15th International Bioactive Lipids Conference  
Casamagna Resort, Puerto Vallarta, Mexico  
Title: Dual Cyclooxygenase-Fatty Acid Amide Hydrolase Inhibitor Exhibits a Unique Mechanism of Cyclooxygenase-2 Inhibition: Serine-530 as a Key Residue
2. August 2016  
Vanderbilt Institute of Chemical Biology Student Symposium  
Vanderbilt University, Nashville, TN  
Title: Cyclooxygenase-2 (COX-2) Dimer Interface Kinetics and Inhibition
3. August 2015  
250th American Chemical Society National Meeting & Exposition  
Boston Convention Center & Exhibition Center, Boston, MA  
Title: The Investigation of the Chemical Mechanism and Inhibition of Microsomal Prostaglandin E2 Synthase 1 (mPGES-1)
4. August 2014  
Vanderbilt Institute of Chemical Biology Student Symposium  
Vanderbilt University, Nashville, TN  
Title: The Investigation of the Chemical Mechanism and Inhibition of Microsomal Prostaglandin E2 Synthase 1 (mPGES-1)
5. May 2014  
36th Annual Steenbock Symposium  
University of Wisconsin-Madison, Madison, WI  
Title: The Investigation of the Chemical Mechanism and Inhibition of Microsomal Prostaglandin E2 Synthase 1 (mPGES-1)
6. May 2014  
Biomolecular Structure, Dynamics, and Function: Membrane Proteins  
Vanderbilt University, Nashville, TN  
Title: The Investigation of the Chemical Mechanism and Inhibition of Microsomal Prostaglandin E2 Synthase 1 (mPGES-1)

**OTHER PRESENTATIONS**

Oral Presentations:

1. October 2016  
Magnet Academy Career Presentation  
Barren County High School, Glasgow, KY  
Title: Cyclooxygenase-2 (COX-2) Dimer Interface Kinetics and Inhibition
2. October 2014  
Center in Molecular Toxicology Enzymology Meeting  
Vanderbilt University, Nashville, TN  
Title: Investigation of the Chemical Mechanism and Inhibition of mPGES-1

3. March 2014  
Center in Molecular Toxicology Enzymology Meeting  
Vanderbilt University, Nashville, TN  
Title: Investigation of the Chemical Mechanism and Inhibition of mPGES-1

### **TECHNICAL RESEARCH SKILLS**

- Standard molecular biology techniques including PCR, cloning, western blotting, slot blotting, and site-directed mutagenesis
- Recombinant protein expression in *Escherichia coli*
- Recombinant protein expression in *Spodoptera frugiperda* (Sf9 cells)
- Sterile cell culture
- Murine tissue/organ harvest and analysis
- Protein purification, including membrane proteins
- Membrane protein association with nanodiscs
- Protein sequencing with mass spectrometry
- Enzymatic synthesis and purification of enzyme substrates
- Confocal microscopy
- Flow cytometry
- Electron paramagnetic resonance (EPR)
- Double electron-electron resonance (DEER)
- Fluorescence anisotropy
- <sup>1</sup>H-NMR
- X-ray crystallography
- Cryo-electron microscopy (Cryo-EM)
- Stopped-flow enzyme kinetics
- UV, HPLC, and LC-MS/MS-based enzyme assays
- Software: Prism, ChemDraw, Chimera, PyMOL, QualBrowser, PEAKS, MassXpert, Microsoft Office Suite

### **AWARDS AND HONORS**

- Christopher C. Harris Travel Award for Graduate Students, 15th International Bioactive Lipids Conference (2017)
- Vanderbilt University Department of Biochemistry Armstrong-Morgenstern Travel Award (2017)
- Vanderbilt Institute of Chemical Biology Certificate in Chemical Biology, Vanderbilt University (2014)
- Training Program in Environmental Toxicology Trainee, Vanderbilt University (2013 – 2015)
- Vanderbilt Institute of Chemical Biology Fellow, Vanderbilt University (2012 – 2013)
- Department of Chemistry Departmental Honors, University of Kentucky (2011)
- Merck Index Research Award, University of Kentucky (2011)
- Dean's List, University of Kentucky (2007, 2010 – 2011)

## ACADEMIC AFFILIATIONS

- American Chemical Society Student Member (2014 – present)
- Vanderbilt University Chemical Biology Association of Students (2012 – present)
- Vanderbilt University Center in Molecular Toxicology Student Fellow (2013 – 2015)
- Vanderbilt University Institute of Chemical Biology Student Fellow (2012 – 2013)
- University of Kentucky College of Arts & Sciences Student Ambassadors (2009 – 2010)
- University of Kentucky American Medical Student Association (2008 – 2010)

## PROFESSIONAL REFERECES

Lawrence J. Marnett, Ph.D. (Current Advisor)  
Dean of Basic Sciences  
Vanderbilt University School of Medicine  
University Professor  
Mary Geddes Stahlman Professor of Cancer Research  
Professor of Biochemistry, Chemistry, and Pharmacology  
Email: larry.marnett@vanderbilt.edu  
Phone: (615) 343-7329

Charles R. Sanders, Ph. D. (Provisional Advisor in lieu of Richard N. Armstrong, Ph.D.)  
Professor of Biochemistry  
Associate Editor of Biochemistry  
Aileen M. Lange and Annie Mary Lyle Chair of Cardiovascular Research  
Vanderbilt University  
Email: chuck.sanders@vanderbilt.edu  
Phone: (615) 936-3756

D. Allan Butterfield, Ph.D.  
The Alumni Association Endowed Professor of Biological Chemistry  
Director, Redox Metabolism Shared Resource Facility, Markey Cancer Center  
Faculty, Sanders-Brown Center on Aging  
Faculty Associate, Spinal Cord and Brain Injury Research Center  
Associate Vice President for Research  
University of Kentucky  
Email: dabens@uky.edu  
Phone: (859) 257-3184

Ralf Morgenstern, Ph.D.  
Professor, Institute of Environmental Medicine  
Division of Biochemical Toxicology  
Karolinska Institutet, Stockholm Sweden  
Email: ralf.morgenstern@ki.se  
Phone: +46 8-524 875 74

## **ADDITIONAL REFERENCES**

Shu Xu, Ph.D.  
Research instructor  
Department of Biochemistry, Vanderbilt University  
Email: shu.xu@vanderbilt.edu  
Phone: (615) 343-7329

Matthew K. Thompson, Ph.D.  
Assistant Professor  
Department of Chemistry, University of Alabama  
Email: matthew.k.thompson@vanderbilt.edu  
Phone: (919) 455-1775

Mary E. Keithly, Ph.D.  
Assistant Professor  
Department of Chemistry, Missouri Southern State University  
Email: keithly-m@mssu.edu  
Phone: (615) 428-9487

## REFERENCES

1. Ferrero-Miliani, L., Nielsen, O. H., Andersen, P. S., and Girardin, S. E. (2007) Chronic inflammation: importance of NOD2 and NALP3 in interleukin-1beta generation. *Clinical and experimental immunology* **147**, 227-235
2. Kumar, R., Clermont, G., Vodovotz, Y., and Chow, C. C. (2004) The dynamics of acute inflammation. *Journal of theoretical biology* **230**, 145-155
3. Khor, B., Gardet, A., and Xavier, R. J. (2011) Genetics and pathogenesis of inflammatory bowel disease. *Nature* **474**, 307-317
4. Porter, N. A., Caldwell, S. E., and Mills, K. A. (1995) Mechanisms of free radical oxidation of unsaturated lipids. *Lipids* **30**, 277-290
5. Dennis, E. A., and Norris, P. C. (2015) Eicosanoid storm in infection and inflammation. *Nature reviews. Immunology* **15**, 511-523
6. Bergstrom, S., Carlson, L. A., and Weeks, J. R. (1968) The prostaglandins: a family of biologically active lipids. *Pharmacological reviews* **20**, 1-48
7. Perez, R., Matabosch, X., Llebaria, A., Balboa, M. A., and Balsinde, J. (2006) Blockade of arachidonic acid incorporation into phospholipids induces apoptosis in U937 promonocytic cells. *Journal of lipid research* **47**, 484-491
8. Irvine, R. F. (1982) How is the level of free arachidonic acid controlled in mammalian cells? *The Biochemical journal* **204**, 3-16
9. Sun, G. Y., Chuang, D. Y., Zong, Y., Jiang, J., Lee, J. C., Gu, Z., and Simonyi, A. (2014) Role of cytosolic phospholipase A2 in oxidative and inflammatory signaling pathways in different cell types in the central nervous system. *Molecular neurobiology* **50**, 6-14
10. Smith, W. L., DeWitt, D. L., and Garavito, R. M. (2000) Cyclooxygenases: structural, cellular, and molecular biology. *Annual review of biochemistry* **69**, 145-182
11. Kroetz, D. L., and Zeldin, D. C. (2002) Cytochrome P450 pathways of arachidonic acid metabolism. *Current opinion in lipidology* **13**, 273-283
12. Kuhn, H., and O'Donnell, V. B. (2006) Inflammation and immune regulation by 12/15-lipoxygenases. *Progress in lipid research* **45**, 334-356
13. Smith, W. L. (1989) The eicosanoids and their biochemical mechanisms of action. *The Biochemical journal* **259**, 315-324
14. Nebert, D. W., Wikvall, K., and Miller, W. L. (2013) Human cytochromes P450 in health and disease. *Philosophical transactions of the Royal Society of London. Series B, Biological sciences* **368**, 20120431
15. Capdevila, J. H., and Falck, J. R. (2002) Biochemical and molecular properties of the cytochrome P450 arachidonic acid monooxygenases. *Prostaglandins & other lipid mediators* **68-69**, 325-344
16. Spector, A. A., Fang, X., Snyder, G. D., and Weintraub, N. L. (2004) Epoxyeicosatrienoic acids (EETs): metabolism and biochemical function. *Progress in lipid research* **43**, 55-90
17. Hill, E., Fitzpatrick, F., and Murphy, R. C. (1992) Biological activity and metabolism of 20-hydroxyeicosatetraenoic acid in the human platelet. *British journal of pharmacology* **106**, 267-274
18. Kuhn, H., Banthiya, S., and van Leyen, K. (2015) Mammalian lipoxygenases and their biological relevance. *Biochimica et biophysica acta* **1851**, 308-330
19. Andreou, A., and Feussner, I. (2009) Lipoxygenases - Structure and reaction mechanism. *Phytochemistry* **70**, 1504-1510
20. Haeggstrom, J. Z., and Funk, C. D. (2011) Lipoxygenase and leukotriene pathways: biochemistry, biology, and roles in disease. *Chemical reviews* **111**, 5866-5898
21. Sharma, J. N., and Mohammed, L. A. (2006) The role of leukotrienes in the pathophysiology of inflammatory disorders: is there a case for revisiting leukotrienes as therapeutic targets? *Inflammopharmacology* **14**, 10-16



22. Peters-Golden, M., and Brock, T. G. (2003) 5-lipoxygenase and FLAP. *Prostaglandins, leukotrienes, and essential fatty acids* **69**, 99-109
23. Silverman, E. S., and Drazen, J. M. (1999) The biology of 5-lipoxygenase: function, structure, and regulatory mechanisms. *Proceedings of the Association of American Physicians* **111**, 525-536
24. Murphy, R. C., and Gijon, M. A. (2007) Biosynthesis and metabolism of leukotrienes. *The Biochemical journal* **405**, 379-395
25. Bohm, I., Speck, U., and Schild, H. (2005) A possible role for cysteinyl-leukotrienes in non-ionic contrast media induced adverse reactions. *European journal of radiology* **55**, 431-436
26. Drazen, J. M., Israel, E., and O'Byrne, P. M. (1999) Treatment of asthma with drugs modifying the leukotriene pathway. *The New England journal of medicine* **340**, 197-206
27. Haeggstrom, J. Z., Rinaldo-Matthis, A., Wheelock, C. E., and Wetterholm, A. (2010) Advances in eicosanoid research, novel therapeutic implications. *Biochemical and biophysical research communications* **396**, 135-139
28. Pettersen, D., Davidsson, O., and Whatling, C. (2015) Recent advances for FLAP inhibitors. *Bioorganic & medicinal chemistry letters* **25**, 2607-2612
29. Crofford, L. J. (1997) COX-1 and COX-2 tissue expression: implications and predictions. *The Journal of rheumatology. Supplement* **49**, 15-19
30. Garavito, R. M., and DeWitt, D. L. (1999) The cyclooxygenase isoforms: structural insights into the conversion of arachidonic acid to prostaglandins. *Biochimica et biophysica acta* **1441**, 278-287
31. Vane, J. R. (1971) Inhibition of prostaglandin synthesis as a mechanism of action for aspirin-like drugs. *Nature: New biology* **231**, 232-235
32. Marnett, L. J. (2009) The COXIB experience: a look in the rearview mirror. *Annual review of pharmacology and toxicology* **49**, 265-290
33. Bergstroem, S., Danielsson, H., and Samuelsson, B. (1964) THE ENZYMATIC FORMATION OF PROSTAGLANDIN E2 FROM ARACHIDONIC ACID PROSTAGLANDINS AND RELATED FACTORS 32. *Biochimica et biophysica acta* **90**, 207-210
34. Van, D., Beerthuis, R. K., Nugteren, D. H., and Vonkeman, H. (1964) THE BIOSYNTHESIS OF PROSTAGLANDINS. *Biochimica et biophysica acta* **90**, 204-207
35. Hamberg, M., and Samuelsson, B. (1967) On the mechanism of the biosynthesis of prostaglandins E-1 and F-1-alpha. *The Journal of biological chemistry* **242**, 5336-5343
36. Hemler, M. E., Cook, H. W., and Lands, W. E. (1979) Prostaglandin biosynthesis can be triggered by lipid peroxides. *Archives of biochemistry and biophysics* **193**, 340-345
37. Vanderhoek, J. Y., and Lands, W. E. (1973) Acetylenic inhibitors of sheep vesicular gland oxygenase. *Biochimica et biophysica acta* **296**, 374-381
38. Lecomte, M., Lecocq, R., Dumont, J. E., and Boeynaems, J. M. (1990) Covalent binding of arachidonic acid metabolites to human platelet proteins. Identification of prostaglandin H synthase as one of the modified substrates. *The Journal of biological chemistry* **265**, 5178-5187
39. Landino, L. M., Crews, B. C., Timmons, M. D., Morrow, J. D., and Marnett, L. J. (1996) Peroxynitrite, the coupling product of nitric oxide and superoxide, activates prostaglandin biosynthesis. *Proceedings of the National Academy of Sciences of the United States of America* **93**, 15069-15074
40. van der Donk, W. A., Tsai, A. L., and Kulmacz, R. J. (2002) The cyclooxygenase reaction mechanism. *Biochemistry* **41**, 15451-15458
41. Marnett, L. J. (2000) Cyclooxygenase mechanisms. *Current opinion in chemical biology* **4**, 545-552
42. Spencer, A. G., Woods, J. W., Arakawa, T., Singer, II, and Smith, W. L. (1998) Subcellular localization of prostaglandin endoperoxide H synthases-1 and -2 by immunoelectron microscopy. *The Journal of biological chemistry* **273**, 9886-9893
43. Garavito, R. M., Malkowski, M. G., and DeWitt, D. L. (2002) The structures of prostaglandin endoperoxide H synthases-1 and -2. *Prostaglandins & other lipid mediators* **68-69**, 129-152

44. Kulmacz, R. J., and Lands, W. E. (1984) Prostaglandin H synthase. Stoichiometry of heme cofactor. *The Journal of biological chemistry* **259**, 6358-6363
45. Kulmacz, R. J., van der Donk, W. A., and Tsai, A. L. (2003) Comparison of the properties of prostaglandin H synthase-1 and -2. *Progress in lipid research* **42**, 377-404
46. Rowlinson, S. W., Crews, B. C., Lanzo, C. A., and Marnett, L. J. (1999) The binding of arachidonic acid in the cyclooxygenase active site of mouse prostaglandin endoperoxide synthase-2 (COX-2). A putative L-shaped binding conformation utilizing the top channel region. *The Journal of biological chemistry* **274**, 23305-23310
47. Neumann, W., Xu, S., Sarosi, M. B., Scholz, M. S., Crews, B. C., Ghebreselasie, K., Banerjee, S., Marnett, L. J., and Hey-Hawkins, E. (2016) nido-Dicarbaborate Induces Potent and Selective Inhibition of Cyclooxygenase-2. *ChemMedChem* **11**, 175-178
48. Vecchio, A. J., Simmons, D. M., and Malkowski, M. G. (2010) Structural basis of fatty acid substrate binding to cyclooxygenase-2. *The Journal of biological chemistry* **285**, 22152-22163
49. Kulmacz, R. J., and Wang, L. H. (1995) Comparison of hydroperoxide initiator requirements for the cyclooxygenase activities of prostaglandin H synthase-1 and -2. *The Journal of biological chemistry* **270**, 24019-24023
50. Luong, C., Miller, A., Barnett, J., Chow, J., Ramesha, C., and Browner, M. F. (1996) Flexibility of the NSAID binding site in the structure of human cyclooxygenase-2. *Nature structural biology* **3**, 927-933
51. Kurumbail, R. G., Stevens, A. M., Gierse, J. K., McDonald, J. J., Stegeman, R. A., Pak, J. Y., Gildehaus, D., Miyashiro, J. M., Penning, T. D., Seibert, K., Isakson, P. C., and Stallings, W. C. (1996) Structural basis for selective inhibition of cyclooxygenase-2 by anti-inflammatory agents. *Nature* **384**, 644-648
52. Rieke, C. J., Mulichak, A. M., Garavito, R. M., and Smith, W. L. (1999) The role of arginine 120 of human prostaglandin endoperoxide H synthase-2 in the interaction with fatty acid substrates and inhibitors. *The Journal of biological chemistry* **274**, 17109-17114
53. Kozak, K. R., Crews, B. C., Morrow, J. D., Wang, L. H., Ma, Y. H., Weinander, R., Jakobsson, P. J., and Marnett, L. J. (2002) Metabolism of the endocannabinoids, 2-arachidonylglycerol and anandamide, into prostaglandin, thromboxane, and prostacyclin glycerol esters and ethanolamides. *The Journal of biological chemistry* **277**, 44877-44885
54. Kozak, K. R., Rowlinson, S. W., and Marnett, L. J. (2000) Oxygenation of the endocannabinoid, 2-arachidonylglycerol, to glyceryl prostaglandins by cyclooxygenase-2. *The Journal of biological chemistry* **275**, 33744-33749
55. Di Marzo, V., De Petrocellis, L., and Bisogno, T. (2005) The biosynthesis, fate and pharmacological properties of endocannabinoids. *Handbook of experimental pharmacology*, 147-185
56. Sharma, P., Murthy, P., and Bharath, M. M. (2012) Chemistry, metabolism, and toxicology of cannabis: clinical implications. *Iranian journal of psychiatry* **7**, 149-156
57. Prusakiewicz, J. J., Kingsley, P. J., Kozak, K. R., and Marnett, L. J. (2002) Selective oxygenation of N-arachidonylglycine by cyclooxygenase-2. *Biochemical and biophysical research communications* **296**, 612-617
58. Laneuville, O., Breuer, D. K., Xu, N., Huang, Z. H., Gage, D. A., Watson, J. T., Lagarde, M., DeWitt, D. L., and Smith, W. L. (1995) Fatty acid substrate specificities of human prostaglandin-endoperoxide H synthase-1 and -2. Formation of 12-hydroxy-(9Z, 13E/Z, 15Z)- octadecatrienoic acids from alpha-linolenic acid. *The Journal of biological chemistry* **270**, 19330-19336
59. Rowlinson, S. W., Crews, B. C., Goodwin, D. C., Schneider, C., Gierse, J. K., and Marnett, L. J. (2000) Spatial requirements for 15-(R)-hydroxy-5Z,8Z,11Z, 13E-eicosatetraenoic acid synthesis within the cyclooxygenase active site of murine COX-2. Why acetylated COX-1 does not synthesize 15-(R)-hete. *The Journal of biological chemistry* **275**, 6586-6591

60. Rouzer, C. A., and Marnett, L. J. (2005) Structural and functional differences between cyclooxygenases: fatty acid oxygenases with a critical role in cell signaling. *Biochemical and biophysical research communications* **338**, 34-44
61. Dong, L., Vecchio, A. J., Sharma, N. P., Jurban, B. J., Malkowski, M. G., and Smith, W. L. (2011) Human cyclooxygenase-2 is a sequence homodimer that functions as a conformational heterodimer. *The Journal of biological chemistry* **286**, 19035-19046
62. Dong, L., Sharma, N. P., Jurban, B. J., and Smith, W. L. (2013) Pre-existent asymmetry in the human cyclooxygenase-2 sequence homodimer. *The Journal of biological chemistry* **288**, 28641-28655
63. Kudalkar, S. N., Nikas, S. P., Kingsley, P. J., Xu, S., Galligan, J. J., Rouzer, C. A., Banerjee, S., Ji, L., Eno, M. R., Makriyannis, A., and Marnett, L. J. (2015) 13-Methylarachidonic acid is a positive allosteric modulator of endocannabinoid oxygenation by cyclooxygenase. *The Journal of biological chemistry* **290**, 7897-7909
64. Mitchener, M. M., Hermanson, D. J., Shockley, E. M., Brown, H. A., Lindsley, C. W., Reese, J., Rouzer, C. A., Lopez, C. F., and Marnett, L. J. (2015) Competition and allostery govern substrate selectivity of cyclooxygenase-2. *Proceedings of the National Academy of Sciences of the United States of America* **112**, 12366-12371
65. Sidhu, R. S., Lee, J. Y., Yuan, C., and Smith, W. L. (2010) Comparison of cyclooxygenase-1 crystal structures: cross-talk between monomers comprising cyclooxygenase-1 homodimers. *Biochemistry* **49**, 7069-7079
66. Cairns, J. A. (2007) The coxibs and traditional nonsteroidal anti-inflammatory drugs: a current perspective on cardiovascular risks. *The Canadian journal of cardiology* **23**, 125-131
67. Kalgutkar, A. S., Crews, B. C., Rowlinson, S. W., Garner, C., Seibert, K., and Marnett, L. J. (1998) Aspirin-like molecules that covalently inactivate cyclooxygenase-2. *Science (New York, N.Y.)* **280**, 1268-1270
68. Vane, J. R., and Botting, R. M. (2003) The mechanism of action of aspirin. *Thrombosis research* **110**, 255-258
69. Smith, W. L., and Lands, W. E. (1971) Stimulation and blockade of prostaglandin biosynthesis. *The Journal of biological chemistry* **246**, 6700-6702
70. Hochgesang, G. P., Rowlinson, S. W., and Marnett, L. J. (2000) Tyrosine-385 Is Critical for Acetylation of Cyclooxygenase-2 by Aspirin. *Journal of the American Chemical Society* **122**, 6514-6515
71. Meade, E. A., Smith, W. L., and DeWitt, D. L. (1993) Differential inhibition of prostaglandin endoperoxide synthase (cyclooxygenase) isozymes by aspirin and other non-steroidal anti-inflammatory drugs. *The Journal of biological chemistry* **268**, 6610-6614
72. Rome, L. H., and Lands, W. E. (1975) Structural requirements for time-dependent inhibition of prostaglandin biosynthesis by anti-inflammatory drugs. *Proceedings of the National Academy of Sciences of the United States of America* **72**, 4863-4865
73. Mancini, J. A., Riendeau, D., Falguyret, J. P., Vickers, P. J., and O'Neill, G. P. (1995) Arginine 120 of prostaglandin G/H synthase-1 is required for the inhibition by nonsteroidal anti-inflammatory drugs containing a carboxylic acid moiety. *The Journal of biological chemistry* **270**, 29372-29377
74. Greig, G. M., Francis, D. A., Falguyret, J. P., Ouellet, M., Percival, M. D., Roy, P., Bayly, C., Mancini, J. A., and O'Neill, G. P. (1997) The interaction of arginine 106 of human prostaglandin G/H synthase-2 with inhibitors is not a universal component of inhibition mediated by nonsteroidal anti-inflammatory drugs. *Molecular pharmacology* **52**, 829-838
75. Kalgutkar, A. S., Crews, B. C., Rowlinson, S. W., Marnett, A. B., Kozak, K. R., Rimmel, R. P., and Marnett, L. J. (2000) Biochemically based design of cyclooxygenase-2 (COX-2) inhibitors: facile conversion of nonsteroidal antiinflammatory drugs to potent and highly selective COX-2 inhibitors. *Proceedings of the National Academy of Sciences of the United States of America* **97**, 925-930

76. Prusakiewicz, J. J., Felts, A. S., Mackenzie, B. S., and Marnett, L. J. (2004) Molecular basis of the time-dependent inhibition of cyclooxygenases by indomethacin. *Biochemistry* **43**, 15439-15445
77. Blobaum, A. L., Uddin, M. J., Felts, A. S., Crews, B. C., Rouzer, C. A., and Marnett, L. J. (2013) The 2'-Trifluoromethyl Analogue of Indomethacin Is a Potent and Selective COX-2 Inhibitor. *ACS medicinal chemistry letters* **4**, 486-490
78. Kurumbail, R. G., Kiefer, J. R., and Marnett, L. J. (2001) Cyclooxygenase enzymes: catalysis and inhibition. *Current opinion in structural biology* **11**, 752-760
79. Bhattacharyya, D. K., Lecomte, M., Rieke, C. J., Garavito, M., and Smith, W. L. (1996) Involvement of arginine 120, glutamate 524, and tyrosine 355 in the binding of arachidonate and 2-phenylpropionic acid inhibitors to the cyclooxygenase active site of ovine prostaglandin endoperoxide H synthase-1. *The Journal of biological chemistry* **271**, 2179-2184
80. So, O. Y., Scarafia, L. E., Mak, A. Y., Callan, O. H., and Swinney, D. C. (1998) The dynamics of prostaglandin H synthases. Studies with prostaglandin h synthase 2 Y355F unmask mechanisms of time-dependent inhibition and allosteric activation. *The Journal of biological chemistry* **273**, 5801-5807
81. Rowlinson, S. W., Kiefer, J. R., Prusakiewicz, J. J., Pawlitz, J. L., Kozak, K. R., Kalgutkar, A. S., Stallings, W. C., Kurumbail, R. G., and Marnett, L. J. (2003) A novel mechanism of cyclooxygenase-2 inhibition involving interactions with Ser-530 and Tyr-385. *The Journal of biological chemistry* **278**, 45763-45769
82. Mancini, J. A., Vickers, P. J., O'Neill, G. P., Boily, C., Falguyret, J. P., and Riendeau, D. (1997) Altered sensitivity of aspirin-acetylated prostaglandin G/H synthase-2 to inhibition by nonsteroidal anti-inflammatory drugs. *Molecular pharmacology* **51**, 52-60
83. Windsor, M. A., Valk, P. L., Xu, S., Banerjee, S., and Marnett, L. J. (2013) Exploring the molecular determinants of substrate-selective inhibition of cyclooxygenase-2 by lumiracoxib. *Bioorganic & medicinal chemistry letters* **23**, 5860-5864
84. Blobaum, A. L., and Marnett, L. J. (2007) Structural and Functional Basis of Cyclooxygenase Inhibition. *Journal of medicinal chemistry* **50**, 1425-1441
85. Gierse, J. K., Koboldt, C. M., Walker, M. C., Seibert, K., and Isakson, P. C. (1999) Kinetic basis for selective inhibition of cyclo-oxygenases. *The Biochemical journal* **339 ( Pt 3)**, 607-614
86. Walker, M. C., Kurumbail, R. G., Kiefer, J. R., Moreland, K. T., Koboldt, C. M., Isakson, P. C., Seibert, K., and Gierse, J. K. (2001) A three-step kinetic mechanism for selective inhibition of cyclo-oxygenase-2 by diarylheterocyclic inhibitors. *The Biochemical journal* **357**, 709-718
87. Blobaum, A. L., Xu, S., Rowlinson, S. W., Duggan, K. C., Banerjee, S., Kudalkar, S. N., Birmingham, W. R., Ghebreselasie, K., and Marnett, L. J. (2015) Action at a distance: mutations of peripheral residues transform rapid reversible inhibitors to slow, tight binders of cyclooxygenase-2. *The Journal of biological chemistry* **290**, 12793-12803
88. Prusakiewicz, J. J., Duggan, K. C., Rouzer, C. A., and Marnett, L. J. (2009) Differential sensitivity and mechanism of inhibition of COX-2 oxygenation of arachidonic acid and 2-arachidonoylglycerol by ibuprofen and mefenamic acid. *Biochemistry* **48**, 7353-7355
89. Duggan, K. C., Hermanson, D. J., Musee, J., Prusakiewicz, J. J., Scheib, J. L., Carter, B. D., Banerjee, S., Oates, J. A., and Marnett, L. J. (2011) (R)-Profens are substrate-selective inhibitors of endocannabinoid oxygenation by COX-2. *Nature chemical biology* **7**, 803-809
90. Musee, J., and Marnett, L. J. (2012) Prostaglandin H synthase-2-catalyzed oxygenation of 2-arachidonoylglycerol is more sensitive to peroxide tone than oxygenation of arachidonic acid. *The Journal of biological chemistry* **287**, 37383-37394
91. Orlando, B. J., and Malkowski, M. G. (2016) Substrate-selective Inhibition of Cyclooxygenase-2 by Fenamic Acid Derivatives Is Dependent on Peroxide Tone. *The Journal of biological chemistry* **291**, 15069-15081
92. Maclouf, J., Kindahl, H., Granstrom, E., and Samuelsson, B. (1980) Interactions of prostaglandin H2 and thromboxane A2 with human serum albumin. *European journal of biochemistry* **109**, 561-566

93. Gudis, K., Tatsuguchi, A., Wada, K., Futagami, S., Nagata, K., Hiratsuka, T., Shinji, Y., Miyake, K., Tsukui, T., Fukuda, Y., and Sakamoto, C. (2005) Microsomal prostaglandin E synthase (mPGES)-1, mPGES-2 and cytosolic PGES expression in human gastritis and gastric ulcer tissue. *Laboratory investigation; a journal of technical methods and pathology* **85**, 225-236
94. Tanioka, T., Nakatani, Y., Semmyo, N., Murakami, M., and Kudo, I. (2000) Molecular identification of cytosolic prostaglandin E2 synthase that is functionally coupled with cyclooxygenase-1 in immediate prostaglandin E2 biosynthesis. *The Journal of biological chemistry* **275**, 32775-32782
95. Hara, S., Kamei, D., Sasaki, Y., Tanemoto, A., Nakatani, Y., and Murakami, M. (2010) Prostaglandin E synthases: Understanding their pathophysiological roles through mouse genetic models. *Biochimie* **92**, 651-659
96. Yamada, T., and Takusagawa, F. (2007) PGH2 degradation pathway catalyzed by GSH-heme complex bound microsomal prostaglandin E2 synthase type 2: the first example of a dual-function enzyme. *Biochemistry* **46**, 8414-8424
97. Watanabe, K., Ito, S., and Yamamoto, S. (2008) Studies on membrane-associated prostaglandin E synthase-2 with reference to production of 12L-hydroxy-5,8,10-heptadecatrienoic acid (HHT). *Biochemical and biophysical research communications* **367**, 782-786
98. Takusagawa, F. (2013) Microsomal prostaglandin E synthase type 2 (mPGES2) is a glutathione-dependent heme protein, and dithiothreitol dissociates the bound heme to produce active prostaglandin E2 synthase in vitro. *The Journal of biological chemistry* **288**, 10166-10175
99. Ueno, N., Takegoshi, Y., Kamei, D., Kudo, I., and Murakami, M. (2005) Coupling between cyclooxygenases and terminal prostanoid synthases. *Biochemical and biophysical research communications* **338**, 70-76
100. Jakobsson, P. J., Morgenstern, R., Mancini, J., Ford-Hutchinson, A., and Persson, B. (2000) Membrane-associated proteins in eicosanoid and glutathione metabolism (MAPEG). A widespread protein superfamily. *American journal of respiratory and critical care medicine* **161**, S20-24
101. Jakobsson, P. J., Morgenstern, R., Mancini, J., Ford-Hutchinson, A., and Persson, B. (1999) Common structural features of MAPEG -- a widespread superfamily of membrane associated proteins with highly divergent functions in eicosanoid and glutathione metabolism. *Protein science : a publication of the Protein Society* **8**, 689-692
102. Holm, P. J., Bhakat, P., Jegerschold, C., Gyobu, N., Mitsuoka, K., Fujiyoshi, Y., Morgenstern, R., and Hebert, H. (2006) Structural basis for detoxification and oxidative stress protection in membranes. *Journal of molecular biology* **360**, 934-945
103. Jegerschold, C., Pawelzik, S. C., Purhonen, P., Bhakat, P., Gheorghe, K. R., Gyobu, N., Mitsuoka, K., Morgenstern, R., Jakobsson, P. J., and Hebert, H. (2008) Structural basis for induced formation of the inflammatory mediator prostaglandin E2. *Proceedings of the National Academy of Sciences of the United States of America* **105**, 11110-11115
104. Ago, H., Kanaoka, Y., Irikura, D., Lam, B. K., Shimamura, T., Austen, K. F., and Miyano, M. (2007) Crystal structure of a human membrane protein involved in cysteinyl leukotriene biosynthesis. *Nature* **448**, 609-612
105. Ferguson, A. D., McKeever, B. M., Xu, S., Wisniewski, D., Miller, D. K., Yamin, T. T., Spencer, R. H., Chu, L., Ujjainwalla, F., Cunningham, B. R., Evans, J. F., and Becker, J. W. (2007) Crystal structure of inhibitor-bound human 5-lipoxygenase-activating protein. *Science (New York, N.Y.)* **317**, 510-512
106. Back, M. (2009) Inhibitors of the 5-lipoxygenase pathway in atherosclerosis. *Current pharmaceutical design* **15**, 3116-3132
107. Morgenstern, R., Svensson, R., Bernat, B. A., and Armstrong, R. N. (2001) Kinetic analysis of the slow ionization of glutathione by microsomal glutathione transferase MGST1. *Biochemistry* **40**, 3378-3384

108. Rinaldo-Matthis, A., Ahmad, S., Wetterholm, A., Lachmann, P., Morgenstern, R., and Haeggstrom, J. Z. (2012) Pre-steady-state kinetic characterization of thiolate anion formation in human leukotriene C(4) synthase. *Biochemistry* **51**, 848-856
109. Ahmad, S., Niegowski, D., Wetterholm, A., Haeggstrom, J. Z., Morgenstern, R., and Rinaldo-Matthis, A. (2013) Catalytic characterization of human microsomal glutathione S-transferase 2: identification of rate-limiting steps. *Biochemistry* **52**, 1755-1764
110. Jakobsson, P. J., Mancini, J. A., Riendeau, D., and Ford-Hutchinson, A. W. (1997) Identification and characterization of a novel microsomal enzyme with glutathione-dependent transferase and peroxidase activities. *The Journal of biological chemistry* **272**, 22934-22939
111. Gillard, J., Ford-Hutchinson, A. W., Chan, C., Charleson, S., Denis, D., Foster, A., Fortin, R., Leger, S., McFarlane, C. S., Morton, H., and et al. (1989) L-663,536 (MK-886) (3-[1-(4-chlorobenzyl)-3-t-butyl-thio-5-isopropylindol-2-yl]-2,2 - dimethylpropanoic acid), a novel, orally active leukotriene biosynthesis inhibitor. *Canadian journal of physiology and pharmacology* **67**, 456-464
112. Miller, D. K., Gillard, J. W., Vickers, P. J., Sadowski, S., Leveille, C., Mancini, J. A., Charleson, P., Dixon, R. A., Ford-Hutchinson, A. W., Fortin, R., and et al. (1990) Identification and isolation of a membrane protein necessary for leukotriene production. *Nature* **343**, 278-281
113. Jakobsson, P. J., Thoren, S., Morgenstern, R., and Samuelsson, B. (1999) Identification of human prostaglandin E synthase: a microsomal, glutathione-dependent, inducible enzyme, constituting a potential novel drug target. *Proceedings of the National Academy of Sciences of the United States of America* **96**, 7220-7225
114. Thoren, S., and Jakobsson, P. J. (2000) Coordinate up- and down-regulation of glutathione-dependent prostaglandin E synthase and cyclooxygenase-2 in A549 cells. Inhibition by NS-398 and leukotriene C4. *European journal of biochemistry* **267**, 6428-6434
115. Murakami, M., Naraba, H., Tanioka, T., Semmyo, N., Nakatani, Y., Kojima, F., Ikeda, T., Fueki, M., Ueno, A., Oh, S., and Kudo, I. (2000) Regulation of prostaglandin E2 biosynthesis by inducible membrane-associated prostaglandin E2 synthase that acts in concert with cyclooxygenase-2. *The Journal of biological chemistry* **275**, 32783-32792
116. Thoren, S., Weinander, R., Saha, S., Jegerschold, C., Pettersson, P. L., Samuelsson, B., Hebert, H., Hamberg, M., Morgenstern, R., and Jakobsson, P. J. (2003) Human microsomal prostaglandin E synthase-1: purification, functional characterization, and projection structure determination. *The Journal of biological chemistry* **278**, 22199-22209
117. Gomez, I., Foudi, N., Longrois, D., and Norel, X. (2013) The role of prostaglandin E2 in human vascular inflammation. *Prostaglandins, leukotrienes, and essential fatty acids* **89**, 55-63
118. Hamberg, M., and Samuelsson, B. (1971) On the metabolism of prostaglandins E 1 and E 2 in man. *The Journal of biological chemistry* **246**, 6713-6721
119. Bygdeman, M. (2003) Pharmacokinetics of prostaglandins. *Best practice & research. Clinical obstetrics & gynaecology* **17**, 707-716
120. Levy, B. D., Clish, C. B., Schmidt, B., Gronert, K., and Serhan, C. N. (2001) Lipid mediator class switching during acute inflammation: signals in resolution. *Nature immunology* **2**, 612-619
121. Koeberle, A., and Werz, O. (2009) Inhibitors of the microsomal prostaglandin E(2) synthase-1 as alternative to non steroidal anti-inflammatory drugs (NSAIDs)--a critical review. *Current medicinal chemistry* **16**, 4274-4296
122. Konya, V., Marsche, G., Schuligoi, R., and Heinemann, A. (2013) E-type prostanoid receptor 4 (EP4) in disease and therapy. *Pharmacology & therapeutics* **138**, 485-502
123. Sjogren, T., Nord, J., Ek, M., Johansson, P., Liu, G., and Geschwindner, S. (2013) Crystal structure of microsomal prostaglandin E2 synthase provides insight into diversity in the MAPEG superfamily. *Proceedings of the National Academy of Sciences of the United States of America* **110**, 3806-3811
124. He, S., Wu, Y., Yu, D., and Lai, L. (2011) Microsomal prostaglandin E synthase-1 exhibits one-third-of-the-sites reactivity. *The Biochemical journal* **440**, 13-21

125. Rinaldo-Matthis, A., Wetterholm, A., Martinez Molina, D., Holm, J., Niegowski, D., Ohlson, E., Nordlund, P., Morgenstern, R., and Haeggstrom, J. Z. (2010) Arginine 104 is a key catalytic residue in leukotriene C4 synthase. *The Journal of biological chemistry* **285**, 40771-40776
126. Brock, J. S., Hamberg, M., Balagunaseelan, N., Goodman, M., Morgenstern, R., Strandback, E., Samuelsson, B., Rinaldo-Matthis, A., and Haeggstrom, J. Z. (2016) A dynamic Asp-Arg interaction is essential for catalysis in microsomal prostaglandin E2 synthase. *Proceedings of the National Academy of Sciences of the United States of America* **113**, 972-977
127. Raouf, J., Rafique, N., Goodman, M. C., Idborg, H., Bergqvist, F., Armstrong, R. N., Jakobsson, P. J., Morgenstern, R., and Spahiu, L. (2016) Arg126 and Asp49 Are Essential for the Catalytic Function of Microsomal Prostaglandin E2 Synthase 1 and Ser127 Is Not. *PLoS one* **11**, e0163600
128. Hammarberg, T., Hamberg, M., Wetterholm, A., Hansson, H., Samuelsson, B., and Haeggstrom, J. Z. (2009) Mutation of a critical arginine in microsomal prostaglandin E synthase-1 shifts the isomerase activity to a reductase activity that converts prostaglandin H2 into prostaglandin F2alpha. *The Journal of biological chemistry* **284**, 301-305
129. Murakami, M., and Kudo, I. (2006) Prostaglandin E synthase: a novel drug target for inflammation and cancer. *Current pharmaceutical design* **12**, 943-954
130. Pawelzik, S. C., Uda, N. R., Spahiu, L., Jegerschold, C., Stenberg, P., Hebert, H., Morgenstern, R., and Jakobsson, P. J. (2010) Identification of key residues determining species differences in inhibitor binding of microsomal prostaglandin E synthase-1. *The Journal of biological chemistry* **285**, 29254-29261
131. Psarra, A., Nikolaou, A., Kokotou, M. G., Limnios, D., and Kokotos, G. (2017) Microsomal prostaglandin E2 synthase-1 inhibitors: a patent review. *Expert opinion on therapeutic patents* **27**, 1047-1059
132. Mbalaviele, G., Pauley, A. M., Shaffer, A. F., Zweifel, B. S., Mathialagan, S., Mnich, S. J., Nemirovskiy, O. V., Carter, J., Gierse, J. K., Wang, J. L., Vazquez, M. L., Moore, W. M., and Masferrer, J. L. (2010) Distinction of microsomal prostaglandin E synthase-1 (mPGES-1) inhibition from cyclooxygenase-2 inhibition in cells using a novel, selective mPGES-1 inhibitor. *Biochemical pharmacology* **79**, 1445-1454
133. Bruno, A., Di Francesco, L., Coletta, I., Mangano, G., Alisi, M. A., Polenzani, L., Milanese, C., Anzellotti, P., Ricciotti, E., Dovizio, M., Di Francesco, A., Tacconelli, S., Capone, M. L., and Patrignani, P. (2010) Effects of AF3442 [N-(9-ethyl-9H-carbazol-3-yl)-2-(trifluoromethyl)benzamide], a novel inhibitor of human microsomal prostaglandin E synthase-1, on prostanoid biosynthesis in human monocytes in vitro. *Biochemical pharmacology* **79**, 974-981
134. Xu, D., Rowland, S. E., Clark, P., Giroux, A., Cote, B., Guiral, S., Salem, M., Ducharme, Y., Friesen, R. W., Methot, N., Mancini, J., Audoly, L., and Riendeau, D. (2008) MF63 [2-(6-chloro-1H-phenanthro[9,10-d]imidazol-2-yl)-isophthalonitrile], a selective microsomal prostaglandin E synthase-1 inhibitor, relieves pyresis and pain in preclinical models of inflammation. *The Journal of pharmacology and experimental therapeutics* **326**, 754-763
135. Leclerc, P., Pawelzik, S. C., Idborg, H., Spahiu, L., Larsson, C., Stenberg, P., Korotkova, M., and Jakobsson, P. J. (2013) Characterization of a new mPGES-1 inhibitor in rat models of inflammation. *Prostaglandins & other lipid mediators* **102-103**, 1-12
136. Leclerc, P., Idborg, H., Spahiu, L., Larsson, C., Nekhotiaeva, N., Wannberg, J., Stenberg, P., Korotkova, M., and Jakobsson, P. J. (2013) Characterization of a human and murine mPGES-1 inhibitor and comparison to mPGES-1 genetic deletion in mouse models of inflammation. *Prostaglandins & other lipid mediators* **107**, 26-34
137. Luz, J. G., Antonysamy, S., Kuklish, S. L., Condon, B., Lee, M. R., Allison, D., Yu, X. P., Chandrasekhar, S., Backer, R., Zhang, A., Russell, M., Chang, S. S., Harvey, A., Sloan, A. V., and Fisher, M. J. (2015) Crystal Structures of mPGES-1 Inhibitor Complexes Form a Basis for the Rational Design of Potent Analgesic and Anti-Inflammatory Therapeutics. *Journal of medicinal chemistry* **58**, 4727-4737

138. Prage, E. B., Pawelzik, S. C., Busenlehner, L. S., Kim, K., Morgenstern, R., Jakobsson, P. J., and Armstrong, R. N. (2011) Location of inhibitor binding sites in the human inducible prostaglandin E synthase, MPGES1. *Biochemistry* **50**, 7684-7693
139. Riendeau, D., Aspiotis, R., Ethier, D., Gareau, Y., Grimm, E. L., Guay, J., Guiral, S., Juteau, H., Mancini, J. A., Methot, N., Rubin, J., and Friesen, R. W. (2005) Inhibitors of the inducible microsomal prostaglandin E2 synthase (mPGES-1) derived from MK-886. *Bioorganic & medicinal chemistry letters* **15**, 3352-3355
140. Prage, E. B., Morgenstern, R., Jakobsson, P. J., Stec, D. F., Voehler, M. W., and Armstrong, R. N. (2012) Observation of two modes of inhibition of human microsomal prostaglandin E synthase 1 by the cyclopentenone 15-deoxy-Delta(12,14)-prostaglandin J(2). *Biochemistry* **51**, 2348-2356
141. Fitzpatrick, F. A., and Wynalda, M. A. (1983) Albumin-catalyzed metabolism of prostaglandin D2. Identification of products formed in vitro. *The Journal of biological chemistry* **258**, 11713-11718
142. Chen, W. J., Boehlert, C. C., Rider, K., and Armstrong, R. N. (1985) Synthesis and characterization of the oxygen and desthio analogues of glutathione as dead-end inhibitors of glutathione S-transferase. *Biochemical and biophysical research communications* **128**, 233-240
143. Brose, S. A., Thuen, B. T., and Golovko, M. Y. (2011) LC/MS/MS method for analysis of E(2) series prostaglandins and isoprostanes. *Journal of lipid research* **52**, 850-859
144. Orlando, B. J., Lucido, M. J., and Malkowski, M. G. (2015) The structure of ibuprofen bound to cyclooxygenase-2. *Journal of structural biology* **189**, 62-66
145. Venkataraman, H., den Braver, M. W., Vermeulen, N. P., and Commandeur, J. N. (2014) Cytochrome P450-mediated bioactivation of mefenamic acid to quinoneimine intermediates and inactivation by human glutathione S-transferases. *Chemical research in toxicology* **27**, 2071-2081
146. Charlier, C., and Michaux, C. (2003) Dual inhibition of cyclooxygenase-2 (COX-2) and 5-lipoxygenase (5-LOX) as a new strategy to provide safer non-steroidal anti-inflammatory drugs. *European journal of medicinal chemistry* **38**, 645-659
147. Sasso, O., Migliore, M., Habrant, D., Armirotti, A., Albani, C., Summa, M., Moreno-Sanz, G., Scarpelli, R., and Piomelli, D. (2015) Multitarget fatty acid amide hydrolase/cyclooxygenase blockade suppresses intestinal inflammation and protects against nonsteroidal anti-inflammatory drug-dependent gastrointestinal damage. *FASEB journal : official publication of the Federation of American Societies for Experimental Biology* **29**, 2616-2627
148. Zhang, G., Panigrahy, D., Hwang, S. H., Yang, J., Mahakian, L. M., Wettersten, H. I., Liu, J. Y., Wang, Y., Ingham, E. S., Tam, S., Kieran, M. W., Weiss, R. H., Ferrara, K. W., and Hammock, B. D. (2014) Dual inhibition of cyclooxygenase-2 and soluble epoxide hydrolase synergistically suppresses primary tumor growth and metastasis. *Proceedings of the National Academy of Sciences of the United States of America* **111**, 11127-11132
149. Selinsky, B. S., Gupta, K., Sharkey, C. T., and Loll, P. J. (2001) Structural analysis of NSAID binding by prostaglandin H2 synthase: time-dependent and time-independent inhibitors elicit identical enzyme conformations. *Biochemistry* **40**, 5172-5180
150. Ouellet, M., and Percival, M. D. (1995) Effect of inhibitor time-dependency on selectivity towards cyclooxygenase isoforms. *The Biochemical journal* **306 ( Pt 1)**, 247-251
151. Callan, O. H., So, O. Y., and Swinney, D. C. (1996) The kinetic factors that determine the affinity and selectivity for slow binding inhibition of human prostaglandin H synthase 1 and 2 by indomethacin and flurbiprofen. *The Journal of biological chemistry* **271**, 3548-3554
152. Laneuville, O., Breuer, D. K., Dewitt, D. L., Hla, T., Funk, C. D., and Smith, W. L. (1994) Differential inhibition of human prostaglandin endoperoxide H synthases-1 and -2 by nonsteroidal anti-inflammatory drugs. *The Journal of pharmacology and experimental therapeutics* **271**, 927-934
153. Palermo, G., Favia, A. D., Convertino, M., and De Vivo, M. (2016) The Molecular Basis for Dual Fatty Acid Amide Hydrolase (FAAH)/Cyclooxygenase (COX) Inhibition. *ChemMedChem* **11**, 1252-1258



154. Lucido, M. J., Orlando, B. J., Vecchio, A. J., and Malkowski, M. G. (2016) Crystal Structure of Aspirin-Acetylated Human Cyclooxygenase-2: Insight into the Formation of Products with Reversed Stereochemistry. *Biochemistry* **55**, 1226-1238
155. Migliore, M., Habrant, D., Sasso, O., Albani, C., Bertozzi, S. M., Armirotti, A., Piomelli, D., and Scarpelli, R. (2016) Potent multitarget FAAH-COX inhibitors: Design and structure-activity relationship studies. *European journal of medicinal chemistry* **109**, 216-237
156. Vecchio, A. J., Orlando, B. J., Nandagiri, R., and Malkowski, M. G. (2012) Investigating substrate promiscuity in cyclooxygenase-2: the role of Arg-120 and residues lining the hydrophobic groove. *The Journal of biological chemistry* **287**, 24619-24630
157. Mileni, M., Kamtekar, S., Wood, D. C., Benson, T. E., Cravatt, B. F., and Stevens, R. C. (2010) Crystal structure of fatty acid amide hydrolase bound to the carbamate inhibitor URB597: discovery of a deacylating water molecule and insight into enzyme inactivation. *Journal of molecular biology* **400**, 743-754
158. Favia, A. D., Habrant, D., Scarpelli, R., Migliore, M., Albani, C., Bertozzi, S. M., Dionisi, M., Tarozzo, G., Piomelli, D., Cavalli, A., and De Vivo, M. (2012) Identification and characterization of carprofen as a multitarget fatty acid amide hydrolase/cyclooxygenase inhibitor. *Journal of medicinal chemistry* **55**, 8807-8826
159. Bai, X. C., McMullan, G., and Scheres, S. H. (2015) How cryo-EM is revolutionizing structural biology. *Trends in biochemical sciences* **40**, 49-57
160. Efremov, R. G., Gatsogiannis, C., and Raunser, S. (2017) Lipid Nanodiscs as a Tool for High-Resolution Structure Determination of Membrane Proteins by Single-Particle Cryo-EM. *Methods in enzymology* **594**, 1-30
161. Bayburt, T. H., and Sligar, S. G. (2010) Membrane protein assembly into Nanodiscs. *FEBS letters* **584**, 1721-1727
162. Orlando, B. J., McDougle, D. R., Lucido, M. J., Eng, E. T., Graham, L. A., Schneider, C., Stokes, D. L., Das, A., and Malkowski, M. G. (2014) Cyclooxygenase-2 catalysis and inhibition in lipid bilayer nanodiscs. *Archives of biochemistry and biophysics* **546**, 33-40